UQAC
Université du Québec
à Chicoutimi

Conception d'un modèle de laboratoire d'un évacuateur de crue pour étudier l'érosion des masses rocheuses

Par

Koulibaly Aboubacar Sidiki

Mémoire présenté à l'Université du Québec à Chicoutimi en vue de l'obtention du grade de Maître ès-sciences appliquées en Maitrise en géologie et génie géologique

Québec, Canada

©Koulibaly Aboubacar Sidiki, 2021

REMERCIEMENTS

Je voudrais remercier tout particulièrement mes directeurs de recherche **Ali Saeidi**, **Alain Rouleau** et **Marco Quirion** de m'avoir guidé et soutenu tout au long de la réalisation de ce projet. Je voudrais également exprimer ma grande gratitude aux organismes partenaires ayant contribué de quelconques manières à la réalisation de ce projet, dont l'**UQAC**, **Hydro-Québec**, **Uniper**, **R2EAU** et **CRSNG/NSERC**.

Je voudrais enfin exprimer ma profonde reconnaissance à toute ma famille, pour leurs encouragements et leur soutien moral au cours de la réalisation de ce mémoire.

TABLE DES MATIERES

REMERCIEMENTS iii

LISTE DES TABLEAUX ix

LISTE DES FIGURES xi

LISTE DES ANNEXES xviii

LISTE DES SYMBOLES ET ABRÉVIATIONS xix

RÉSUMÉ xxi

AVANT-PROPOS xxiii

CHAPITRE 1 INTRODUCTION 1

1.1 MISE EN CONTEXTE 1

1.2 PROBLÉMATIQUE 2

1.3 OBJECTIFS 9

1.4 MÉTHODOLOGIE 10

1.4.1 LA RECHERCHE DE DONNÉES 11

1.4.2 L'IDENTIFICATION DES PARAMÈTRES CARACTÉRISTIQUES DE L'ÉROSION HYDRAULIQUE 12

1.4.2.1 LES INDICES UTILISÉS POUR LA FORCE ÉROSIVE DE L'EAU 12

1.4.2.2 REPRÉSENTATIVITÉ DES PARAMÈTRES HYDRAULIQUES À UNE ÉCHELLE RÉDUITE 13

1.4.3 REPRÉSENTATIVITÉ DES PARAMÈTRES GÉOMÉCANIQUES À UNE ÉCHELLE RÉDUITE 15

1.4.4 CONCEPTION, CONSTRUCTION ET VALIDATION DU MODÈLE PHYSIQUE RÉDUIT 17

1.4.5 RECOMMANDATIONS 17

1.5 STRUCTURE DU MÉMOIRE 17

CHAPITRE 2 20

IDENTIFICATION DES PARAMÈTRES HYDRAULIQUES INFLUENÇANT L'ÉRODABILITÉ HYDRAULIQUE DES CANAUX D'ÉCOULEMENT DES DÉVERSOIRS 20

2.1 INTRODUCTION 22

2.2 TYPES OF SPILLWAYS AND THEIR OPERATING MODE 28

2.3 METHODS FOR ESTIMATING THE EROSIVE FORCE OF WATER IN SPILLWAYS 31

2.3.1 AVERAGE SHEAR STRESS AT THE SURFACE OF THE FLOW CHANNEL 31

2.3.2 AVERAGE FLOW VELOCITY IN OPEN CHANNELS 43

2.3.3 APPLIED STRESSES INSIDE JOINTS AND THE BLOCK LIFTING FORCE 54

2.3.4 INDICES OF ENERGY DISSIPATION 58

2.4 DISCUSSION 67

2.5 CONCLUSION AND FUTURE RESEARCH DIRECTIONS 71

CHAPITRE 3 74

MÉTHODE POUR DÉTERMINER L'APPLICABILITÉ DES INDICES UTILISÉS POUR REPRÉSENTER LA FORCE ÉROSIVE DE L'EAU DANS LE PROCESSUS D'ÉROSION HYDRAULIQUE 74

3.1 INTRODUCTION 76

3.2 DESCRIPTION OF THE METHODOLOGY 86

3.2.1 DATA SET DEVELOPMENT 88

3.2.2 SELECTION OF A PARAMETER OF THE EROSIVE FORCE OF WATER ($umean, \tau b$ and ΠUD) 88

3.2.3 SELECTION OF ROCK MASS INDEX (K_h, $eGSI$ and $RMEI_B$) 89

3.2.4 CLASSIFICATION OF THE DATA SET ACCORDING TO SELECTED ROCK MASS INDEX 90

3.2.5 ORGANIZATION OF THE DATA ACCORDING TO DAMAGE CLASSES FOR THE SELECTED ROCK MASS CLASS 91

3.2.6 CALCULATION OF THE MEAN VALUE OF THE ROCK MASS INDEX AND INTENSITY PARAMETER FOR EACH DAMAGE CLASS 92

3.2.7 GRAPHICAL REPRESENTATION OF THE EROSIVE FORCE OF WATER VS. RESISTANCE INDICES OF THE ROCK MASS 94

3.3 RESULTS AND DISCUSSION 95

3.3.1 u_{mean} AS A FUNCTION OF ROCK MASS RESISTANCE INDEX 95
3.3.2 τ_b AS A FUNCTION OF ROCK MASS RESISTANCE INDEX 98
3.3.3 Π_{UD} AS A FUNCTION OF ROCK MASS RESISTANCE INDEX 100
3.4 CONCLUSION 104
CHAPITRE 4 106
DÉVELOPPEMENT D'UNE MÉTHODE VECTORIELLE POUR LE CALCUL EXACT DU VOLUME DU BLOC DE ROCHE 106
4.1 INTRODUCTION 109
4.2 DEVELOPMENT OF AN ANALYTICAL MODEL FOR CALCULATION OF THE BLOCK VOLUME 116
4.2.1 SELECTION OF THE SIGNIFICANT PARAMETERS FOR BLOCK SIZE CALCULATION 117
4.2.2 MODEL DEVELOPMENT 119
4.2.3 MODEL VALIDATION 123
4.3 COMPARISON OF THE METHODS FOR BLOCK VOLUME CALCULATION 127
4.3.1 PREPARATION OF THE DATABASE 127
4.3.2 BLOCK VOLUME CALCULATION 129
4.3.3 ROOT MEAN SQUARE ERROR (RMSE) CALCULATION 130
4.4 DISCUSSION 131
4.5 CONCLUSION 133
4.6 DECLARATIONS 134
CHAPITRE 5 135
CONCEPTION D'UN MODÈLE PHYSIQUE RÉDUIT D'ÉVACUATEUR DE CRUES POUR L'ÉVALUATION DE L'ÉRODABILITÉ HYDRAULIQUE D'UN MASSIF ROCHEUX FRACTURÉ 135
5.1 INTRODUCTION 137
5.2 DESIGN METHODOLOGY 147
5.2.1 MECHANISSME OF ROCK MASS HYDRAULIQUE EROSION 148

5.2.2 IDENTIFICATION OF THE RELEVANT PARAMETERS IN THE EROSION PROCESS 151

5.2.3 DIMENSIONAL ANALYSIS FOR CHOOSING THE HYDRAULIC PARAMETERS OF PHYSICAL MODEL 154

5.2.4 DESIGN OF ROCK MASS TEST SECTION 157

5.2.5 MONITORING AND INSTRUMENTATION DESIGN 163

5.2.6 TEST DESIGN FOR STUDYING THE EFFECT OF GEOMECHANICAL PARAMETER 165

5.2.6.1 Design for evaluating the effect of blocks orientation on the erosion . 165

5.2.6.2 Design for evaluating the effect of joint shear strength on erosion 168

5.2.6.3 Design for evaluating the effect of block volume (V_b) and weight (G_b)169

5.2.6.4 Design for studying the Nature of Potentially Erodible Surface (*NPES*) 170

5.3 RESULTS FROM THE VALIDATION TESTS OF THE REDUCE PHYSICAL MODEL 172

5.3.1 THE EFFECTS OF THE INFLOW RATE ON THE WATER PRESSURE .. 173

5.3.2 THE EFFECT OF THE OPENING JOINT (J_o) UNDER THE BLOCK AND PROTRUSION (*NPES*) ON THE PRESSURE 174

5.3.3 THE EFFECT OF THE OPENING JOINT (J_o) ON THE PRESSURE 176

5.4 DISCUSSIONS, RECOMMENDATIONS AND RESEARCH PERSPECTIVE. 178

5.5 CONCLUSION 179

CHAPITRE 6 CONCLUSION 180

6.1 IDENTIFICATION DES PARAMÈTRES HYDRAULIQUES INFLUANTS L'ÉRODABILITÉ HYDRAULIQUE 181

6.2 QUELLE EST L'APPLICABILITÉ DES INDICES REPRÉSENTANT LA FORCE ÉROSIVE DE L'EAU?..... 183

6.3. DÉVELOPPEMENT D'UNE MÉTHODE VECTORIELLE POUR LE CALCUL EXACT DU VOLUME DES BLOCS DE ROCHE..... 184

6.4. CONCEPTION D'UN MODÈLE PHYSIQUE RÉDUIT D'ÉVACUATEUR DE CRUE POUR L'ÉVALUATION DU PROCESSUS D'ÉROSION HYDRAULIQUE 184

RÉFÉRENCES 187
ANNEXES 194
Annexe A. Hydraulic and geomechanical data used in chapter 3 (Pells 2016a) 194
Annexe B. Graphics data sources 196
Annexe C. Avancement de la construction du modèle réduit 199

LISTE DES TABLEAUX

Tableau 1-1 : Résumé des méthodes connues pour évaluer le processus d'érosion hydraulique.....3

Table 2-1: General characteristics of methods for calculating the shear stress at the surface of a flow channel 35

Table 3-1. Empirical methods for evaluating the hydraulic erosion process 77

Table 3-2. Class of rock mass in terms of ease of excavation (Kirsten 1982a) 89

Table 3-3. Class of rock mass according to Pells (2016) *eGSI*, derived from the *GSI* of Hoek (Hoek *et al.* 1998) 89

Table 3-4. Class of rock mass according to Pells' $RMEI_B$ index 90

Table 3-5. Erosion classes as defined by Van Schalkwyk *et al.* (1994).....91

Table 3-6. Erosion classes as defined by Pells *et al.* 2016.....91

Table 3-7. Summary of steps 5 to 7 of the methodology applied to the parameters u_{mean} and *eGSI* parameters, considering only Class 2 of the *eGSI* index. 93

Table 3-8. Summary of steps 1 to 7 of the methodology applied to the paired parameters u_{mean} and *eGSI*. 94

Table 4-1: Methods for calculation of the block volume of a fractured rock mass 110

Table 4-2: Block volume calculation for a rock mass that includes three joint sets by Eq. 4-3 and 3DEC software 117

Table 4-3: Discontinuity's characteristics used for comparison of block volume calculation by analytical and numerical methods 124

Table 4-4: Characteristic data of the database summarizing the case studies of Pells (Pells 2016b) 128

Table 4-5: RMSE of block volume calculation results obtained by previously developed methods compared with the method developed in this study (Eq. 4-17-Method "A") for the cases of Figure 4-5 131

Table 5-1. Methods currently used to assess hydraulic erosion of rock mass. 139

Table 5-2. Summary of reduced physical models of spillways developed to study the effects of the geomechanical parameters of the rock mass on erosion. 144

Table 5-3. Summary of the parameters evaluated by the existing scale model 145

Table 5-4. Summary of the dimensional parameters of the real model and the RSPM 156

Table 5-5. Characteristics of measuring instruments 165

LISTE DES FIGURES

Figure 1-1 : Méthodologie de recherche appliquée dans ce mémoire..... 10

Figure 1-2 : Aspect typique d'un massif rocheux fracturé (Modifié de D. Hantz 2015)..... 16

Figure 2-1: Erosion by block removal or the dynamic block impulse (Bollaert et Schleiss 2002; Annandale 2006b)..... 24

Figure 2-2: Erosion by brittle fracture or instant hydrofracturing (Annandale 2006b) 24

Figure 2-3: Erosion by the continuous fragile fracturing of a rock mass or hydrofracturing by fatigue (Annandale 2006b)..... 25

Figure 2-4: Types of spillways. (a) Typical longitudinal section through an unlined spillway of a large embankment dam (Pells 2016a); (b) schematic representation of a free jet (© A.S Koulibaly, 2021), and (c) schematic representation of discharge over a drop structure (© A.S Koulibaly, 2021)..... 30

Figure 2-5: Schema of (a) uniform and (b) non-uniform flow (modified from Graf and Altinakar (Graf et Altinakar 2000))..... 33

Figure 2-6: Schematic illustration of the areas determined by the merged perpendicular method (Khodashenas *et al.* 2008)..... 36

Figure 2-7. Regions of the inner and outer laws of the boundary layer (Yen 1991). 48

Figure 2-8. Schematic representation of a plunging flow according to Annandale (Annandale 1995) 61

Figure 2-9. Flow conditions of a hydraulic jump (Annandale 1995) 62

Figure 2-10. Schematic of a knickpoint flow (Annandale 1995) 63

Figure 2-11. Schematic of a plunging flow according to Pells (Pells 2016a) 65

Figure 2-12. The block removal erosion mechanism for flow parallel to the bottom of the flow channel (modified from Annandale (Annandale 1995)) 70

Figure 3-1. Methods for evaluating the hydraulic erodibility of rock mass in the flow channels of spillways, presenting the methods developed by (a) Annandale (1995), (b) Van Schalkwyk *et al.* (1994b), and (c, d) Pells *et al.* (2016). 81

Figure 3-2. Examples of estimates when applying the different indices used to represent the erosive force of water (Pells 2016a). 83

Figure 3-3. Methodology for determining the relevance of the index for the erosive force of water 87

Figure 3-4. Observed erosion damage plotted using u_{mean} as the intensity of the erosive force of water vs. the various resistance indices of the rock mass (K_h, *eGSI*, and $RMEI_B$) 96

Figure 3-5. Observed erosion damage plotted using τ_b as the intensity of the erosive force of water vs. the various resistance indices of the rock mass (K_h, *eGSI* and $RMEI_B$) 99

Figure 3-6. Observed erosion damage plotted using ΠUD as the intensity of the erosive force of water vs. the various resistance indices of the rock mass (K_h, *eGSI* and $RMEI_B$) 101

Figure 4-1: The structural characteristics of a rock mass (Wyllie et Mah 2004) 118

Figure 4-2. The methodology used for the analytical calculation of the block volume. (a) a model comprising three joint sets, (b) blocks that not cut by the boundaries of the model and boundary blocks (c) all the intact blocks are identical in dimension and volume (© A.S Koulibaly et al., 2021) 120

Figure 4-3. Block volume calculation method (a) an intact block that produced by three joint sets. (b) normal to joint set (N_{J1}, N_{J2} and N_{J3}), edge vectors (A, B, and C) and true spacing of joint set 1 (S_1) as well as the angle between edge vector A and S_1 (θ_1) and the angle between joint set 1 and 2 (γ_3) (© A.S Koulibaly et al., 2021) . 120

Figure 4-4. A 20x20 m rock mass that includes three joint sets with dip/dip direction according to case number 6 of Table 4-3, but with different spacings (2, 3, and 4 meters for joint sets 1, 2, and 3, respectively) (© A.S Koulibaly et al., 2021). 126

Figure 4-5. Graphical representation of the block volumes for the cases presented in Table 4-4, that are calculated by models of Table 4-1 and the method that is developed in this article (method "A"). NB: method C and D give the same results, which is why curve C is visible. (© A.S Koulibaly et al., 2021) 129

Figure 5-1. The design stages of the physical model 148

Figure 5-2. Erosion by instantaneous brittle fracture (Annandale 2006b). 149

Figure 5-3. Erosion by continuous fragile fracturing of rock mass or hydrofracturing by fatigue (Annandale 2006b). 150

Figure 5-4. Erosion by block removal called dynamic block impulses, (a) erosion by removal of blocks in a plunging stream (Bollaert et Schleiss 2002; Annandale 2006b), and (b) erosion by removal of blocks in a flow parallel to the bottom of the flow channel (Annandale 1995)..... 151

Figure 5-5. Spillway of Romaine IV dam (Hydro-Québec) 155

Figure 5-6. Location of areas subject to erosion on an inclined spillway, a) downstream erosion at the Copeton dam in Australia (Pells 2016a), and b) area sensitive to erosion an inclined flow channel (Kirsten 2000)..... 158

Figure 5-7. Plan of the test section of the RSPM (dimension in centimeters) (© A.S Koulibaly, 2021) 159

Figure 5-8. Cross-section of the test section of the RSPM at upstream (A-A) and downstream (B-B) location along flume (dimension in centimeters) (© A.S Koulibaly, 2021). 159

Figure 5-9. The designed RSPM of the spillway. (a) 3D view, and (b) sectional view of the system (© A.S Koulibaly, 2021)..... 160

Figure 5-10. View of the double valve system in model (© A.S Koulibaly, 2021) . 161

Figure 5-11. Schematic view of the initial configuration of casing of concrete blocks. (a) Plan view of concrete blocks and (b) Longitudinal profile of concrete blocks (dimension in centimeters) (© A.S Koulibaly, 2021)..... 162

Figure 5-12. Example of concrete block instrumented to measure the water pressure on each side (© A.S Koulibaly, 2021)..... 163

Figure 5-13. a) ¼" diameter copper pipes, of different shapes depending on the pressure measurement points, b) Wooden mold with copper pipes installed on each face of the block, mold for blocks with smooth surface, c) Wooden mold with 3D printing of a rough profile, mold for blocks with a rough surface, d) Pouring a concrete block, and e) Pressure sensor installed on a concrete block for a pressure measurement for validation test on each face of the block (© A.S Koulibaly, 2021). 164

Figure 5-14. Arrangement of the blocks with respect to the direction of water flow (DWF) (distance in centimeters) (© A.S Koulibaly, 2021). 167

Figure 5-15. Altered joint behavior of a rock mass under the effect of forces of different nature (© A.S Koulibaly, 2021) 168

Figure 5-16. Smooth and rough faces of concrete blocks, water inlet in red and water outlet in green (© A.S Koulibaly, 2021)..... 169

Figure 5-17. Different size and density of the concrete blocks (© A.S Koulibaly, 2021)..... 170

Figure 5-18. Some examples of the arrangement of concrete blocks with different protrusion (© A.S Koulibaly, 2021)..... 171

Figure 5-19. Condition tests to evaluate the effect of the inflow rate on the pressure (© A.S Koulibaly, 2021)..... 173

Figure 5-20. Effect of flow water inflow rate on the apply pressure on the rock mass (© A.S Koulibaly, 2021)..... 174

Figure 5-21. Condition tests to evaluate the effect of the spacing under the rock block and the protrusion on the apply pressure under and on it (© A.S Koulibaly, 2021)..... 175

Figure 5-22. a) Effect of the variation of J_o under the block on the uplift pressure, and b) effect of the protrusion (NPES) on the apply on the block (© A.S Koulibaly, 2021)..... 175

Figure 5-23. Condition tests to evaluate the effect of the spacing around the rock block on the apply pressure (© A.S Koulibaly, 2021)..... 176

Figure 5-24. Effect of the variation of *Jo* around the block on the pressure (© A.S Koulibaly, 2021) 177

LISTE DES ANNEXES

Annexe A. Hydraulic and geomechanical data used in chapter 3 (Pells 2016a) 194

Annexe B. Graphics data sources 196

Annexe C. Avancement de la construction du modèle réduit 199

LISTE DES SYMBOLES ET ABRÉVIATIONS

(.): The point is an inner product of a pair of vectors

(×): The multiplication sign is a cross product

($\%SFw$): Percentage of shear force

A: The area of the observation zone (m^2)

$\vec{A}, \vec{B}, and\ \vec{C}$: Edge vectors of the intact block

a_1: Longest dimension of the block (m)

a_3: Shortest dimension of the block (m)

B_f: Width of a flow section measured at the water surface (m)

C : Flow resistance coefficient of Chezy

D_1, D_2, *and* D_3: Dip of the joint set 1, 2 and 3

DD_1, DD_2, *and* DD_3: Dip direction of the joint set 1, 2 and 3

d_p: Pipe diameter (m)

$eGSI$: Geological strength index for erodibility

E_{doa}: Erosion, discontinuity orientation adjustment

F: Limit correction factor for stress intensity

F_O: Force on a block (kN)

F_u: Force under a block (kN)

Fr: Upstream Froude number

f: Flow resistance coefficient of Darcy

G_b : Submerged weight of a rock block (kN)

g: Acceleration due to gravity ($m.s^{-2}$)

H: Total energy charge or water height (m)

HEC-RAS: Hydrologic Engineering Centers River Analysis System

H_f: Friction energy loss over a pipe length (m)

I_{impuls}: Dynamic impulse or block lifting force ($Kg.m.s^{-1}$)

J_a: Joint alteration number

J_f: Average energy slope

J_n: Number of joint sets

J_o: Joint aperture (m)

J_r: Joint roughness number

J_s: Relative block structure

J_v: Number of joints intersecting a volume of $1m^3$ of rock (m^{-3})

K: Relative roughness coefficient

K_h: Kirsten's index

$K_{I,in}$: In situ resistance of a rock mass ($MPa.m^{1/2}$)

K_I: Sub-hydrostatic pressure factor of flow

K_s: Equivalent wall surface roughness

L: The characteristic length of the rock mass or pipe (m)

L_f: Total joint length (m)

l_i: The joint length (m)

m: Mass of rock (kg)

N: Non-uniformity of the channel in both profiles

N_{J1}, N_{J2}, *and* N_{J3}: Normal vectors to joint set J_1, J_2, and J_3 plane

N_r: Number of random joints in the real location
n: Resistance coefficient of Manning
$P_{(b)}$, $P_{(w)}$: The wetted perimeter of the bed and sidewalls of the flow channel, respectively (m)
P_i: Joint persistence
Q: Water flow rate ($m^3.s^{-1}$)
q: Discharge per unit width of the channel ($m^2.s^{-1}$)
R_H: Hydraulic radius (m)
RQD: Rock quality designation
$RMEI$: Rock mass erodibility index
$RMSE$: Root Mean Square Error
S: Average joint spacing measured along the drill core (m)
S_a: Average joint spacing of all sets (m)
S_f: Friction slope, the gradient of the total hydraulic energy line
S_i: Average spacing of joint set i (m)
T: Total power (W)
U: Degree of flow unsteadiness
u_{mean}: Average velocity (m.s-1)
$\overrightarrow{u_A}$, $\overrightarrow{u_B}$, and $\overrightarrow{u_C}$: Unit vectors of $\vec{A}, \vec{B}, and\ \vec{C}$
V_b: Volume of blocks (m^3)
V_b^A: The analytically calculated block volume (m^3)
$V_{\Delta tpulse}$: Flow or fluid velocity ($m.s^{-1}$)
wJd: Weighted joint density
y_c: Critical spray depth (m)
y_l: Downstream flow depth (m)
z: Elevation above a datum (m)
η_0: Cross-sectional geometric shape
γ_1, γ_2, and γ_3: Angle between each pair of joint sets
β: Form factor of the blocks
θ : Channel tilt angle (°)
ν : Kinematic viscosity ($m.s^{-1}$)
ξ : Slope of the dividing line
ρ : Density of water ($kg.m^{-3}$)
ψ : Ratio of the energy dissipation capacity
τ_b: Shear stress at the surface of the flow channel (kPa)
$\prod_{UD}$: Energy dissipation ($W.m^{-2}$)

RÉSUMÉ

L'érosion hydraulique du massif rocheux d'un évacuateur de crues résulte de l'action de l'eau sur celui-ci, un phénomène évalué par différentes méthodes en utilisant la corrélation entre la force érosive de l'eau et la capacité d'une masse rocheuse à y résister. L'érosion se produit lorsque la force érosive de l'eau dépasse la capacité de résistance des formations rocheuses. La résistance d'un massif rocheux est alors estimée par différents indices ainsi que la force érosive de l'eau. Avec ces indices et sur la base de certaines études de laboratoire, des méthodes d'évaluation d'érosion hydraulique ont été développées. Cependant les résultats obtenus par ces méthodes comportent plusieurs incohérences, notamment l'utilisation de certains paramètres hydrauliques et géomécaniques jugés non pertinents dans la détermination des forces en cause du processus d'érosion hydraulique. Le contenu de ce mémoire présente de nouvelles avancées dans l'investigation du phénomène d'érosion hydraulique. Notamment, l'identification des incohérences liées aux anciennes méthodes d'évaluation de l'érosion hydraulique à travers une revue de littérature, à la suite de laquelle nous essaierons de développer une méthode permettant la détermination de l'applicabilité des paramètres hydraulique dans le processus d'érosion. De nouvelles solutions sont donc proposées dans le but de mieux caractériser le

processus d'érosion hydraulique, dont le développement d'une nouvelle méthode de détermination du volume exact des blocs de roche dans un massif rocheux. La conception d'un modèle physique réduit d'évacuateur de crue a également été nécessaire dans le but de pouvoir de caractériser le phénomène d'érosion. Ce modèle regroupe tous les paramètres considérés comme pertinents dans le processus d'érosion et sa représentativité dans l'étude de l'interaction entre la force érosive de l'eau et les paramètres géomécaniques a été validée à travers des essais d'écoulement. Les paramètres hydrauliques considérés dans la conception du modèle sont le débit, la vitesse d'écoulement, la pression d'eau et la pente du canal. Concernant les paramètres géomécaniques, nous avons le volume des blocs, la résistance en cisaillement des joints, la disposition des blocs par rapport à la direction de l'écoulement, l'ouverture des joints, l'altération des joints et la nature de la surface du canal potentiellement érodable.

AVANT-PROPOS

Ce mémoire présente les résultats de nos travaux de recherche sur la caractérisation du phénomène d'érosion des massifs rocheux des évacuateurs de crue.

D'entrée de jeu, nous tenons à préciser que la structure de ce mémoire est particulière, car son contenu est entièrement présenté à l'aide d'articles, et ce dépendamment de la méthodologie de recherche développée. Dans l'introduction (***chapitre 1***), un résumé sommaire du processus d'érosion est présenté, suivi par la problématique générale de recherche. Pour résoudre cette problématique, un objectif principal a été émis, consistant à mieux caractériser l'érosion à travers un modèle physique réduit. Pour atteindre cet objectif, des problématiques intermédiaires ont été mises en place. Dans la recherche de solution à ces problématiques, des méthodologies de recherche spécifiques ont été élaborées et des efforts ont été fournis pour présenter les résultats obtenus sous forme d'article.

Le premier article (***chapitre 2***) présente une revue de littérature générale, dans laquelle nous cherchons à identifier les incohérences liées aux méthodes existantes, et en même temps identifier les paramètres à considérer dans la conception du modèle réduit. D'après cette revue, deux sources potentielles d'incohérences ont été identifiées et font l'objet des articles 2 et 3.

Le deuxième article (***chapitre 3***) répond à la première problématique de la revue de littérature. Dans cet article, nous cherchons à déterminer l'applicabilité des indices utilisée pour représenter la force érosive de l'eau.

L'article trois (***chapitre 4***) traite la seconde problématique découlant de la revue de littérature et d'une particularité de l'objectif général. Dans cet article une nouvelle méthode de détermination de la taille des blocs d'un massif rocheux a été développée pour mieux caractériser ce paramètre géomécanique.

À la lumière de ces trois articles, nous présentons dans l'article quatre (***chapitre 5***) la méthodologie de conception du modèle physique réduit selon les paramètres hydrauliques et géomécaniques identifiés précédemment.

Pour clore cet avant-propos, nous spécifions que chaque article dans le mémoire présente une section discussion/perspectives de recherche et un résumé de chaque article est présenté dans la conclusion du mémoire (***chapitre 6***).

CHAPITRE 1 INTRODUCTION

1.1 MISE EN CONTEXTE

La notion d'érodabilité hydraulique d'un massif rocheux est apparue vers 1900, après que des observations de la dégradation du massif rocheux sous les ponts aient été faites (Keaton 2013; Pells *et al.* 2016b). Par la suite, plusieurs cas d'érosion ont été observés en aval des déversoirs de barrages comme par exemple, le cas du barrage de Kariba en Zambie en 1962 (Bollaert *et al.* 2012) et celui de Tarbela au Pakistan en 1976 (Lowe *et al.* 1979). Depuis lors, plusieurs chercheurs se sont efforcés de comprendre ce phénomène, et plusieurs méthodes ont été développées pour évaluer l'érodabilité hydraulique des massifs rocheux soutenant ces barrages à l'aide de méthodes semi-empiriques et semi-analytiques. Ces méthodes utilisent le concept de "ligne de seuil" (Annandale 1995; Pells *et al.* 2016b), une corrélation entre la force érosive de l'eau et la capacité de la roche à résister à sa destruction. Ce concept est établi sur la base de trois mécanismes d'érosion, à savoir la fracturation fragile instantanée, la fracturation fragile continue de la masse rocheuse et l'érosion par enlèvement dynamique des blocs (Bollaert et Schleiss 2002; Annandale 2006b; Bollaert 2010). Les résultats obtenus par ces méthodes sont des graphiques sous forme d'abaque mettant en relation trois paramètres à savoir l'intensité de la force érosive de l'eau, la résistance du massif rocheux et les classes

d'érosion ou classes de dommages subis par le massif rocheux. Cependant, ces abaques présentent plusieurs incohérences quant à l'évaluation du processus d'érosion hydraulique. Les cas d'érosions qualifiés de négligeables sur le terrain sont dans la majorité des cas qualifiés d'érosion mineure à moyenne selon les abaques et vice-versa. Ce type d'incohérence existe pour les différentes classes d'érosion, de négligeable à extensive. Par ailleurs, les études de laboratoires ayant servi de base au développement de ces méthodes comportent des limites quant à l'estimation de l'érosion. De nombreux facteurs sont identifiés comme pouvant être la source de ces incohérences, dont l'incertitude liée à la représentativité de la force érosive de l'eau, l'incertitude liée à la détermination de la taille exacte des blocs d'un massif rocheux et la détermination de l'influence des différents paramètres géomécaniques sur la force érosive de l'eau. Le but de ce mémoire est donc à la recherche de solution à ces différentes sources d'incohérences.

1.2 PROBLÉMATIQUE

Le phénomène d'érosion hydraulique des massifs rocheux est une problématique qui affecte grandement la stabilité des ouvrages de rétention d'eau et notamment les barrages hydroélectriques sur lesquels ils reposent. Les dégâts peuvent aller de simples dommages aux ouvrages, jusqu'à leur rupture complète. Les méthodes développées pour évaluer ce phénomène utilisent une corrélation

entre la force érosive de l'eau et la résistance du massif rocheux. La plupart de ces méthodes sont de nature empirique (Tableau 1-1).

Tableau 1-1 : Résumé des méthodes connues pour évaluer le processus d'érosion hydraulique.

Auteurs	**Fonction de corrélation**		**Types de méthodes**
Moore *et al.* (1994)	Dissipation d'énergie Vs. Indice de Kirsten	$\prod_{UD} = f(K)$	Méthodes empiriques à semi-empiriques
Van Schalkwyk *et al.* (1994)			
Annandale (1995)			
Kirsten *et al.* (2000)			
Pells (2016a)	Dissipation d'énergie Vs. Indice de force géologique pour l'érodabilité	$\prod_{UD}$ Vs. *eGSI*	
	Dissipation d'énergie Vs. Indice de la masse rocheuse pour l'érodabilité	$\prod_{UD}$ Vs. *RMEI*	
Bollaert et Schleiss (2002; 2005); Bollaert 2004; Bollaert *et al.* (2012; 2016)	Contrainte appliquée au massif rocheux Vs. Résistance de la masse rocheuse in-situ	K_I Vs. $K_{I\text{-}in}$	Méthode semi-analytique

La force érosive de l'eau est le plus souvent représentée par la dissipation de l'énergie ($\prod_{UD}$; Tableau 1-1). Différentes méthodes d'estimation de cet indice sont proposées dans la littérature et ces méthodes d'estimation donnent systématiquement des résultats différents. D'autres indices sont également utilisés pour représenter la force érosive de l'eau, dont la vitesse moyenne d'écoulement (u_{mean}), la contrainte de cisaillement moyenne sur le lit d'un canal (τ_b) et la contrainte (K_I) appliquée aux joints dans le massif rocheux. L'ensemble de ces indices utilisés pour représenter la force érosive de l'eau considèrent différents

paramètres hydrauliques dans la détermination cette force. Cependant, l'utilisation de ces indices pour représenter la force érosive de l'eau est largement critiquée dans l'évaluation du processus d'érosion hydraulique (Van Schalkwyk *et al.* 1994; Annandale 2006a; Pells *et al.* 2016a). Les chapitres 2 et 3 de ce mémoire sont principalement dédiés aux indices utilisés pour représenter la force érosive de l'eau.

Concernant la résistance du massif rocheux, différents indices ont été développés sur la base des paramètres de la roche intacte et du massif rocheux (Tableau 1-1).

- L'INDICE DE KIRSTEN (K_h)

L'indice de Kirsten a été établi pour évaluer la résistance d'un massif rocheux face à une force d'excavation. Il a par la suite été adapté pour évaluer le phénomène d'érosion hydraulique en remplaçant la force d'excavation par la force érosive de l'eau (Moore *et al.* 1994; Van Schalkwyk *et al.* 1994; Annandale 1995; Kirsten *et al.* 2000). Cet indice s'exprime par l'équation 1.

$$K_h = Ms \cdot K_b \cdot K_d \cdot Js \,, \qquad (1)$$

Où Ms est la résistance à la compression confinée de la roche intacte, représentée par le produit de la résistance à la compression uniaxiale (*UCS,* en MPa) et du coefficient de densité (*Cr*) dépendant de la masse volumique d'une roche; K_b est le

paramètre estimatif de la taille des blocs équivalant à RQD/J_n, où, *RQD* est le *Rock Quality Designation* (Deere et Deere 1989), une mesure de la fréquence des joints contenue dans un massif rocheux, et J_n désigne le nombre de famille de joints dans un massif rocheux, déterminé lors de levés structuraux; K_d est la résistance en cisaillement des joints, définie par le rapport de la rugosité de la face des joints (J_r) et le degré d'altération (J_a), et J_s représente la structure relative des blocs, qui prend en compte l'effet de la forme et de l'orientation des blocs par rapport à la direction d'écoulement de l'eau dans le canal.

- LE *GEOLOGICAL STRENGTH INDEX POUR L'ÉRODABILITÉ* (*eGSI*)

Le *Geological Strength Index* (*GSI*) est un indice de la masse rocheuse obtenu à partir de l'indice *Rock Mass Rating* (*RMR*) de Bieniawski (Bieniawski 1989; Hoek *et al.* 1998). C'est un indice de résistance des massifs rocheux utilisé dans la conception des tunnels. Cet indice est modifié par l'ajout d'un facteur d'ajustement considérant l'effet des discontinuités sur l'érodabilité (Pells *et al.* 2016a). L'équation 2 est utilisée pour déterminer le *eGSI*.

$$eGSI = GSI + E_{doa} , \qquad (2)$$

Où E_{doa} est le facteur d'ajustement de l'effet des discontinuités sur l'érodabilité, similaire au facteur J_s de l'indice de Kirsten, et *GSI* est le *Géological Strength Index* à déterminer en utilisant le graphique de Hoek (Hoek *et al.* 1998).

- *ROCK MASS EROSION INDEX* (*RMEI*) (Pells *et al.* 2016a)

Le *Rock Mass Erosion Index* (*RMEI)* est un indice de résistance de la masse rocheuse, basé sur la quantification de probabilité de détachement et de déplacement des blocs. L'indice ne considère que les paramètres géologiques les plus importants contrôlant le mécanisme d'érosion, et est déterminé de deux manières différentes (Éqs. 3 et 4), soit $RMEI_A$ et $RMEI_B$. Le $RMEI_A$ a une plage de valeurs de 10 à 50 et le $RMEI_B$ peut avoir des valeurs comprises entre 36 et 4500.

$$RMEI_A = [RF_{P1}LF_{P1}] + [RF_{P2}LF_{P2}] + [RF_{P3}LF_{P3}] + [RF_{P4}LF_{P4}] + [RF_{P5}LF_{P5}]\,, \qquad (3)$$

$$RMEI_B = (RF_{P1}.LF_{P1}).(RF_{P2}.LF_{P2}).(RF_{P3}.LF_{P3}) + (RF_{P4}.LF_{P4}) + (RF_{P5}.LF_{P5})\,, \qquad (4)$$

Où *RF* est le facteur d'importance relative pour les paramètres de vulnérabilité à l'érosion, *LF* est le facteur de vraisemblance pour les paramètres de vulnérabilité à l'érosion de P_1 à P_5, P_1 est le mécanisme cinématique viable pour le détachement d'un bloc, P_2 représente la nature de la surface potentiellement érodable, P_3 la nature des discontinuités (résistance des joints), P_4 et P_5 représentent respectivement l'espacement des discontinuités basales et la forme des blocs.

- RÉSISTANCE IN SITU DU MASSIF ROCHEUX *($K_{I,in}$)*

La résistance in situ du massif rocheux ($K_{I\text{-}in}$, en MPa.m$^{1/2}$) est un indice de résistance de la masse rocheuse, défini comme étant la ténacité à la rupture in situ de la masse rocheuse (Bollaert 2004). Cet indice utilise soit la résistance à la traction

(T), ou la résistance à la compression non confinée (UCS) de la roche (Éq. 5 et Éq. 6).

$$K_{I,in} = (0{,}105\ to\ 0{,}132)T + (0{,}054\sigma_c) + 0{,}53\ , \quad (5)$$

$$K_{I,in} = (0{,}008\ to\ 0{,}010)UCS + (0{,}054\sigma_c) + 0{,}42\ , \quad (6)$$

Où T est la résistance à la traction de la roche (MPa), UCS est la résistance à la compression non confinée, et σ_c la contrainte de confinement in situ (MPa).

Pour développer ces méthodes d'évaluation de l'érodabilité hydraulique (Tableau 1-1), la plupart des auteurs ont procédé de manière empirique ou semi-analytique, et parmi ces auteurs, certains ont effectué des études de laboratoire sur des modèles physiques réduits. L'objectif de ces modèles réduits était de valider des hypothèses ou pour étudier les caractéristiques hydrauliques de l'écoulement ainsi que les phénomènes d'érosion dans les matériaux granulaires ou dans les massifs rocheux. Ces modèles physiques réduits permettent en général l'acquisition de données à partir d'essais sur différentes configurations d'évacuateurs de crues et différents types de massifs rocheux. Cependant, ces modèles physiques réduits comportent des limitations du point de vue de la représentativité du processus d'érosion hydraulique. Le chapitre 5 de ce mémoire étant principalement dédié à la conception d'un modèle physique réduit, une revue de littérature bien détaillée sur ces modèles est présentée.

À la lumière de cette revue de littérature sommaire, il ressort que le processus d'érosion hydraulique n'est que partiellement étudié par les différents modèles physiques réduits mis en place pour étudier ce processus. De plus, la représentativité des indices utilisés pour représenter les forces caractéristiques de l'érosion hydraulique est mise en cause. Selon, Boumaiza *et al.* (2019a), les indices de résistance de la masse rocheuse utilisent certains paramètres géomécaniques non pertinents pour le processus d'érosion hydraulique (M_s, J_s et K_b) et d'énormes critiques viennent à l'encontre de l'utilisation des indices connus pour représenter la force érosive de l'eau. Et parmi les paramètres qualifiés de pertinents pour l'érosion hydraulique, le volume des blocs (V_b) représente un paramètre géomécanique très important, car il est intrinsèquement lié aux poids des blocs qui influencent grandement la force nécessaire au déplacement des blocs. Cependant, il ressort que les méthodes de quantification de ce paramètre (V_b) le sous-estiment ou le surestiment dans la caractérisation des massifs rocheux (Elci et Turk 2014). Nous reviendrons plus en détail sur ce point dans le chapitre 4. Ces critiques rendent nécessaires de nouvelles études pour compléter la caractérisation du processus d'érosion hydraulique, en commençant par l'évaluation de la pertinence des indices utilisés pour représenter la force érosive de l'eau, puis la recherche de nouvelles méthodes d'estimation du volume des blocs et enfin l'évaluation

complète de l'interaction entre la force érosive de l'eau et les paramètres géomécaniques.

1.3 OBJECTIFS

L'objectif principal consiste à mettre en place un modèle physique réduit d'évacuateur de crue, permettant une caractérisation complète du processus d'érosion hydraulique. Pour ce faire, quelques objectifs spécifiques sont nécessaires pour répondre à l'objectif principal. Ces objectifs spécifiques sont les suivants :

1- Identifier les différents paramètres caractéristiques de l'érosion hydraulique, c'est-à-dire les paramètres caractéristiques de la force érosive de l'eau et ceux caractéristiques de la résistance du massif rocheux,

2- Étudier la pertinence et l'applicabilité des paramètres caractéristiques de la force érosive de l'eau,

3- Rechercher une nouvelle méthode d'estimation du volume des blocs in situ d'un massif rocheux,

4- Étudier la représentativité des différents paramètres hydrauliques et géomécaniques à une échelle réduite;

5- Concevoir et construire le modèle physique réduit,

6- Valider la représentativité du modèle physique réduit construit.

1.4 MÉTHODOLOGIE

La méthodologie adoptée tout au long de cette recherche pour atteindre les objectifs énumérés ci-dessus est présentée à la Figure 1-1 sous forme de diagramme et les sections suivantes expliquent en détail chaque étape de cette méthodologie.

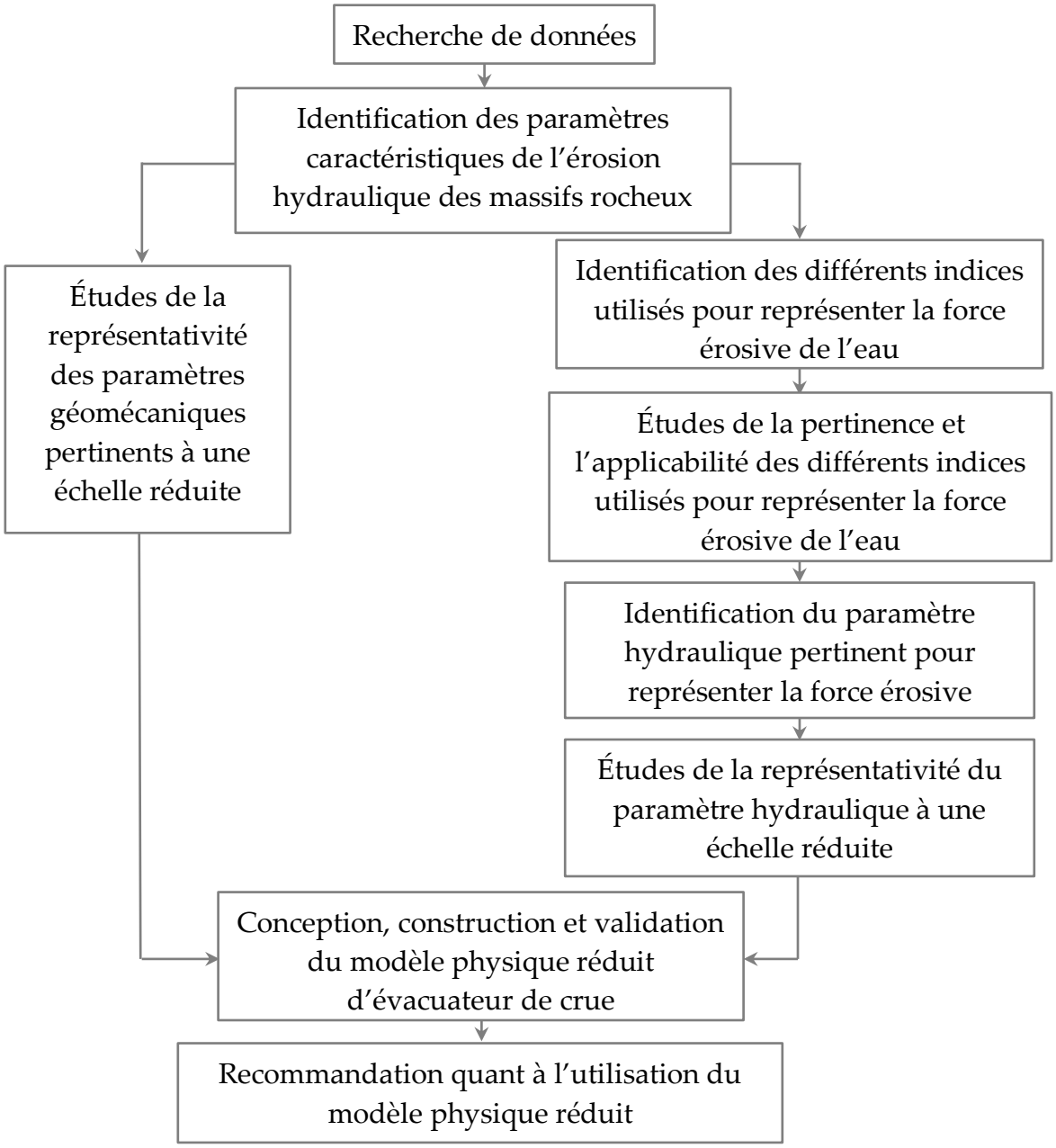

Figure 1-1 : Méthodologie de recherche appliquée dans ce mémoire

1.4.1 LA RECHERCHE DE DONNÉES

Dans la littérature, il existe de nombreuses études concernant la caractérisation du processus d'érosion hydraulique. Pour entamer cette recherche, une compilation des anciennes méthodes d'évaluation du processus d'érosion hydraulique est effectuée dans le but de définir l'état des connaissances sur le phénomène d'érosion hydraulique des évacuateurs de crue, et de valider les objectifs de conception du modèle physique réduit à l'étude. L'ensemble des mécanismes d'érosion sont étudiés et les différents paramètres caractéristiques de l'érosion hydraulique ont été répertoriés. Les approximations liées aux anciennes méthodes ont été identifiées et les objectifs de conception du modèle physique réduit ont été bonifiés par l'ajout des nouvelles perspectives de recherches dans le but de pouvoir mettre en place un modèle physique réduit complet. De plus, une base de données de plus de 100 études de cas d'érosions d'évacuateurs de crue a été compilée sur la base des données existantes, dont principalement ceux de Van Schalkwyk (Van Schalkwyk *et al.* 1994) et de Pells (Pells 2016a). Les données compilées portent sur les paramètres caractéristiques de l'hydraulique des évacuateurs de crue, dont le débit d'écoulement (Q), la décharge (q) et les pertes de charges liées aux écoulements (S_f ou S_0). À l'opposé les paramètres géomécaniques compilés sont le *RQD*, *Jn*, *Jr*, *Ja*, *Js*, *Jo*, *Ms*, la persistance des joints, la rugosité des joints (*JRC*), l'espacement entre les joints (S), le pendage et la direction de pendage

des joints (Dip/Dip-Direction), la direction des écoulements et les classes de dommages pour chaque cas d'études.

1.4.2 L'IDENTIFICATION DES PARAMÈTRES CARACTÉRISTIQUES DE L'ÉROSION HYDRAULIQUE

1.4.2.1 LES INDICES UTILISÉS POUR LA FORCE ÉROSIVE DE L'EAU

L'érosion hydraulique étant caractérisée par le résultat de l'action de la force érosive de l'eau sur un massif rocheux, les méthodes développées pour prédire ce processus sont basés sur la corrélation entre cette force et la résistance du massif rocheux. Les cas d'érosion sont définis lorsque la force érosive de l'eau excède la résistance du massif rocheux et le contraire est qualifié de non-érosion. Pour ce faire, des méthodes d'estimation de ces forces ont été développées de différentes manières et représentées par différents indices de force, soit les indices de force érosive et les indices de résistances de la masse rocheuse. Étant donné que les résultats obtenus des différentes corrélations entre ces indices présentent des incohérences quant à la prédiction des classes de dommage, la source de ces incohérences est définie comme étant liée aux indices de force caractéristiques des deux paramètres de corrélation. Cependant, Boumaiza *et al.* (2019a), a effectué une étude sur les indices de résistances de la masse rocheuse, et leur conclusion était que ces différents indices considèrent certains paramètres géomécaniques non

pertinents pour l'érosion hydraulique pour définir la résistance des massifs rocheux.

Dans ce mémoire, les indices de force érosive sont investigués en première position dans le but d'identifier les paramètres hydrauliques pertinents à prendre en compte dans la conception du modèle physique réduit à l'étude. Ensuite, ces indices sont critiqués sur la base d'une interprétation du comportement des paramètres hydrauliques dans les mécanismes d'érosion (chapitre 2). En utilisant la base de données compilée précédemment, une méthodologie a été mise en place pour évaluer l'applicabilité de ces différents indices. Et le paramètre hydraulique essentiel à considérer dans la conception du modèle physique réduit est doublement identifié (chapitre 3).

1.4.2.2 REPRÉSENTATIVITÉ DES PARAMÈTRES HYDRAULIQUES À UNE ÉCHELLE RÉDUITE

L'une des problématiques majeures liée aux anciens modèles physiques réduits d'évacuateur de crue est la représentativité des paramètres caractéristiques de l'érosion. Par exemple, les débits utilisés étaient généralement faibles ou trop élevés comparativement aux débits d'écoulement d'un évacuateur de crue. Pour remédier à ces problèmes dans la présente conception, la notion d'analyse dimensionnelle (Cengel 2014) utilisée dans le domaine de la mécanique des fluides pour assurer l'invariance des paramètres géométriques, cinématiques et

dynamiques à différentes échelles a été appliquée. Pour ce faire, différentes étapes sont nécessaires dont :

1- La sélection d'un prototype (modèle à grande échelle, c'est-à-dire un évacuateur de crue sur place) permettant d'avoir les dimensions géométriques, les données cinématiques et dynamiques d'un évacuateur de crue réel,

2- La sélection d'un facteur d'échelle (*Fe*) et d'un nombre adimensionnel pour effectuer la transposition des différentes données,

3- La validation de l'analyse dimensionnelle.

Sur la base des propositions reçues d'Hydro-Québec, l'évacuateur de crue du barrage Romaine – 04 (RN-04) a été choisi comme modèle réel à l'étude. Par la suite, le nombre de Froude (*Fr*), étant le nombre adimensionnel permettant d'utiliser l'eau comme fluide à différentes échelles (Cengel 2014), a été utilisé avec un facteur d'échelle *Fe* = 1/40 pour déterminer les dimensions du modèle physique réduit dépendamment des dimensions de la RN-04. Cependant, le modèle physique réduit a été conçu d'une manière à pouvoir l'adapter à d'autres conditions d'écoulement, car le débit, la vitesse d'écoulement et la pente du canal sont variables ainsi que les paramètres géomécaniques. Et la validation de l'analyse dimensionnelle a été effectuée en utilisant le nombre Reynolds (*Re*).

L'analyse dimensionnelle est valide lorsque le prototype et le modèle physique réduit sont caractérisés par le même mode d'écoulement, à savoir l'écoulement turbulent.

1.4.3 REPRÉSENTATIVITÉ DES PARAMÈTRES GÉOMÉCANIQUES À UNE ÉCHELLE RÉDUITE

L'objectif principal de conception de ce modèle physique réduit est la possibilité d'étudier l'effet de la variation des différents paramètres géomécaniques sur la force érosive de l'eau. Cependant, l'ensemble des paramètres géomécaniques affectant un massif rocheux, font en sorte qu'un massif rocheux soit constitué d'un assemblage de blocs de différentes tailles et de multitudes dispositions donnant des configurations variées (Figure 1-2). Pour mieux représenter le massif rocheux dans cas le présent, des ensembles de blocs de béton ont été confectionnés avec différentes formes, différentes tailles, différentes densités et en ayant également des surfaces allant de lisses à très rugueuses. Ces blocs sont confectionnés de sorte à pouvoir tenir compte de tous les paramètres géomécaniques pertinents dans l'érosion hydraulique, dont J_n, J_r, J_a, J_o, E_{dao}, K_d, V_b et *NPES*. Par ailleurs, il a été constaté que les méthodes détermination du volume des blocs (V_b) ne sont pas viables (Elci et Turk 2014), nous présentons plus détails sur ce sujet dans le chapitre 4.

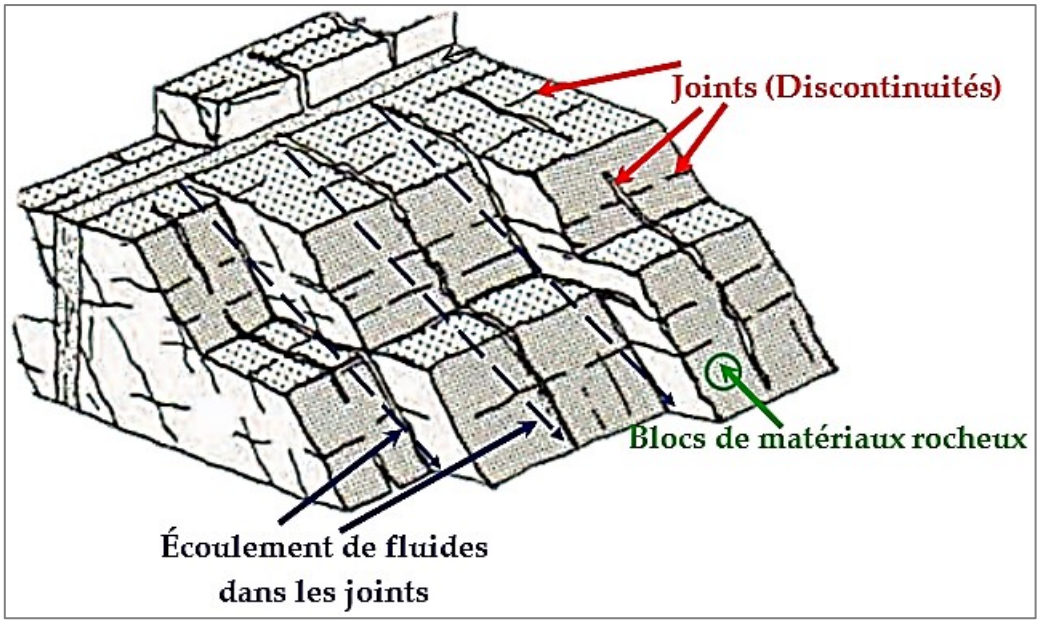

Figure 1-2 : Aspect typique d'un massif rocheux fracturé (Modifié de D. Hantz 2015).

On sait que la pression liée à l'écoulement de l'eau est le paramètre le plus important dans le processus d'érosion hydraulique. La valeur de cette pression et sa variation selon des paramètres géomécaniques sont mesurées à l'aide de capteurs de pression situés à différents endroits sur chaque face des blocs de béton. Par ailleurs, à la suite de l'interprétation des différents mécanismes d'érosion, il ressort que certains paramètres géomécaniques n'ont pas d'influence directe sur la pression hydraulique, mais plutôt sur le déplacement relatif des blocs. C'est pourquoi les blocs de béton sont également munis de capteur de déplacement (accéléromètre) dans le but d'évaluer ce paramètre.

1.4.4 CONCEPTION, CONSTRUCTION ET VALIDATION DU MODÈLE PHYSIQUE RÉDUIT

Après savoir résolu les problèmes de représentativité des différents paramètres caractéristiques de l'érosion hydraulique, le plan du modèle physique réduit est conceptualisé avant de passer à la construction. Après la mise en place de ce modèle, des essais devront être réalisés pour valider la représentativité du modèle réduit ainsi conçu. On s'attend à ce que la pression liée à la circulation d'eau dans les joints (autour et en dessous des blocs de béton) varie selon différentes configurations d'assemblage des blocs de béton.

1.4.5 RECOMMANDATIONS

À la suite des essais, des recommandations seront émises quant à l'amélioration du modèle, son utilisation et les différents essais d'écoulement à effectuer pour évaluer le processus d'érosion hydraulique de manière complète.

1.5 STRUCTURE DU MÉMOIRE

Comme expliqué en avant-propos ce mémoire est le recueil de quatre manuscrits d'articles scientifiques (Chapitre 2, 3, 4 et 5) dont un publié, et dont le premier auteur est l'auteur de ce mémoire. Le mémoire contient six chapitres résumés comme suit :

Le chapitre 1 (le présent chapitre): Introduction qui comprend la mise en contexte, l'énoncé de la problématique de recherche, les objectifs de la recherche, la méthodologie mise en place pour atteindre ces objectifs et un résumé de la structure du mémoire.

Le chapitre 2 : Revue de littérature des méthodes d'estimation de la force érosive de l'eau qui répond à l'***objectif 1***. Dans ce chapitre, nous cherchons à identifier les différents indices connus pour représenter la force érosive de l'eau, présenter les méthodes d'estimation de ces indices, présenter les critiques concernant les insuffisances liées à ces indices par rapport à leurs pertinences pour représenter la force érosive de l'eau. Des pistes de recherche sont proposées pour améliorer l'indice le plus pertinent.

Le chapitre 3 : Pour répondre à l'***objectif 2***, ce chapitre présente une méthode développée pour évaluer l'applicabilité des indices connus pour représenter la force érosive de l'eau.

Le chapitre 4 : Concernant l'***objectif 3***, ce chapitre présente le développement d'une nouvelle méthode vectorielle de détermination du volume des blocs d'un massif rocheux, et une étude comparative entre cette nouvelle méthode et les anciennes méthodes de détermination du volume des blocs.

Le chapitre 5 : Présente en détail le modèle physique réduit conçu en laboratoire (***objectifs 4, 5 et 6***). Ce modèle physique réduit conçu prend en compte les

paramètres propres à la force érosive de l'eau et les paramètres géomécaniques pertinents dans la définition de la résistance des massifs rocheux dans le processus d'érosion hydraulique.

Le chapitre 6 : Chapitre de conclusion contenant également des recommandations et les perspectives de recherche avec le modèle physique réduit conçu en laboratoire.

CHAPITRE 2

IDENTIFICATION DES PARAMÈTRES HYDRAULIQUES INFLUENÇANT L'ÉRODABILITÉ HYDRAULIQUE DES CANAUX D'ÉCOULEMENT DES DÉVERSOIRS

Ce chapitre présente un article dont le 1er auteur est l'auteur de ce mémoire. Le but ce chapitre est l'identification des différents paramètres hydrauliques influençant le processus d'érosion hydraulique des massifs rocheux des canaux d'écoulement des évacuateurs de crue. Cet article a été publié par la revue Hydraulics and Hydronamics dans la section Water, le 20 octobre 2021 et est disponible en ligne : https://www.mdpi.com/2073-4441/13/21/2950

Review

IDENTIFICATION OF HYDRAULIC PARAMETERS INFLUENCING THE HYDRAULIC ERODIBILITY OF SPILLWAY FLOW CHANNELS

Aboubacar Sidiki Koulibaly[1*], Ali Saeidi[1], Alain Rouleau[1], Marco Quirion[2]

[1] Département des Sciences Appliquées, Université du Québec à Chicoutimi, 555 boulevard de l'Université, Chicoutimi, Québec, G7H 2B1; Canada; ali_saeidi@uqac.ca; alain_rouleau@uqac.ca

[2] Hydro-Québec, Unité de Production et d'Expertise en barrages, 75 boulevard René-Lévesque Ouest, Montréal, Québec, H2Z 1A4, Canada; quirion.marco@hydro.qc.ca

* Correspondence: Aboubacar-sidiki.koulibaly1@uqac.ca; Tel.: +1-581-235-1247

Abstract: The rock mass erosion of dam spillways, a phenomenon involving the interaction between the hydraulic load of water and the capability of the rock mass to resist its destruction, remains a critical safety issue. The erosion resistance of a rock mass can be estimated through several erodibility indices, including that of Kirsten, Pells, and Bollaert. Several indices have been developed to link rock resistance to the hydraulic parameters of water, i.e., the hydraulic load applied on a rock mass. The developed indices use the average flow velocity, the average shear stress on the bottom of the flow channel, the stress applied to the internal

joints of fractured rock mass, the dynamic impulse force, and the power dissipation of water to represent the erosive force of water. From these indices, several methods of assessing hydraulic erosion have been developed, and all use the threshold line concept. Nonetheless, several uncertainties are associated with these methods. This paper presents and discusses the various means of calculating the erosive force of water as a hazard parameter for predicting potential rock erosion. The representativeness of these approaches is also discussed, and we clarify nuances associated with each method. We then provide guidelines for future research aimed at improving estimates of the erosive force of the water within spillway flow channels.

Keywords: Hydraulic erodibility, Hydraulic jump, Hydraulic load, Plunging flow, Power dissipation, Rock mass.

2.1 INTRODUCTION

The notion of the hydraulic erodibility of a rock mass emerged around 1900 after observations of the degradation of rock masses under bridges (Keaton 2013). Several cases of erosion downstream of dam spillways have since been observed, for example, the Tarbela dam in Pakistan in 1976 (Lowe *et al.* 1979) and the Kariba dam in Zambia in 1962 (Bollaert *et al.* 2012). Much research has focused on understanding this phenomenon, and several methods have been developed for

evaluating the hydraulic erodibility of a rock mass using semi-empirical and semi-analytical methods. These methods have applied the concept of the "threshold line,"(Annandale 1995; Pells *et al.* 2016b) a correlation between a hydraulic hazard parameter (e.g., shear stress, hydraulic power, and hydraulic energy) and the capacity of the rock to resist destruction. This concept is based on three erosion mechanisms in particular: dynamic block removal, brittle fracturing, and the continuous fragile fracturing of the rock mass (Bollaert et Schleiss 2002; Annandale 2006b; Bollaert 2010). Turbulent flow is the flow mode that can produce these different erosion mechanisms.

Erosion by the removal of blocks is a process that depends on the water pressure within the joints of the fractured rock mass. The amplitude of the fluctuating pressure changes with time during a turbulent flow, and the pressure applied inside the rock joints can increase pressure directly below the blocks. Moreover, the rock mass is eroded by the dynamic expulsion of the blocks when the lifting pressure under the block exceeds the resistance force of the block in the rock mass (Figure 2-1). The parameters affecting the resistance of the block are the submerged weight of the block (G_b), the pressure on top of the block (F_o), and the shear resistance along the sides of the block (F_{sh}).

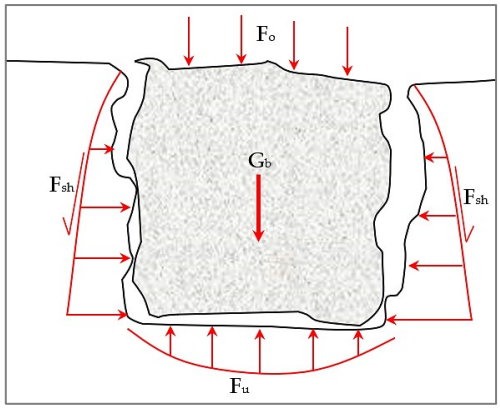

Figure 2-1: Erosion by block removal or the dynamic block impulse (Bollaert et Schleiss 2002; Annandale 2006b)

The second mechanism enabling the erosion of a rock mass is brittle fracturing or instant hydrofracturing. This mechanism occurs when the intensity of the fluctuating pressure-induced stress in the joints is greater than the resistance of the rock, and, hence, the rock mass breaks into small pieces owing to fragile failure (Figure 2-2).

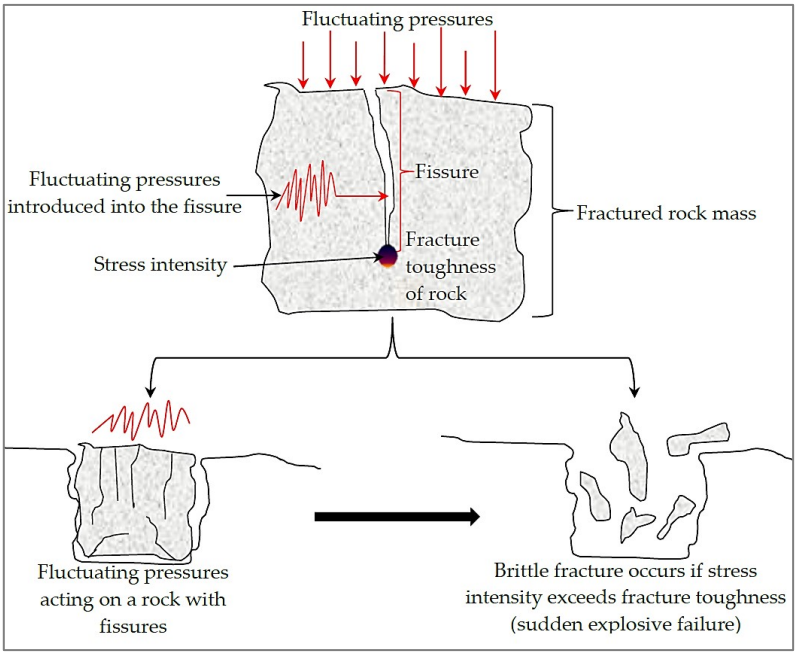

Figure 2-2: Erosion by brittle fracture or instant hydrofracturing (Annandale 2006b)

The final mechanism of erosion is continuous fragile fracturing or fatigue erosion. This mechanism occurs when the instantaneous brittle fracture of rock mass is not possible, as the intensity of the stress in the joints does not exceed the resistance of the rock mass. The rock mass is eroded, however, by fatigue pressure loads that exist in the joints. This type of erosion is highly dependent on time (Figure 2-3).

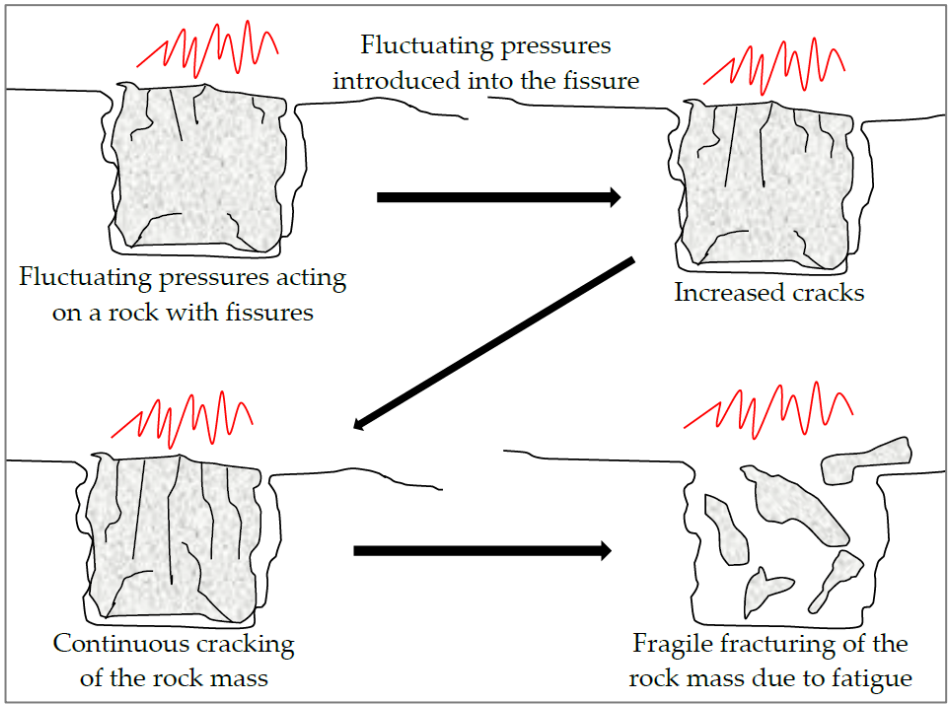

Figure 2-3: Erosion by the continuous fragile fracturing of a rock mass or hydrofracturing by fatigue (Annandale 2006b)

From these three erosion mechanisms, various indices have been developed to represent the resistance of a rock mass. These indices include the Kirsten index (K_h), Bollaert's in situ resistance of a rock mass ($K_{I,in}$), and the indices of Pells, which are the geological strength index for erodibility ($eGSI$) and the rock

mass erodibility index ($RMEI$). The hydraulic hazard parameter of water has been mainly represented by the dissipation of energy rate (Π_{UD} in kW m^{-2}), although other parameters have been used. For example, Bollaert et al. (Bollaert et Schleiss 2002) estimated the hydraulic hazard parameter of water in terms of the stress applied in a joint present within a rock mass (K_I in MPa m$^{1/2}$) and in the form of force dynamic impulse or block lifting force (I_{impuls} in Kg m s^{-1}). Pells (Pells 2016a) illustrated that the average flow velocity ($\bar{u}$ in m s^{-1}) and the average shear stress on the bottom surface of flow channel ($\bar{\tau}_b$ in Pa) are suitable indicators for representing the hydraulic erosion hazard for a fractured rock mass. Among these above-listed parameters, energy dissipation was selected by Bieniawski (Bieniawski 1989), Moore (Moore *et al.* 1994), Annandale (Annandale 1995; Annandale *et al.* 1998), Kirsten (Kirsten *et al.* 2000), and Pells (Pells *et al.* 2016b) (among others) to estimate the hydraulic hazard parameter of different possible flow conditions in spillways. Annandale (Annandale 1995) maintained that the dissipation of hydraulic power (Π_{UD}) provides a good approximation of turbulent fluctuations. Moreover, a large combination of spillway geometry and flow types can be associated with a given measure of Π_{UD}. Because the determination of Π_{UD} is relatively easy to perform, this also greatly favors the use of Π_{UD}.

Although the resistance indices of the rock mass and the hydraulic power indices have been commonly used to evaluate the hydraulic erodibility, these

methods have produced inconsistencies in some cases. These inconsistencies likely stem from two sources: the estimation of erosive force and the uncertainty linked to the indices for defining the resistance of a fractured rock mass. Previously, Boumaiza et al. (Boumaiza *et al.* 2019b) evaluated the weaknesses of the resistance of rock mass indices for the hydraulic erosion process. Here, we review the indices of the erosive force to determine whether erodibility assessment methods are also influenced by these hydraulic power indices and therefore represent (or not) a source of the produced inconsistencies in assessments of the hydraulic erodibility of a rock mass. Because of the large number of proposed indices, we review the various estimation methods of indices developed to represent the erosive force of water (waterpower) for various spillway flow modes. We highlight the advantages and disadvantages of each index and discuss the representativeness of each. We suggest that these indices do not effectively represent the erosive force of the water; we therefore offer potential research avenues to develop a better characterization of the erosive force of water.

In the following sections, we summarize the types of spillways and their operating mode. The different methods for estimating the hydraulic hazard parameters for rock mass erosion are then presented, including the estimation of the average shear stress at the bottom surface of a flow channel, the average flow velocity in open channels, the applied stresses inside joints, the block lifting force,

and the dissipation of power or energy from a flow channel. We also discuss the limitations of these methods.

2.2 TYPES OF SPILLWAYS AND THEIR OPERATING MODE

The overflow structures in dams can be divided into two categories on the basis of their frequency of use: spillways (fuse-plug or emergency spillways) and regulation structures (service or auxiliary spillways). A spillway returns the excess water arriving at the dam during periods of flooding to the river. The return period of flooding determines the frequency of this occasional use. In contrast, regulation structures manage the flow rate, ensuring a relatively continuous transfer of water to the river. Despite the significant operational differences between the two structures, their designs and configurations are similar. Structures in each category vary in their specific configurations depending on site topography and geology. These on-site properties determine the types of spillway that are installed, for example (Khatsuria 2004):

- ogee spillway,
- chute spillway,
- side-channel spillway,
- shaft or tunnel spillway,
- siphon spillway,
- and free over-fall spillway.

The energy of the discharging water must be dissipated before returning to the river; therefore, and depending on the operational mode of the specific spillway, these structures are equipped with a flow channel or a transition zone between the end of the profiled threshold and the final dissipation zone of an evacuation structure (Figure 2-4a). In other cases, a simple basin, constituting a plunge pool, dissipates the energy immediately at the foot of the spillway (Figure 2-4b and c). The flow channels dissipate and direct the torrential regime flow toward the final dissipation zone. In this latter case, the observed flow modes differ depending on the nature of the channel, i.e., flows on an inclined slope, hydraulic jumps, flows at knickpoints, and plunging flows into the receiving pool.

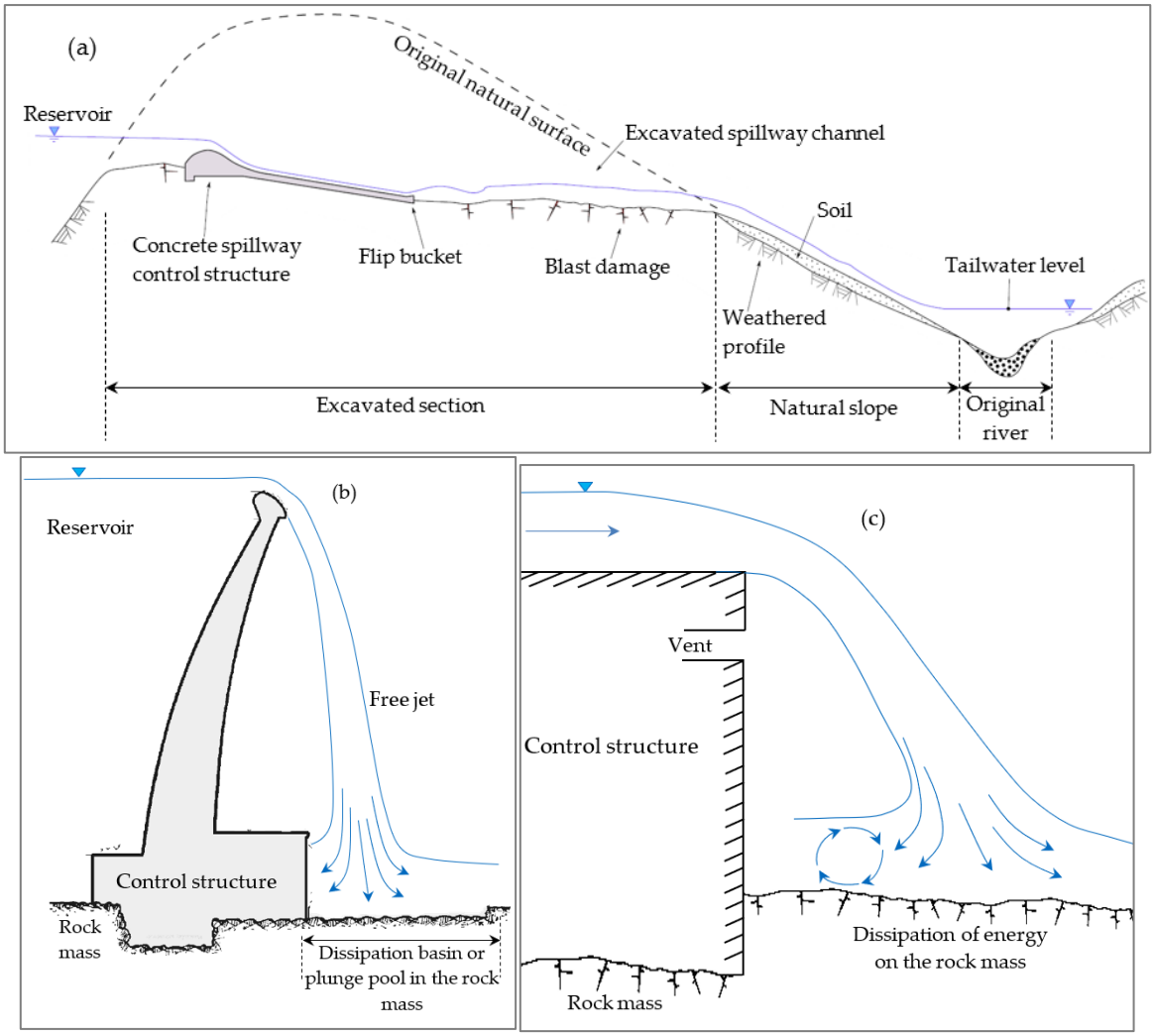

Figure 2-4: Types of spillways. (a) Typical longitudinal section through an unlined spillway of a large embankment dam (Pells 2016a); (b) schematic representation of a free jet (© A.S Koulibaly, 2021), and (c) schematic representation of discharge over a drop structure (© A.S Koulibaly, 2021)

Several spillways around the world have been designed and built involving a combination of a discharge channel and a dissipation or stabilization zone. Examples of these combined spillways include the Robert-Bourassa dam spillway (Quebec, Canada) and the Hell Hole dam spillway (California, USA) (Khatsuria 2004). Moreover, in most cases, the dissipation structures are excavated into the rock mass, including the plunge pool or the combination of an evacuation channel

and dissipation zone. An important aspect of these unlined spillways is the phenomenon of hydraulic erosion of rock mass. For these spillways, the proper estimation of the erosive force of water is critical.

2.3 METHODS FOR ESTIMATING THE EROSIVE FORCE OF WATER IN SPILLWAYS

Various methods have been applied to estimate the erosive force of water in erosion processes, and different indices of erosive force have been obtained, including the average shear stress at the bottom surface of a flow channel, the average flow velocity in open channels, the applied stresses inside joints, the block lifting force, and the dissipation of energy from a flow channel.

2.3.1 AVERAGE SHEAR STRESS AT THE SURFACE OF THE FLOW CHANNEL

The velocity profile of a fluid is proportional to the applied shear force, and the linear proportionality factor is the dynamic viscosity ($\tau = \mu . du/dy$) (Schlichting 1979; Pells *et al.* 2016b). Given that the viscosity of water is well known, the average shear stress at the bottom surface of a flow channel therefore mainly depends on the variation of flow velocity, which is a function of the nature of the flow. The calculation of shear stress varies, however, depending on the type of flow. The shear stresses for a uniform flow depend on the slope of the flow

channel. In the case of non-uniform flow, the total energy gradient is used to estimate the shear stresses in the channel. Figure 2-5 illustrates possible cases of the distribution and variation of flow velocity. The cases depend on the nature of flow; in the first case, the velocity of a flow is uniform (Figure 2-5a), whereas the second case has a variable velocity for a non-uniform flow (Figure 2-5b). Depending on the nature of the flow, shear stress on the bottom of the channel can be estimated using either Eq. ***(2-1)*** or Eq.***(2-2)***.

$$\bar{\tau}_b = \rho.\mathrm{g}.R_H.S\cos\theta \ \text{(Uniform flow)}, \qquad (2\text{-}1)$$

$$\bar{\tau}_b = \rho.\mathrm{g}.R_H.S_f\cos\theta \ \text{(non-uniform flow)}, \qquad (2\text{-}2)$$

where μ is the dynamic viscosity of water, u is the flow velocity, R_H is the hydraulic radius, S is the slope of the channel equal to dz/dx, x is the distance along the channel, z is the elevation above a datum, g is the gravitational acceleration, θ is the angle of inclination of the channel, and S_f is the total energy gradient equal to $dH/dx = H_f/L.\cos\theta$, and H_f is the energy loss by friction (in m) over distance L, which can be determine using Eq. *(2-19)* (section 3.2).

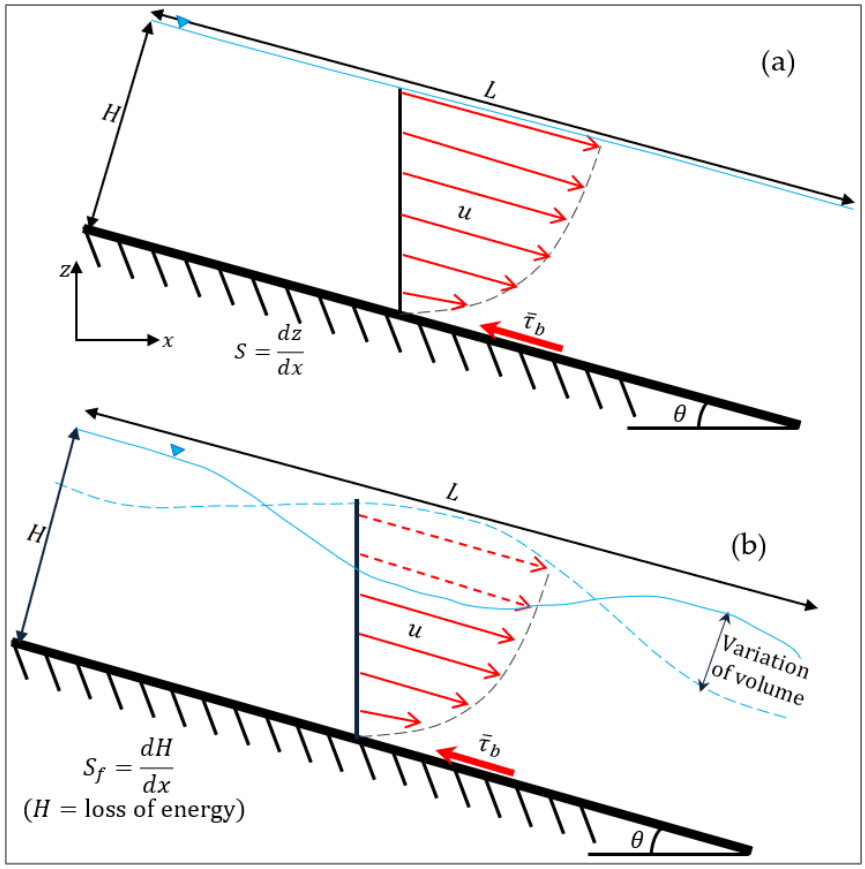

Figure 2-5: Schema of (a) uniform and (b) non-uniform flow (modified from Graf and Altinakar (Graf et Altinakar 2000))

It should be noted that $\bar{\tau}_b$ represents the mean hydraulic shear stress on the surface of the channel. The actual shear stress at each point along the channel can always vary because of the presence of relatively rougher parts of the channel. Given this variability, the shear stress term ($\bar{\tau}_b$) is generally replaced by the shear velocity (u_*), which is calculated using Eq.***(2-3)***.

$$u_* = \sqrt{\frac{\rho.\mathrm{g}.R_H \sin\theta}{\rho}} = \sqrt{\mathrm{g}.R_H \sin\theta} \ \ \& \ \bar{\tau}_b = \rho u_*^2 \ . \qquad (2\text{-}3)$$

According to Streeter (Streeter *et al.* 1998), estimating the shear stress in a flow channel is quite complex for turbulent flow because of the variable internal

shear stress, which depends on the velocity over the entire depth of the flow profile and the substantial changes along a channel. A simple solution, for this case, is to substitute the dynamic viscosity (μ) with the eddy viscosity (η) to calculate the shear stress for turbulent flow (Eq.***(2-4)***) (Streeter *et al.* 1998). For this to be possible, the eddy viscosity must be estimated for each flow type, as this parameter is not a constant characteristic of the fluid and varies throughout the profile of the fluid over time. This parameter depends upon the density of the fluid, the velocity gradient, and the mixing length, and it generally varies from point to point in the flow field.

$$\tau_t = \eta . \frac{du}{dy} \qquad (2\text{-}4)$$

In addition to Eqs.***(2-1)***, ***(2-2)***, ***(2-3)***, and ***(2-4)***, expressions exist for estimating the shear stress at the surface of a flow channel. **Table 2-1** summarizes some existing methods used to calculate this surficial shear stress. Most of these methods are adapted for calculating the local average shear stresses of straight and prismatic flow channels of rectangular, trapezoidal, and circular sections, either with or without a flat or compound bed. Moreover, these methods differ in their assumptions, which can lead to divergent shear stress estimates. We detail some of the methods presented in **Table 2-1** below.

Table 2-1: General characteristics of methods for calculating the shear stress at the surface of a flow channel

Method	Cross-sectional shape	Boundary roughness distribution
Lundgren and Jonsson (1964)	General	Homogeneous and rough
Flintham and Carling (1988)	Rectangular, trapezoidal	Homogeneous
Pizzuto (1991)	General	Homogeneous
Christensen and Fredsoe (1998)	General	Homogeneous
Khodashenas and Paquier (1999)	General	Homogeneous
Ramana Prasad and Russell Manson (2002)	Rectangular, trapezoidal	Homogeneous
Berlamont et al. (2003)	Rectangular, circular (with or without a flat bed)	Homogeneous
Yang and Lim (2005) and Yang et al. 2004	Rectangular, trapezoidal, circular, V-notch, compounded	Homogeneous
Guo and Julien (2005)	Rectangular	Homogeneous and smooth
Seckin et al. (2006)	Rectangular	Homogeneous and smooth
Severy and Felder (2017)	Rectangular	Homogeneous and smooth

Modified: from (Khodashenas *et al.* 2008)

- **Merged perpendicular method** (Khodashenas *et al.* 2008)

The merged perpendicular method (MPM) is a geometric method for calculating the local shear stress in an irregular cross section of a channel. This method is derived from the normal area method, which relies on the concept of

hydraulic radius separation based on the subdivision of a cross-sectional region delimited by walls into three subareas that correspond to the lateral walls and channel bed. The wetted area is then divided into small subareas using the lines normal to the wetted perimeter (Figure 2-6). The local shear stress (τ_i) is thus obtained using Eq.***(2-5)***.

$$\tau_i = \rho . g . R . J_f \ , \qquad (2\text{-}5)$$

where R is the local hydraulic radius, and J_f is the average energy slope. Subsequently, the average boundary stresses acting on the channel bed and sides are determined by the numerical integration of the local values. However, this method neglects secondary flow structures and the momentum transfer in an irregularly shaped channel. Moreover, the roughness distribution along the wetted perimeter is not considered when the wetted area is divided into subzones.

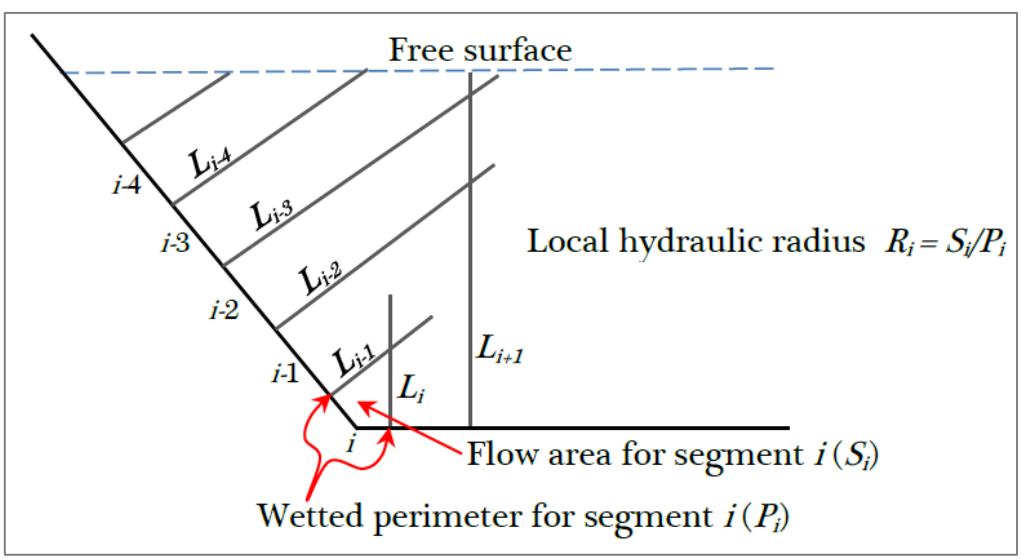

Figure 2-6: Schematic illustration of the areas determined by the merged perpendicular method (Khodashenas *et al.* 2008)

- **Ramana Prasad and Russell Manson method** (Ramana Prasad et Russell Manson 2002)

This method is based on an analytical approach for calculating the percentage of shear force ($\%SFw$) carried by the sidewall in prismatic channels of a trapezoidal cross section having a homogeneous roughness. The percentage of shear force is given in terms of the width–depth ratio (b/h) without accounting for the effect of secondary currents (Eq.***(2-6)***).

$$\%SFw = \frac{100\bar{\tau}_{(w)}}{\bar{\tau}_{(w)} + \bar{\tau}_{(b)}\left(\frac{P_{(b)}}{P_{(w)}}\right)} = \begin{cases} 25\left(4 - \frac{b}{h}\right) & \frac{b}{h} \leq 2 \\ \frac{100}{b/h} & \frac{b}{h} \geq 2 \end{cases}, \qquad (2\text{-}6)$$

where $P_{(b)}$ and $P_{(w)}$ represent the wetted perimeter of the bed and sidewalls, respectively. Knowing $\%SFw$, the following equations are used to determine the shear stress of the bed and the walls of a channel ($\bar{\tau}_{(b)}$ and $\bar{\tau}_{(w)}$):

$$\begin{cases} \frac{\bar{\tau}_{(b)}}{\rho g h J_f} = (1 - 0.01\%SFw)\left(1 + \frac{P_{(w)}}{P_{(b)}}\right) \\ \frac{\bar{\tau}_{(w)}}{\rho g h J_f} = 0.01\%SFw\left(1 + \frac{P_{(b)}}{P_{(w)}}\right) \end{cases}. \qquad (2\text{-}7)$$

- **Yang and Lim method** (Yang et Lim 2005)

This method uses an analytical approach for calculating the distribution of shear stresses in prismatic channels and is based on the concept of excess energy transport over a minimum relative distance within a uniform and fully developed turbulent flow. The relative distance is defined as the ratio of the shortest

geometric distance to the energy dissipation capacity (EDC) of the boundary. For a smooth boundary, the characteristic length representing the EDC of the boundary is scaled using the viscous length scale (ν/u_*) (Yang et Lim 2005), where ν is the kinematic viscosity of the fluid, and u_* is the shear rate. And for an approximate limit, the characteristic length is scaled using the roughness height of the limit. From this concept, Yang and Lim divide the flow zone into subzones on the basis of the shape of the cross section and the roughness of its wetted perimeter; however, secondary currents are not considered. The distribution of average shear stresses along the bed ($\bar{\tau}_{(b)}$) and side wall ($\bar{\tau}_{(w)}$) for a smooth trapezoidal channel are determined using equations ***(2-8)*** through ***(2-11)***.

$$\begin{cases} \dfrac{\bar{\tau}_{(b)}}{\rho g h J_f} = 1 + \dfrac{h}{b}\dfrac{1}{\tan\beta} - \psi\dfrac{h}{b}\dfrac{1}{\sin\beta} \\ \dfrac{\bar{\tau}_{(w)}}{\rho g h J_f} = \dfrac{1}{2}\psi \end{cases}, \qquad (2\text{-}8)$$

where h is the flow depth, b is the width of the channel bed, β is the angle between the sidewall and the water surface, and ψ is the ratio of the EDC of the lateral wall to the EDC of the bottom $\left(\psi = u_{*(b)}/u_{*(w)}\right)$. Equation ***(2-8)*** is applicable and valid under the following conditions:

$$\begin{cases} \frac{b}{h} \geq 2\frac{1-\cos\beta}{\sin\beta} \\ (1-\psi\cos\beta) \leq 0 \end{cases}. \qquad (2\text{-}9)$$

The conditions of Eq. ***(2-9)*** regarding the applicability of Eq. ***(2-8)*** involve the case where the intersection of the dividing lines is located above the water surface in

wide channels. In those cases where the dividing lines are located below the water surface in narrow and deep channels, the average stress at the limits is given by Eq.***(2-10)***.

$$\begin{cases} \frac{\bar{\tau}_{(b)}}{\rho g h J_f} = \frac{b}{4h}\xi \\ \frac{\bar{\tau}_{(w)}}{\rho g h J_f} = \frac{b}{4h\psi^2}\xi \end{cases}, \qquad (2\text{-}10)$$

where ξ is the slope of the dividing line, which is defined as $\xi = \frac{\sin\beta}{\psi - \cos\beta}$. Similarly, for wide channels, Eq. ***(2-10)*** is only valid if

$$\begin{cases} \frac{b}{h} \leq 2\frac{1-\cos\beta}{\sin\beta} \\ (1 - \psi\cos\beta) \leq 0 \end{cases}. \qquad (2\text{-}11)$$

Thus, for channels having a rough and homogeneous trapezoidal section, the local bed and sidewall average stresses are obtained using Eqs. ***(2-8)*** and ***(2-10)***, with $\psi = 1$, assuming that the dividing lines are the bisectors of the internal base angles of the trapezoid.

- **Guo and Julien method** (Guo et Julien 2005)

Guo and Julien present a formula for determining the average shear stress of the bed and sidewalls within a smooth rectangular open channel. The method uses conformal mapping, assuming in a first approximation a constant vortex viscosity without considering the effect of secondary currents. In a second approximation, they use two grouped empirical correction factors for the effects of secondary

currents, the variable viscosity of the vortices, and other possible effects to calculate the shear stresses (Eq.***(2-12)***).

$$\begin{cases} \frac{\bar{\tau}_{(b)}}{\rho g h J_f} = \frac{4}{\pi}\mathrm{Arctg}\left[\exp\left(\frac{-\pi h}{b}\right)\right] + \frac{4}{\pi}\frac{h}{b}\exp\left(\frac{-h}{b}\right) \\ \frac{\bar{\tau}_{(w)}}{\rho g h J_f} = \frac{b}{2h}\left(1 - \frac{\bar{\tau}_{(b)}}{\rho g h J_f}\right) \end{cases} . \qquad (2\text{-}12)$$

- **Method of Seckin et al.** (Seckin *et al.* 2006)

Drawing on the studies by Knight et al., Seckin et al. (2006) use nonlinear regression to develop equations derived from an experimental analysis to obtain the percentage total mean shear force on the base and the smooth walls of the wetted perimeter in terms of the width-to-depth ratio. From the percentages of the shear force ($\%SFw$), Knight et al. (1984) produce equations to determine this average shear stress (Eq.***(2-13)***).

$$\begin{cases} \frac{\bar{\tau}_{(b)}}{\rho g R S_f} = (1 - 0.01\%SFw)\left(1 + \frac{2H}{B}\right) \\ \frac{\bar{\tau}_{(w)}}{\rho g R S_f} = 0.01\%SFw\left(1 + \frac{B}{2H}\right) \end{cases} , \qquad (2\text{-}13)$$

where R is the hydraulic radius, S_f is the energy gradient, B is the width of the channel, H is the channel depth, and $\%SFw$ is the percentage of the shear force acting on the walls along a unit of channel length, determined by Eq.***(2-14)***.

$$\begin{cases} \log(\%SFw) = -1.4026\log(B/H + 3) + 2.6692 \\ \text{or} \\ SFw = \exp(\alpha), in\ which\ \alpha = -3.23\log(B/H + 3) + 6.146 \end{cases} . \qquad (2\text{-}14)$$

Reanalyzing the Knight et al. equations, Seckin et al. (2006) use a shifted power adjustment model to find $\%SFw$. They then use various function models to estimate the average wall and bed shear stress of a channel. Seckin et al. (2006) apply a rational function model to determine the average bed shear stress, $\bar{\tau}_{(b)}$, and a logistic model to determine the average wall shear stress $\bar{\tau}_{(w)}$. The developed respective equations are

$$\begin{cases} \dfrac{\bar{\tau}_{(b)}}{\rho g R S_f} = \dfrac{a + b(B/H)}{1 + c(B/H) + d(B/H)^2}, \\ where\ a = 0.946, b = 0.117, c = 0.088\ and\ d = 0.0011 \\ \dfrac{\bar{\tau}_{(w)}}{\rho g R S_f} = \dfrac{a}{1 + b\exp[-c(B/H)]}, \\ where\ a = 0.011, b = -0.989\ and\ c = 0.00034 \end{cases}, \qquad (2\text{-}15)$$

where a, b, c, and d represent constants.

- **Severy and Felder method** (Severy et Felder 2017)

By performing flow tests in a smooth rectangular channel, Severy and Felder develop an equation to calculate the average shear stress of a channel from detailed measurements of flow velocity. They use three approaches to compute the boundary shear stress: the logarithmic law within the inner flow region, the velocity defects law in the outer flow region, and the direct-step method. Relying on the equations of Schlichting (1979) and Montes (1998), Severy and Felder develop Eq. ***(2-16)*** as a function of a resistance factor to calculate the local shear stress.

$$\tau_0 = \frac{1}{8} f \rho V^2 \,, \qquad (2\text{-}16)$$

where V is the flow velocity, and f is the Darcy-Weisbach friction factor for gradually varying flows, in this case determined by

$$f = \frac{8.g.S_f.\left(\int_{y=0}^{y=Y_{98}} (1-C)dx\right)^2 \left(\frac{D_H}{4}\right)}{q_w^2} \,, \qquad (2\text{-}17)$$

where S_f is the energy gradient, x is the longitudinal distance in the direction of flow propagation, y is the perpendicular elevation from the channel bed, Y_{98} is the characteristic flow depth, C is the fraction voids in the flow, q_w is the discharge, and D_H is the hydraulic diameter.

In summary, shear stress is a physical measure of the normal force applied to a channel. Shear stress is intrinsically linked to the nature of the velocity profile and indirectly represents many hydraulic characteristics. Pells (Pells 2016a) selected the mean shear stress of the channel as an appropriate indicator of the erosive force of water. Van Schalkwyk (Van Schalkwyk *et al.* 1994) and Pells (Pells 2016a) demonstrated that the amount of observed erosion is well correlated with shear stress. Most researchers hold that the erosion caused by the flow of water in the channel is due to the shear stress exerted by the water at the bottom surface of the flow channel. However, Annandale (Annandale 2006b) showed that this notion is only valid for laminar flow; for turbulent flow, the erosion capacity of water depends on the pressure fluctuations exerted by the water rather than shear stress.

Moreover, shear stress cannot explain all the probable mechanisms of erosion, including erosion by the dynamic expulsion of blocks recessed in a rock mass or erosion by fragile fracture of the rock mass into small pieces because of turbulent flow. In addition, the average shear stress in the flow channel is a hard-to-estimate parameter that can cause considerable uncertainty in estimates of the hydraulic head under differing flow conditions within the spillways (e.g., hydraulic jump). Most equations used to evaluate this parameter (Eqs.***(2-5)*** *to* ***(2-17)***) were developed for narrow, smooth-wall flow channels (e.g., pipes) and then applied analytically to other types of channels. Most of these equations have also been developed using assumptions that do not apply to spillway flow channels, including the homogeneity of the shear stress of the flow channel, the non-inclusion of secondary currents in a flow channel, and the non-differentiation of subcritical and supercritical flows. Finally, these methods are based on different assumptions, which can lead to an approach-dependent shear stress estimate. Their use in the cases of flow channels of spillways is therefore highly questionable.

2.3.2 AVERAGE FLOW VELOCITY IN OPEN CHANNELS

The average flow velocity ($\bar{u}$) can be calculated on a plane that is perpendicular to the flow direction and is given by the shearing movement in a fluid. This movement leads to the continuous dissipation of energy and depends

considerably on the profile of the flow channel surface, the viscosity of the fluid, and the nature of the flow. Various flow resistance coefficients, including the expressions of Darcy-Weisbach, Chézy, and Manning, are to represent the resistance to flow in the calculation of the average flow velocity (Cengel 2014).

First, assuming $\bar{\tau}_0 \propto \bar{u}^2$, Chézy (1769) defined a resistance coefficient to represent the resistance to flow and developed an equation to calculate the average flow velocity as Eq.***(2-18)***.

$$\bar{u} = C\sqrt{R_H.S}; \text{ where } C = \sqrt{\frac{\rho.\mathrm{g}}{K}}, \qquad (2\text{-}18)$$

where $\bar{\tau}_0$ is the shear stress, C is the resistance coefficient of Chézy, $\bar{u}$ is the average cross-sectional flow velocity, and K is a probability coefficient or relative roughness coefficient.

Experiments on fluid flow in pipes led Darcy and Weisbach (1845) to develop a flow resistance coefficient (f) and derive an equation for calculating the average flow velocity on a smooth surface. Subsequently, this index was applied to open-channel flows by replacing the diameter of the pipe with an effective diameter representative of the hydraulic radius of a flow channel. The resulting analytical equation is presented as Eq.***(2-19)***.

$$\bar{u} = \sqrt{\frac{8\mathrm{g}}{f}}\sqrt{R_H.S_f\cos\theta}\,; \text{ where } H_f = f\frac{L}{d_{eff}}\frac{\bar{u}^2}{2\mathrm{g}} = f\frac{L}{R_H}\frac{\bar{u}^2}{8\mathrm{g}}, \qquad (2\text{-}19)$$

where H_f is the energy loss by friction (in m) over a distance L, and d_{eff} is the effective diameter of channel function for the hydraulic radius of the channel ($d_{eff} = 4R_H$).

Moreover, the calculation of the shear stress in a channel can be performed using Darcy's coefficient. Equation ***(2-20)*** was developed for this purpose.

$$\bar{\tau}_b = \rho.\bar{u}^2 \frac{fL}{H_f 8} \frac{H_f}{L.\cos\theta} \cos\theta \implies \bar{\tau}_b = \frac{f}{8}\rho.\bar{u}^2 . \qquad (2\text{-}20)$$

Manning (1890) calculated the average velocity of a uniform flow from a channel with a flow resistance coefficient of n via Eq.***(2-21)***. It is noted that the Manning coefficient (n) depends not only on the shape and roughness of the channel but also on the nature of the flow itself. Hence, this parameter is generally an approximation in calculations, and the known values are specific to river systems.

$$\bar{u} = \frac{1}{n} {R_H}^{2/3} S^{1/2}; \text{ where } n = \frac{{R_H}^{1/6}}{C} = {R_H}^{1/6} \sqrt{\frac{f}{8g}} . \qquad (2\text{-}21)$$

In addition to equations ***(2-19)***, ***(2-20)***, and ***(2-21)***, other equations exist for relating flow velocity to the coefficient of resistance to flow. Knowing that flow resistance is influenced by various parameters, including the shape of the cross section, the non-uniformity of the limits of the flow channel, and the instability of the flow—in addition to the viscosity and the roughness of the walls of a flow channel—flow resistance can be classified into four components: surface or skin

friction, form resistance, wave resistance from free surface distortion, and the resistance associated with local acceleration or flow unsteadiness (Yen 2002). When the Weisbach coefficient of resistance (*f*) is applied, flow resistance can be expressed as:

$$f = F\ (Re, K,\ \eta_0, N, Fr, U)\ , \qquad (2\text{-}22)$$

where F represents a function, Re is the Reynolds number, K is the relative roughness coefficient (usually expressed as k_s/R, where k_s is the equivalent wall surface roughness and R is the hydraulic radius of the flow), η_0 is the cross-sectional geometric shape, N is the non-uniformity of the channel in both profile and plan, Fr is the Froude number, and U is the degree of flow unsteadiness. The parameters of this equation are independent, and the four resistance components (surface, form, wave, and unsteadiness) interact nonlinearly so that any linear separation and combination are artificial.

The internal and external laws of the boundary layer theory are used to explain some components of flow resistance and better define the flow resistance with respect to these parameters. The theory of the boundary layer refers to a zone in a flowing fluid where the viscous effects are as important as the effects of inertia in terms of magnitude. Within this layer, the tangential velocity with respect to the wall changes very quickly, having no velocity at the wall and a greater-than-zero

velocity outside this layer. Thus, the boundary layer represents the interface zone between a body and a surrounding fluid.

According to this theory, the distribution of the velocity (u) along the normal direction (y) to the wall is correctly described by the internal law (or the law of the wall) where the viscous effect dominates and the external law (or velocity defects low) (Rouse 1965; Schlichting 1979). The expressions defined by these laws are

$$\frac{u}{u_*} = F(y^*, k^*) \text{ where: } y^* = \frac{u^* y}{\nu} \text{ , and} \qquad (2\text{-}23)$$

$$\frac{U-u}{u_*} = F\left(\frac{y}{\delta}, H_s\right), \qquad (2\text{-}24)$$

where u_* is the shear velocity (Eq.***(2-3)***), k^* is the Von Karman's constant, y^* is a constant equal to $u^* y/\nu$, ν is the kinematic viscosity of the fluid, U is the free stream velocity at the far end of the outer law, and δ is the boundary layer thickness. H_s is often called a shape factor, a nondimensional parameter associated with the pressure gradient and Reynolds number, and it is usually expressed as the ratio between the displacement and momentum thicknesses of the boundary layer.

Knowing that the inner and outer laws are not mutually exclusive, there is a region of overlap between the lower limit of the outer law and the upper limit of the inner law (Figure 2-7). To characterize this transition zone, researchers have developed equations to satisfy both laws. Rouse (1959) presented a logarithmic function that applies to the laws (Eqs. ***(2-23)*** and ***(2-24)***), and the power-law

distribution of Chen (1991) is also used (Yen 2002). These equations are presented respectively in Eqs. *(2-25)* and ***(2-26)***. More information on the logarithmic function and power-law distribution can be found in of Nezu et al (Nezu et Rodi 1986).

$$\frac{u}{u_*} = c_1 \log y^* + c_2 \text{ , and} \qquad (2\text{-}25)$$

$$\frac{u}{u_*} = c_3 (y^*)^m \text{ ,} \qquad (2\text{-}26)$$

where c_1, c_2, and c_3 are constants for a given channel. From these equations, the open-channel resistance can be derived and extended from the resistance of a uniform flow in a circular rigid pipe.

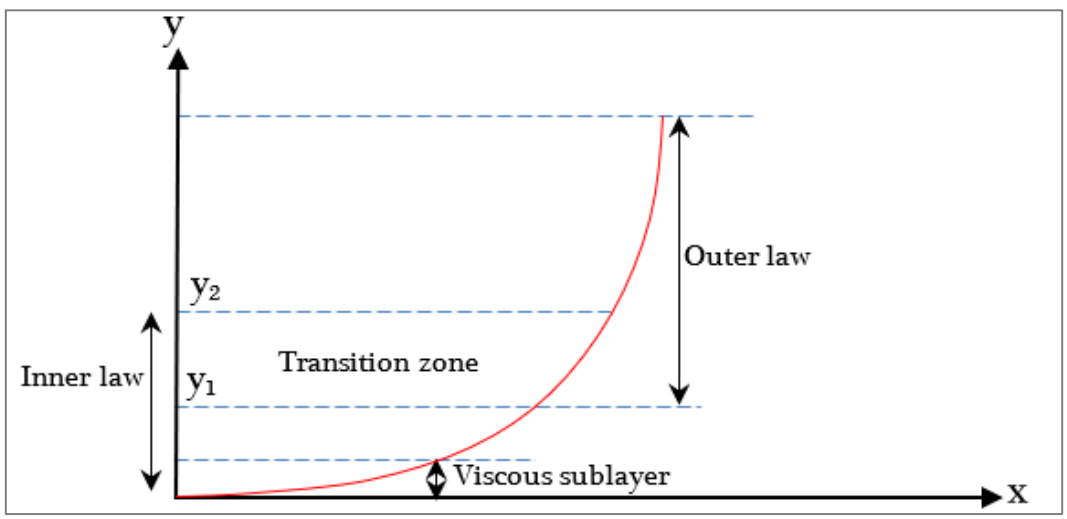

Figure 2-7. Regions of the inner and outer laws of the boundary layer (Yen 1991)

The closest open channel counterpart of a circular pipe (besides a half circle) is the two-dimensional (2D) wide channel. With the shape factor held constant for 2D wide channels or circular pipes, Eqs.***(2-23)*** and ***(2-24)*** imply that, referring to Eq.***(2-22)***, the resistance to a steady uniform flow is solely a function of the

Reynolds number Re and the relative roughness $K = k_s/R$, provided that the Froude number is not high and its effect is negligible. Hence, the resistance factors become

$$f, \frac{n}{R^{1/6}}, \frac{C}{\sqrt{g}}, = F\left(Re, \frac{k_s}{R}\right), \qquad (2\text{-}27)$$

where k_s is the equivalent wall surface roughness, and R is the hydraulic radius.

From Eq.**(2-27)**, various resistance coefficients in the form of Darcy-Weisbach can be derived, depending on Re.

- For a uniform and regular laminar flow with a $Re < 500$, the resistance factor is obtained as

$$f = K_L/Re\ , \qquad (2\text{-}28)$$

  where $K_L = 24$ for wide channels and $K_L = 16$ for circular pipes.

- For $700 < Re < 25000$, the resistance factor for a smooth pipe (and often used as an approximation for wide channels) is

$$f = 0.224/Re^{0.25}\ . \qquad (2\text{-}29)$$

- For $Re > 25000$, the resistance factor becomes

$$\frac{1}{\sqrt{f}} = -K_1 \log\left(\frac{k_s}{K_2 R} + \frac{K_3}{4Re\sqrt{f}}\right)\ , \qquad (2\text{-}30)$$

where K_1, K_2, and K_3 represent Colebrook-White coefficients for a regular uniform flow in open channels with a rigid impermeable limit (Yen 2002). These Colebrook-White coefficients are implicit in the determination of *f*. To overcome this

drawback, Churchill and Bray (Churchill 1973; Bray 1979) assumed full flow in a pipe to then propose an equation for calculating the flow resistance as

$$f = \frac{1}{4}\left[-\log\left(\frac{k_s}{14.8R}\right) + \frac{5.76}{(4R_e)^{0,9}}\right]^{-2}. \qquad (2\text{-}31)$$

From Eq.***(2-31)***, Yen (1991) suggested a formula to calculate the flow resistance for large open channels having a $Re > 3000$ and a $k_s/R < 0.05$ (Yen 2002):

$$f = \frac{1}{4}\left[-\log\left(\frac{k_s}{12R}\right) + \frac{1.95}{{R_e}^{0,9}}\right]^{-2}. \qquad (2\text{-}32)$$

For Eqs.***(2-27)***–***(2-32)***, flow resistance is determined in terms of limit shear, that is, from the perspective of the relationship between force and momentum. This concept determines the flow resistance of open channels in terms of the slope of the impulse resistance along a channel for a channel cross section. However, other work has shown that resistance to flow can also be examined from the concept of energy in terms of the energy loss when a fluid moves across a surface, as well as in terms of the energy slope or, more precisely, the gradient of the mean motion of the dissipated energy. Yen and Akan (Yen et Akan 1999) suggest the rather than applying Eq.***(2-28)***, Eq. ***(2-28)*** can be used for the momentum equation of laminar sheet flow under rain-full conditions with an intensity *i*:

$$f_m = \left[24 + 660\left(\frac{i}{\sqrt[3]{\mathrm{gv}}}\right)^{0.4}\right]\frac{1}{Re}. \qquad (2\text{-}33)$$

In summary, Eqs.***(2-19)***, ***(2-20)***, and ***(2-21)*** indicate that the average flow velocity is directly related to the pressure that is applied to the surface of a rock

mass or inside a joint. Therefore, the average flow velocity is a key element for determining the specific forces that are applied to a rock mass. However, the average flow velocity is sensitive to the problem of "non-uniqueness" in the field of hydraulic erosion. Pells (Pells *et al.* 2016b) and Van Schalkwyk (Van Schalkwyk *et al.* 1994) reported that the average velocity could not be used as a representative value in hydraulic hazard parameters for erosion prediction. Moreover, the average flow velocity is proportional to the flow resistance coefficient, which can be defined by knowing the roughness of the flow channels and spatial variation along the flow channel. To specify the flow resistance, the resistance coefficients of Darcy-Weisbach, Chézy, and Manning are used to estimate mean flow velocity. The equations detailed above (Eqs.***(2-28)–(2-33)***) illustrate the diverse means of determining resistance coefficients, and this diversity of approaches can explain the confusion among users and the inconsistencies among the produced values for the resistance coefficients. The application of these flow resistance coefficients in flood spillways also remains uncertain. Indeed, the theory of the boundary layer served as a basis in the development of some resistance coefficients and this theory would be less effective for flow channels with very rough surface. Under the flow conditions considered for rough unlined spillways, the roughness elements may exceed the thickness of the boundary sublayer (fully turbulent flow) and the velocity profile is fully developed, that is, the thickness of the boundary layer is

equal to the depth of the outflow(Pells *et al.* 2016b). According to Yen(Yen 2002), the inner law region (Figure 2-7) below the transition zone is generally thin and it is difficult to measure velocity, especially when the roughness of the wall is large.

The multiple equations established to determine the resistance to flow of a channel fluid represent the derivative and the extent of the resistance of a uniform and constant flow in a rigid circular pipe. These coefficients are approached either from the perspective of impulse resistance (resistance slope) or energy loss (energy movement gradient). These various Darcy-Weisbach, Manning, and Chézy resistance coefficients can be related (Eq.***(2-27)***), and there is no clear theoretical advantage of one coefficient over the other. The C (Chézy) coefficient is, however, the simplest to use, although there is no generally accepted table or figure of C values. The n (Manning) coefficient has the advantage of being nearly constant and almost independent of flow depth, Reynolds number, or k_s/R for fully developed turbulent flow on a rigid and rough surface (Yen 2002). Determining the resistance coefficient values by Manning, obtained from field data, relies on the head loss energy concept applied to channel reaches. The f (Darcy-Weisbach) coefficient has the advantage of being directly linked to the development of fluid mechanics, and there are known values for this coefficient, the most reliable source for the values of f being the Moody diagram. Generally, f is regarded as a point value related to the velocity distribution, although some hydraulic engineers extend it to cross-

sections or reach values and consider it as an energy loss coefficient. Thus, it appears appropriate to refer to the Darcy-Weisbach *f* for point resistance, whereas Manning's *n* can serve for cross-sectional and reach resistance coefficients. Previous field experiments suggest that *n* is a simpler coefficient when accounting for the effects of other parameters beyond the Reynolds number and relative roughness, as well as from a fluid mechanics perspective. A drawback of Manning's formula is that it is dimensionally non-homogeneous (Yen 2002).

In general, these flow resistance coefficients are not representative of the roughness of a flow channel of a spillway; for example, the Darcy-Weisbach coefficient was specifically developed for pipes having a smooth surface and was then analytically modified for use in open-channel flows. Manning's coefficient is more applicable to river systems; however, the roughness values of an uncoated channel of high-speed spillways is generally greater than those estimated from river systems. Moreover, in practice, the resistance varies among points, in particular along the flow channels of the spillway, whereas the resistance coefficient for a cross section or a range of channels is a spatially weighted average of local resistance. Yen (Yen 2002) concludes that despite the success of resistance coefficients in presenting complex physical processes in flows, much remains to be studied, including the effects of channel geometry and flow instability on resistance to the flow.

2.3.3 APPLIED STRESSES INSIDE JOINTS AND THE BLOCK LIFTING FORCE

Bollaert estimated the hydraulic load on the rock mass by considering the hydrodynamic tensile load of the joints, represented by the stress intensity factors in the various erosion mechanisms (Bollaert et Schleiss 2002; Bollaert 2004; Bollaert et Schleiss 2005; Bollaert 2010). First, erosion is defined as resulting from instantaneous brittle fracture (hydrofracturing), where the hydraulic head is defined by a stress factor ($\boldsymbol{K_I}$). This index represents the stress induced by the water pressure inside the joints and, hence, the brittle fracturing occurs when the intensity of the stress in the joints, owing to fluctuating pressure, is greater than the resistance of the rock mass (Figure 2-2). The semi-analytical index developed by Bollaert is presented in Eq.***(2-34)***.

$$K_I = 0.8.P_{max}.F.\sqrt{\pi.L_f}\,, \qquad (2\text{-}34)$$

where $0.8.P_{max}$ represents 80% of the maximum instantaneous dynamic pressure in the diving tank, F is the correction factor, which depends on the types of cracks when it is persistent, and L_f is the total length of a joint.

In cases where brittle fracture is not likely, another mechanism dominates, i.e., fatigue erosion or the progressive hydrofracturing of a rock mass. If the intensity of the stresses in the joints does not exceed the fracture toughness of the rock mass, the existence of a continuous fluctuating pressure in the joints can

ultimately lead to the failure of the rock because of fatigue (Figure 2-3). In this context, Bollaert considered the hydraulic head via a stress intensity amplitude factor (ΔK_I), which corresponds to the difference in intensity of maximum and minimum stresses inside a joint or, in a rough estimation, could be considered equal to 40% of K_I.

In a fractured rock mass characterized by a system of joint sets that form a block assembly, erosion occurs by the dynamic expulsion of the blocks through water pressure as a lifting force. Bollaert (Bollaert et Schleiss 2002; Bollaert 2004; Bollaert et Schleiss 2005; Bollaert 2010) estimated this load by considering the essential lifting force of the individual block. This lifting force can be expressed as a dynamic impulse index that is obtained by the temporal integration of the net forces applied to a block. These forces include the force applied on top of the block (F_o), the lifting force beneath the block (F_u), the submerged weight of the block (G_b), and the friction along the sides of the block (F_{sh}) (Figure 2-1). The equation developed to define the lifting force of an individual block is presented in Eq. ***(2-35)***.

$$I = \int_0^{\Delta tpulse} (F_u - F_o - G_b - F_{sh}).dt = m.V_{\Delta tpulse}\ , \qquad (2\text{-}35)$$

where $V_{\Delta tpulse}$ is the velocity of the fluid in the joint, and m is the mass of the rock block.

In summary, the Bollaert index (Bollaert et Schleiss 2002; Bollaert 2004; Bollaert et Schleiss 2005; Bollaert 2010) defining the erosive force of water on a rock mass illustrates effectively the three mechanisms of erosion and the importance of the pressure dynamics in hydraulic erosion. These indices (K_I and I) illustrate the erosive force of water, as they are developed on the basis of various erosion mechanisms of a fractured rock mass. To correctly apply these indices, however, some considerations must be addressed. First, these indices are not applicable to other flow modes at spillways; for example, they do not apply to parallel flow along the bottom of the channel and hydraulic jumps. Moreover, the first two factors depend mainly on the maximum instantaneous dynamic pressure (P_{max}). This pressure depends in turn on the average velocity of the jet at the impact point (V_j) and the dynamic pressure coefficient. The latter coefficient is obtained by multiplying the quadratic mean pressure coefficient (C'_{pa}) by a pressure amplification factor in the joints (Γ^+) and then adding a mean dynamic pressure coefficient (C_{pa}). The expression developed to calculate the instantaneous dynamic pressure is presented in Eq.***(2-36)***.

$$P_{max} = 10^{-6}\rho.\left(C_{pa} + \Gamma^+.C'_{pa}\right).\frac{V_j^2}{2\mathrm{g}}, \qquad (2\text{-}36)$$

where the parameters C_{pa} *and* C'_{pa} depend on the toughness of the rock mass and are obtained experimentally. Nonetheless, the toughness of the rock mass is an irrelevant criterion for the erosion of fractured rocks, and no setup can determine

the toughness of a rock (Annandale 2006b). The parameter L_f in Eq. ***(2-34)*** represents the total length of a single joint. However, from the field data obtained by Pells (Pells 2016a), this parameter does not adequately represent the geometry of an entire erosion zone because it is determined using a reduced physical model that is not representative of a fractured rock mass.

The second index developed by Bollaert, the lifting force of a block, also includes some nuances as to its reliability for estimating the erosive force of water. The first is that the index does not consider the shear strength along the sides of the blocks (F_{sh}). Moreover, according to Figure 2-1, the net lifting force of a block also depends on the joint openings. As the openings become larger, the amount of water seeping into the joints increases, which directly influences the pressure below the blocks. Therefore, this index of dynamic block uplift once again ignores an important parameter contributing to the resistance of a block to erosion. Furthermore, the indices developed by Bollaert (Bollaert et Schleiss 2002; Bollaert 2004; Bollaert et Schleiss 2005; Bollaert 2010) apply only to plunging jets, and, hence, these indices are not applicable to other flow conditions. As a result, they must be improved to not only determine the erosive hydraulic force of the plunging jets for which they have been developed but also for their application to other flow modes.

2.3.4 INDICES OF ENERGY DISSIPATION

The dissipation of energy in spillways depends mainly on the flow condition, which is primarily a function of spillway shape. Therefore, hydraulic powers should vary among flow conditions. Several authors have thus developed expressions to calculate the dissipation of energy in relation to the variation of the total energy gradient $\left(\frac{dE}{dx}\right)$ to define the erosive force of water within spillways. Van Schalkwyk (Van Schalkwyk *et al.* 1994) evaluated the energy dissipation for plunging flows. Annandale (Annandale 1995) attempted to develop an expression for estimating the energy gradient for calculating energy dissipation in plunging jets, hydraulic jumps, and knickpoint flows. Similarly, Pells (Pells 2016a) developed expressions to determine the variation of the hydraulic gradient for plunging jets and hydraulic jumps.

Van Schalkwyk (Van Schalkwyk *et al.* 1994) used the ratio between the total power of flow (T) and the surface on which it is dissipated (A) to estimate the energy dissipation, following Eq.***(2-37)***.

$$P = \frac{T}{A}, \text{where } T = \rho g Q \,, \qquad (2\text{-}37)$$

where Q is the water flow rate, and H is the total head.

Equation *(2-37)* was then applied to different flow modes observed at spillways to estimate the energy dissipation of each. Accordingly, energy

dissipation for an inclined channel was calculated on the basis of the power loss over a distance. The energy released owing to variations of the total head corresponds to the slope of the hydraulic gradient, and the produced equation is presented in Eq.***(2-38)***.

$$P = \rho g q S, \text{where } S = \frac{dH}{dx} \text{ and } \frac{dT}{dx} = \rho g Q S\,, \qquad (2\text{-}38)$$

where q is the flow rate per unit length of channel width ($q = Q/B_f$), and B_f is the channel width.

Van Schalkwyk (Van Schalkwyk *et al.* 1994) then reformulated Eq.***(2-37)*** to calculate energy dissipation for a plunging flow by selecting a coefficient of 3 as the energy gradient for the plunging jet. Equation ***(2-39)*** presents the modified Eq.***(2-37)*** for calculating the energy dissipation at a plunging flow.

$$P = 3gq\,. \qquad (2\text{-}39)$$

Equations ***(2-38)*** and ***(2-39)***, developed by Van Schalkwyk, are only applicable to inclined uniform flow and plunging jets; however, some considerations should be noted. For example, the flow within the inclined flow channels of spillways is not uniform; and using a coefficient of 3 as the energy gradient for a plunging jet needs to be evaluated further, as the energy gradient of a plunging jet is highly variable. These equations are therefore not sufficiently comprehensive to evaluate the erosive force of water within spillways.

Annandale (Annandale 1995) also proposed equations for calculating the erosive force of water within spillways. When the density of water, the unit flow rate, and the energy loss of a flow are accounted for, the resulting equation is

$$P = \gamma . q . \Delta E \,, \qquad (2\text{-}40)$$

where ΔE is the energy loss depending on the type of flow, and q is the specific discharge rate equal to the flow rate divided by channel width. Considering a flow channel with a length (w) and depth of water (d) that is measured perpendicular to the flow direction, the unit discharge rate is calculated using Eq.***(2-41)***.

$$q = \frac{Q}{w} = \frac{\bar{u} \times A}{w} = \frac{\bar{u}.w.d}{w} = \bar{u}.d \,. \qquad (2\text{-}41)$$

From Eq.***(2-40)***, Annandale (Annandale 1995) developed several equations to estimate the erosive hazard parameter for various flow modes at spillways, including for lunging jets, hydraulic jumps, and knickpoint flows.

In regard to plunging jets, Figure 2-8 shows the characteristic parameters considered by Annandale, where energy loss (ΔE) is calculated as a function of specific discharges (q_1 *and* q_3). From this, Annandale (Annandale 1995) developed Eqs.*(2-42)* and ***(2-43)*** to determine the energy dissipation for a plunging jet (Figure 2-8).

$$P = \gamma . q . y_c . \left(\frac{\Delta z}{y_c} + \frac{3}{2} - \frac{y_l}{y_c} - \frac{1}{4}\left(\frac{3}{2} + \frac{\Delta z}{y_c}\right)\left(1 + \frac{1.06}{\sqrt{\frac{\Delta z}{y_c} + \frac{3}{2}}}\right)^2 \right) \text{ (depends on } q_1\text{)}, \qquad (2\text{-}42)$$

$$P = \gamma . q . \frac{v^2}{8g}\left(1 + \frac{1.06}{\sqrt{\frac{\Delta z}{y_c} + \frac{3}{2}}}\right)^2 \text{ (depends on } q_3\text{)}, \qquad (2\text{-}43)$$

where y_c is the critical depth of the jet, Δz is the height of the spillway, v is the average flow velocity, and y_l is the downstream flow depth.

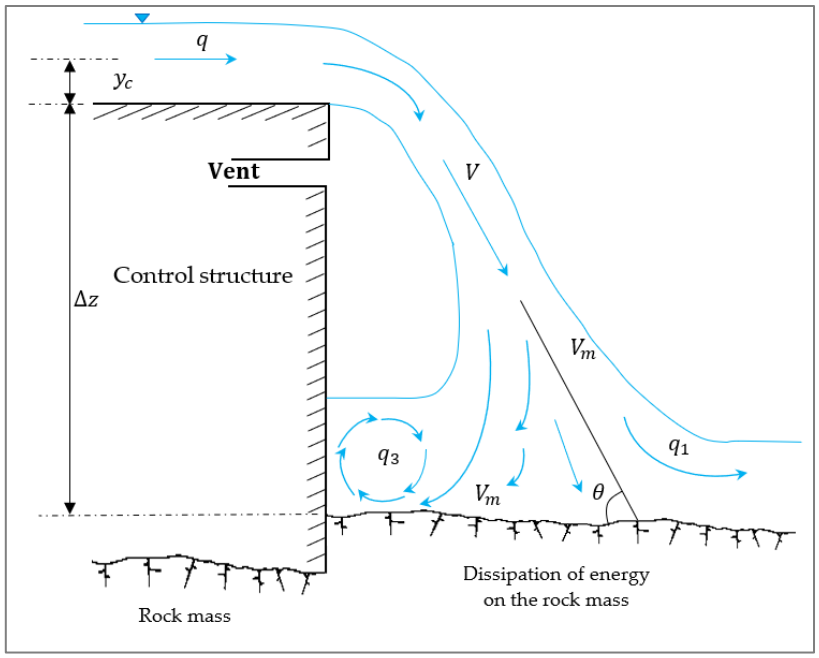

Figure 2-8. Schematic representation of a plunging flow according to Annandale (Annandale 1995)

For a fluid flowing as a hydraulic jump, the significant parameters considered by Annandale for this type of flow are represented in Figure 2-9, and the relevant equation is presented in Eq.***(2-44)***.

$$P = \gamma . q\left(y_l + \frac{q^2}{2gy_l^2} - \frac{y_l}{2}\left(\sqrt{1 + 8F_{r1}^{\ 2}} - 1\right) - \frac{q^2}{2g} - \frac{4}{y_l^2\left(\sqrt{1+8F_{r1}^2} - 1\right)^2}\right). \qquad (2\text{-}44)$$

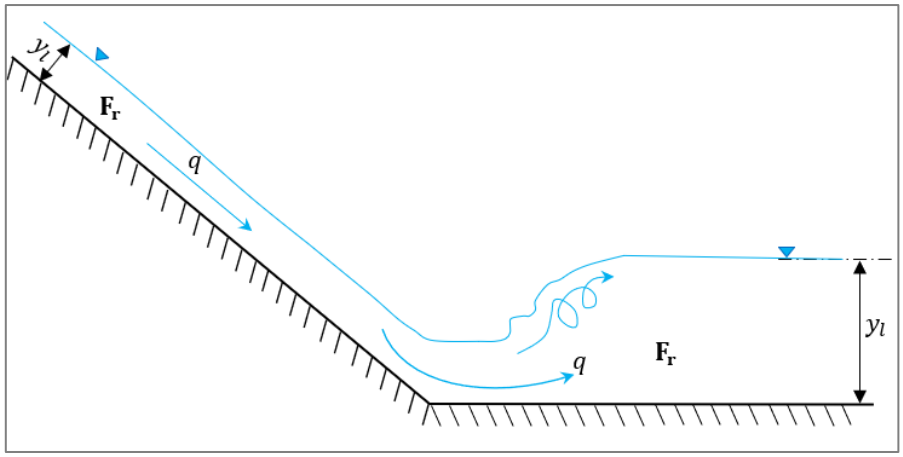

Figure 2-9. Flow conditions of a hydraulic jump (Annandale 1995)

According to Annandale (Annandale 1995), the maximum dissipation of a knickpoint flow occurs at the point where the angle of the flow channel changes from a low to a steep angle (Figure 2-10). Equation ***(2-45)*** is subsequently used to estimate the energy dissipation for a knickpoint flow.

$$P = \gamma . q \left(\frac{1+\cos(\theta-\alpha)}{1-\cos(\theta-\alpha)} K_l \left(\frac{v_g^2}{2g} \right) + S_f . L \right), \qquad (2\text{-}45)$$

where K_l is a probability coefficient estimated at 1 (on the pretense that it provides consistent results), θ is the angle approximated by superimposing the theoretical ogee shape onto the channel bed geometry, and α is the slope angle of the channel.

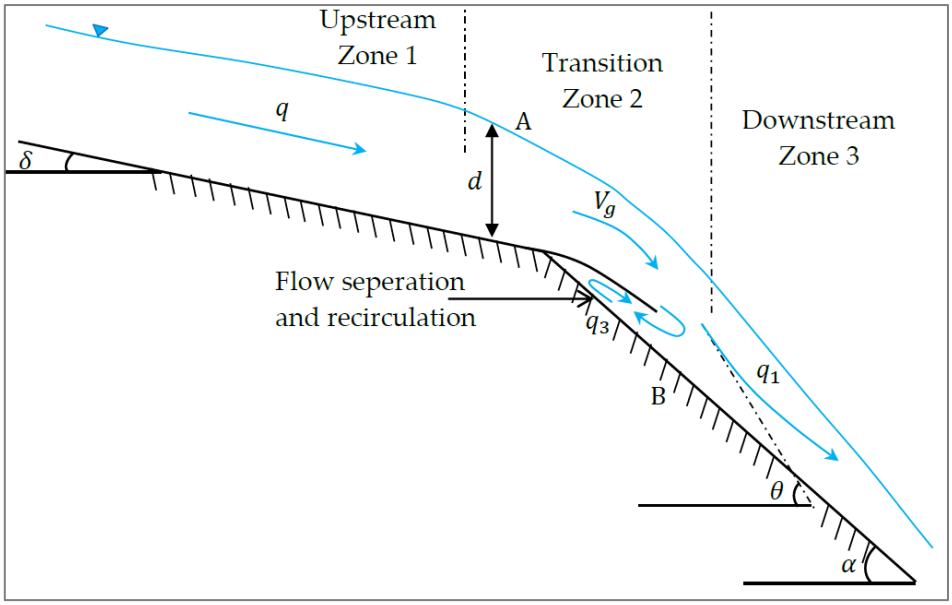

Figure 2-10. Schematic of a knickpoint flow (Annandale 1995)

The equations used by Annandale (Annandale 1995) to estimate the energy dissipation for various flow modes lack clarity and detail and have thus been criticized; for example, Pells (Pells 2016a) points out that the Annandale equation ignores the hydraulic jump length (Δx) in the definition of flow dissipation (i.e., the expression is $\rho g q \Delta E$ rather than the correct form $\rho g q \frac{\Delta E}{\Delta x}$). This issue was modified by Annandale (Annandale 2006b) by using $\Delta x = 1$ m and mentioning that this value provides a conservative estimate in the absence of effective data. Henderson (Henderson 1966) demonstrated that the length of dissipation is a significant parameter at $\Delta x = 6y_2$ (y_2 is the height of the water downstream of the flow channel), where the Froude number lies in the $4.5 < \mathrm{F_r} < 13$ range. Moreover, for the specific discharge rate between 1 and 50 $m^2\ s^{-1}$, Annandale's analytical solution overestimates the unit energy dissipation (Pells 2016a). This dissipation

length is also ignored in the analytical solution of the unit power dissipation of a knickpoint flow condition and downstream of a jet. Finally, the equation provided by Annandale (Annandale 1995) for calculating the energy dissipation of the back roller (Eq.*(2-43)*) disregards the length of the energy dissipation. These criticisms therefore discourage the use of the Annandale equations in this context.

Pells (Pells 2016a) developed Eq. ***(2-46)*** to calculate the erosive force of water in the flow channel of the spillways.

$$\Pi = \rho g Q \left(\frac{P_r}{\rho g} + \frac{\bar{u}^2}{2g} \right), \qquad (2\text{-}46)$$

where P_r is the water pressure, and ρ is the density of water.

The dissipation of the fluid energy represents the velocity at which the power is expended, corresponding to the flux gradient. Hence, by multiplying the slope of the total energy line by $\rho g Q$, a simplified form of the energy dissipation equation is presented in Eq.***(2-47)***.

$$\Pi_{UD} = \rho . g . q \frac{dE}{dx} . \qquad (2\text{-}47)$$

From Eq.***(2-47)***, Pells (Pells 2016a) developed equations related to the various flow modes found in spillways. Figure 2-11 illustrates the different parameters that are considered in plunging flow. From these parameters, the estimation of the energy loss in plunging flows over distance (between points 1 and 4 of Figure 2-11) is presented in Eq.***(2-48)***.

$$\Delta E = z_1 + y_1\left(\frac{3}{2} - \frac{2}{\sqrt{2}\alpha+\frac{3}{2}} - \frac{\left(\sqrt{2}\alpha+\frac{3}{2}\right)^2}{8}\right), \qquad (2\text{-}48)$$

where z_1 is the height of the spillway, y_1 is the height of the water from the surface of the discharge point, and α is a coefficient depending on z_1 and y_1 $\left(\alpha = \sqrt{\frac{3}{2} + \frac{z_1}{y_1}}\right)$.

By combining Eq.***(2-48)*** and Eq.***(2-47)***, Pells (Pells 2016a) proposed an equation (Eq.***(2-49)***) to calculate the energy dissipation for a plunging flow.

$$\Pi_{UD} = \rho.\mathrm{g}.q_1\frac{dE}{dx} = \frac{\rho.\mathrm{g}.q_1}{\sqrt{2z_1y_1}}\left[z_1 + y_1\left(\frac{3}{2} - \frac{2}{\sqrt{2}\alpha+\frac{3}{2}} - \frac{\left(\sqrt{2}\alpha+\frac{3}{2}\right)^2}{8}\right)\right]. \qquad (2\text{-}49)$$

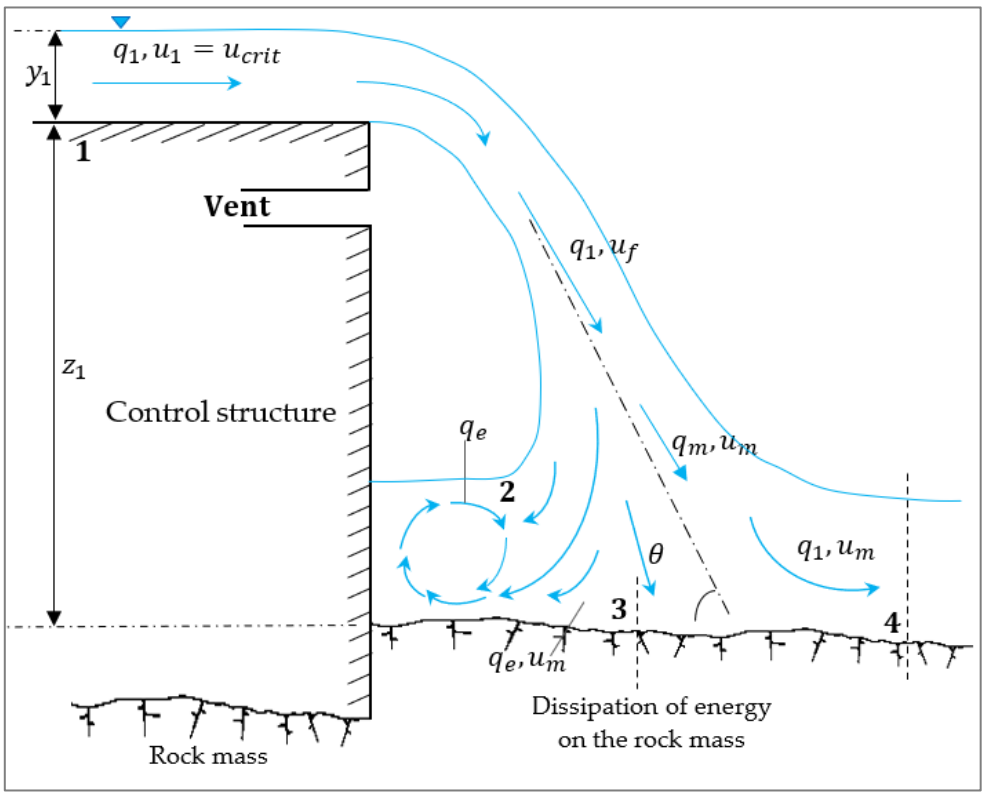

Figure 2-11. Schematic of a plunging flow according to Pells (Pells 2016a)

Subsequently, Pells (Pells 2016a) estimated the energy dissipation for a hydraulic jump flow, a flow characterized by an abrupt change in the flow regime.

By knowing the initial velocity and depth, the downstream depth of the flow can be calculated. Thus, it is possible to calculate the variation in velocity and the energy loss between two points (from upstream to downstream). The resulting equation is presented in Eq.*(2-50)*. By combining Eqs.*(2-50)* and ***(2-47)*** and applying a distance about $6y_2$ between points (for $4.5 < F_{r1}^2 < 13$)(Henderson 1966), Eq.***(2-51)*** allows calculating the energy dissipation for a hydraulic jump.

$$\Delta E = y_1 + \frac{q^2}{2gy_1^2} - \frac{y_1}{2}\left(\sqrt{1+8F_{r1}^2} - 1\right) - \frac{4q^2}{2gy_2^2\left(\sqrt{1+8F_{r2}^2}-1\right)^2}, \qquad (2\text{-}50)$$

$$\Pi_{UD} = \frac{\rho.g.q}{6y_2}\left(y_1 + \frac{q^2}{2gy_1^2} - \frac{y_1}{2}\left(\sqrt{1+8F_{r1}^2} - 1\right) - \frac{q^2}{2g\left(\frac{y_1}{2}\left(\sqrt{1+8F_{r2}^2}-1\right)\right)^2}\right), \qquad (2\text{-}51)$$

where y_2 is the height of the water downstream of the flow channel.

In summary, the analytical methods for estimating energy dissipation presented by Pells (Pells 2016a) appear to be more reliable than other approaches. Generally, energy dissipation is a widely used index for evaluating the hydraulic erodibility of a rock mass and is used to represent the erosive force of water in most modes of hydraulic erosion assessments. These methods are Π_{UD} vs. *RMEI* (Pells *et al.* 2016b), Π_{UD} vs. *eGSI* (Pells *et al.* 2015), and $P = f(K_h)$ (Moore *et al.* 1994; Van Schalkwyk *et al.* 1994; Annandale 1995; Kirsten *et al.* 2000; Annandale 2006b). This energy dissipation index is used because of its simplicity rather than its effectiveness in representing the erosive force. That is, owing to the absence of a

reliable index and the complexity of estimating the actual erosive force of water within a spillway, energy dissipation is used as a simple indicator of erosive hydraulic force. According to Pells (Pells 2016a), the use of energy dissipation by itself is common, although it does not present all the complexities of the erosion process; an infinite number of combinations of spillway geometry and flow modes can be potentially associated with a given measure of energy dissipation. Moreover, a direct interpretation of energy dissipation infers that it is not a direct measurement of erosive capacity but rather represents energy loss linked to the conservation of heat and not to the work performed. It is thus evident that there exists the need to develop an improved index for calculating the erosive force of water to assess the erosion of a fractured rock mass.

2.4 DISCUSSION

The indices reviewed in this paper were developed to represent the erosive force or hazard parameter of water for the purpose of determining rock erosion in the spillways of hydroelectric projects. The previous sections exhaustively discuss the advantages and disadvantages of each method for estimating the erosive force of water.

The non-representativeness of average velocity ($\bar{u}$) is linked to its sensitivity to the problem of "non-uniqueness" in the realm of hydraulic erosion. In short, the

average shear stress at the surface of the flow channel ($\bar{\tau}_b$) is designated as being representative of the hazard parameter of the water within the spillways. However, shear stress cannot explain all possible erosion mechanisms within the spillways, e.g., erosion via the dynamic removal of blocks or erosion by the brittle fracture of large blocks into smaller blocks. This inability to fully explain the erosion mechanisms and the difficulty of estimating shear stress are among the limitations when using this factor to calculate the erosive force of the water. Energy dissipation as an erosive force does not include all the complexities of the erosion process and is used to calculate the erosive hazard parameter of water mainly because it is simple to determine, not because of its representativeness.

In regard to the semi-analytical solutions of Bollaert (Bollaert et Schleiss 2002; Bollaert 2004; Bollaert et Schleiss 2005; Bollaert 2010), they can be used for estimating the erosive force of water as they better explain the principles behind the different mechanisms of hydraulic erosion of rock mass; however, there are some criticisms of these indices. The first index, developed on the basis of the stress applied to joints (K_I), includes parameters that are difficult to determine for a rock mass. Among them, L_f (the total length and shape of the joints) is not representative, as it was developed using a scale model that is not representative of the fractured zone of a rock mass. In addition, uncertainty is associated with the determination of the empirical variables, including C_{pa}, C'_{pa}, and Γ^+. The second

index, the dynamic impulse of the blocks (I_{impuls}), also disregards some important parameters that influence the accuracy of the model, such as the shear strength (F_{sh}) along the block sides. Another essential parameter for estimating the lifting force of a block (see Figure 2-1) is the opening of the joints, a parameter directly influencing the pressure below the blocks, the latter an important parameter neglected by the lifting force of the blocks. Generally, the most important parameter for estimating the Bollaert indices is the maximum dynamic pressures or the peak pressures applied within joints. However, Pells (Pells 2016a) mentions that the pressure fluctuation follows a Gaussian distribution; thus, no pressure peak is observed in the joints. Thus, these indices are only applicable to plunging flows, and modifying the existing indices becomes essential.

Our review found that the main shared factor related to the indices used to represent the erosive force is the pressure applied to the discontinuities of the rock mass. Among all the mechanisms controlling hydraulic erosion, erosion by dynamic block removal appears to be the most common erosion mechanism of fractured rock masses, as evidenced by several cases of erosion observed at the flow channels of spillways around the world. These cases of erosion by removal of the blocks mainly concern the spillways with inclined flow channels. Figure 2-12 shows in detail the mechanism of erosion by removal of the blocks in the inclined flow channels of the spillways. This remark therefore emphasizes that different

flow modes within spillways share similar dynamics of erosion; hence, the dynamic expulsion index of the blocks seems more suitable than the other indices to represent the erosive force of water. Nonetheless, the dynamic expulsion index must be improved, as it neglects important parameters, including shear strength and joint opening. Moreover, this index is only applicable to plunging flows.

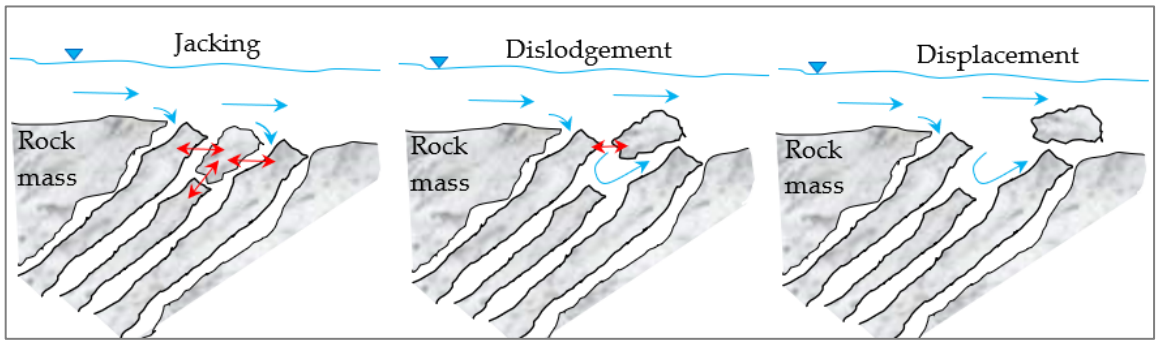

Figure 2-12. The block removal erosion mechanism for flow parallel to the bottom of the flow channel (modified from Annandale (Annandale 1995))

The dynamic expulsion index should be modified to determine the erosive force of water for the various flow modes occurring in spillways. This includes flows on inclined channels, hydraulic jumps, and knickpoints. The mechanism of rock mass erosion in relation to these flow modes is defined using parameters such as the pressure above and under the block, the submerged weight of the block, the opening of the joints, the arrangement of the joints with respect to the direction of flow, and the shear forces along the sides of the block. In this regard, the critical unanswered questions include determining the uplift pressure in the joint as a function of the parameters of the joint and identifying the influence of or the

interaction between the pressure and joint geomechanical parameters, including the joint profile, opening, and roughness of the joint surface. Other relevant parameters are the effect of the submerged weight of the blocks and the surface profile of the open channels on this erosive hydraulic force (the pressure). Future studies should include the characterization of the dynamic pressure variation applied to the discontinuities of the rock mass to reduce these uncertainties.

2.5 CONCLUSION AND FUTURE RESEARCH DIRECTIONS

This paper identifies the most important parameters affecting hydraulic power, such as the instantaneous dynamic pressure for the hydraulic erosion of the rock mass. We also highlight the various geomechanical parameters that can influence this pressure, depending on the various known erosion mechanisms of the rock mass of the spillways. It appears that no index is effective for the moment to represent the erosive force of the water. However some of them can be improved.

Existing and ongoing studies include simulations at the laboratory scale via the use of a physical model of an inclined channel spillway. These models must represent the fractured rock mass as realistically as possible. Instrumentation is also essential to study the pressure changes as a function of the variation in the parameters of the rock mass. This additional information will permit assessing:

- Pressure variation in relation to block shape and size,
- Pressure variation in relation to joint opening,
- Pressure variation in relation to the arrangement of the joints relative to the flowing direction of the water,
- Pressure variation in relation to different flow channel profiles,
- Relative displacement of the blocks as a function of the shear force along the joints affected by pressure.

This experimental setup would help improve our understanding of rock mass erosion and, hence, define the representative indices of hydraulic power and the resistance of the rock mass. This experimental setup would favor developing a reliable method to evaluate hydraulic erosion of fractured rock masses in spillways.

AUTHOR CONTRIBUTIONS: Conceptualization, A.S.K.; methodology, A.S.K, A.S; software, ASK.; validation, A.S.K., A.S., A.R and M.Q.; formal analysis, A.S.K.; investigation, A.S.K.; resources, A.S.K and A.S.; writing—original draft preparation, A.S.K; writing—review and editing, A.S.K., A.S., A.R and M.Q.; visualization, A.S.K., A.S., A.R and M.Q.; supervision, A.S., A.R and M.Q.; project administration, A.S., A.R and M.Q.; funding acquisition, A.S. All authors have read and agreed to the published version of the manuscript.

FUNDING: Natural Sciences and Engineering Research Council of Canada (NSERC), Hydro-Québec for funding through the CRD program (CRD 537350).

INSTITUTION REVIEW BOARD STATEMENT : Not applicable.

INFORMED CONSENT STATEMENT: Not applicable.

AVAILABILITY OF DATA AND HARDWARE: Not applicable

ACKNOWLEDGMENTS: The authors would like to thank the Natural Sciences and Engineering Research Council of Canada (NSERC) and Hydro-Québec for funding the project.

CONFLICTS OF INTEREST / COMPETING INTERESTS: The authors declare that they have no conflicts of interest in regard to the content of this document.

CHAPITRE 3

MÉTHODE POUR DÉTERMINER L'APPLICABILITÉ DES INDICES UTILISÉS POUR REPRÉSENTER LA FORCE ÉROSIVE DE L'EAU DANS LE PROCESSUS D'ÉROSION HYDRAULIQUE

Ce chapitre présente un article dont le 1er auteur est l'auteur de ce mémoire. Le chapitre présente le développement d'une nouvelle méthode permettant d'évaluer l'applicabilité des différents indices utilisés pour représenter la force érosive de l'eau dans le processus d'érosion hydraulique.

L'article est au stade de la révision avant soumission.

METHOD TO DETERMINE THE APPLICABILITY OF INDICES USED TO REPRESENT THE EROSIVE FORCE OF WATER IN DAM SPILLWAYS

Aboubacar Sidiki Koulibaly[1*], Ali Saeidi[1], Alain Rouleau[1], Marco Quirion[2]

[1] Département des Sciences appliquées, Université du Québec à Chicoutimi, 555 boulevard de l'Université, Chicoutimi, Québec, G7H 2B1; ali_saeidi@uqac.ca ; alain_rouleau@uqac.ca

[2] Hydro-Québec, Unité de Production et d'Expertise en barrages, 75 boulevard René-Lévesque Ouest, Montréal, Québec, H2Z 1A4, Canada; quirion.marco@hydro.qc.ca

* Correspondence: Aboubacar-sidiki.koulibaly1@uqac.ca ; Tel.: +1-581-235-1247

Abstract. In the flow channels of unlined spillways, the degree of erosion is determined by the resistance of the rock mass to the intensity of the erosive force of flow water. The methods commonly used to analyze this phenomenon are based on correlating a rock mass resistance parameter or index with the water erosive force; these results serve to predict the degree of damage. Multiple indices have been proposed for both factors to assess rock mass erosion. The selection of an appropriate index is critical when evaluating rock mass erosion. The erosive force of water is often represented by energy dissipation; however, other parameters, including average flow velocity and shear stress along the bed of the flow channel, are also valid. Here we develop a method to determine the applicability of the various indices used to represent the erosive force of water based on the observed erosion at more than 100 study sites. Our results suggest

that the shear stress along the bed of a channel is the most representative parameter of the erosive force of water. We also demonstrate that the dissipation of energy, the index most commonly used to represent the erosive force, is least representative.

Keywords: Rock mass, Hydraulic erosion, Energy dissipation, Shear stress, Kirsten index, Erosion class, Erosive force.

3.1 INTRODUCTION

Spillways are control structures integrated into a dam to evacuate excess water during periods of flooding. Spillway structures have a dissipation zone generally excavated into a rock mass and take the form of a flow channel or a plunge pool. When designing these structures, the rock mass resistance to the erosive force of water is generally assessed. However, marked erosion is commonly observed in a large number of settings, even where the rock mass had been qualified a priori as resistant. The commonly used methods to assess the hydraulic erodibility of a rock mass are based on correlating the erosive force of the water with the resistance of the rock mass. The results obtained from these methods are plotted on graphs in the form of a chart relating three parameters: the intensity of the erosive force of the water, the resistance of the rock mass, and

the rock mass erosion (or damage) classes. These methods are generally empirical, as summarized in Table 3-1.

Table 3-1. Empirical methods for evaluating the hydraulic erosion process

Method		**Correlation parameters**		**Erosion class**
Author	**Type**	**Erosive force**	**Resistance of the rock mass**	
(Moore *et al.* 1994)	Empirical methods	Energy dissipation ($\prod_{UD}$)	Kirsten's index (K_h)	One class of erosion when ($\prod_{UD} > K_h$)
(Van Schalkwyk *et al.* 1994)				No erosion Minor Moderate Large
(Annandale 1995)				One class of erosion when ($\prod_{UD} > K_h$)
(Kirsten *et al.* 2000)				
(Pells *et al.* 2016b)			Geological strength index for erodibility (*eGSI*)	Negligible Minor Moderate Large Extensive
			Erodibility index of the rock mass ($RMEI_B$)	

In these methods, the resistance of the rock mass is evaluated through various indices, including the Kirsten Index (K_h), the Geological Strength Index for Erodibility (*eGSI*), and the Rock Mass Erodibility Index ($RMEI_B$). These indices use different geomechanical parameters related to the rock mass and the intact rock, such as the confined compressive strength of the intact rock (M_s), the size (K_b) or the volume (V_b) of the rock blocks, the shear strength of the rock joints (K_d), and the relative structure of the blocks (either J_s or E_{doa}), which considers the effect of the shape and orientation of the blocks with respect to the flow direction of

water in the canal. The values of K_h, *eGSI*, and $RMEI_B$ are determined using Equations *(3-1)*, *(3-2)* and *(3-3)*, respectively.

$$K_h = Ms \cdot K_b \cdot K_d \cdot Js, \tag{3-1}$$

$$eGSI = GSI + E_{doa}, \tag{3-2}$$

$$RMEI_B = (RF_{P1}.LF_{P1}).(RF_{P2}.LF_{P2}).[(RF_{P3}.LF_{P3})+(RF_{P4}.LF_{P4})+(RF_{P5}.LF_{P5})], \tag{3-3}$$

In Equation *(3-2)*, *GSI* is a rock mass classification index developed by Hoek et al. (1995); it is also used by Pells as the basis for the *eGSI* erodibility index. Equation *(3-3)* defines the resistance of the rock mass by weighting the various geomechanical parameters using factors of relative importance (*RF*) and likelihood (*LF*). The prefixes *P1* to *P5* in Equation *(3-3)* represent various sets of geomechanical parameters, including the viable mechanisms at the kinematic separation of the blocks, the nature of the potentially eroded surface, the nature of the joints contained in the rock mass, the spacing between the joints, and the shape of the blocks (Pells 2016a).

For representing the index of the water erosive force, energy dissipation (Π_{UD}) is used in the erosion evaluation methods; it is controlled by various parameters related to the flow conditions. In the case of unlined spillways, Π_{UD} is determined using Equation *(3-4)*.

$$\Pi_{UD} = \rho.\mathrm{g}.q\frac{dE}{dx}, \tag{3-4}$$

where ρ is the density of water (kg.m^{-3}), g is the gravity acceleration (m.s^{-2}), q is the flow rate per unit length of channel width ($q = Q/B_f$), B_f is the channel width (m), Q is the water flow rate (m^3.s^{-1}), and $\frac{dE}{dx}$ is the energy loss during flow.

From these two indices (i.e., the erosive force of water and the resistance of the rock mass) and the observed damage classes in dam spillways, graphical representations of predicted future damage in spillways can be developed (Figure 3-1). These graphs, developed by various authors, have the erosion class or damage class determined by the scour depth or the amount of eroded material, which is a function of the intensity of the erosive force of the water and the resistance of the rock mass. Generally, a greater erosive force and lower rock mass resistance increase the degree of damage to the rock mass. An extensive damage class corresponds to an erosive force that is markedly greater than the resistance of the rock mass, whereas a negligible damage class suggests the two forces are equal. In addition, rock masses of the same class share similar characteristics and should be eroded at a near-equal intensity when affected by the same erosive force. However, the graphs of Figure 3-1, show that most cases of erosion present a non-proportional relationship between the resistance of the rock mass and the erosive force of the water in all erosion classes. In Figure 3-1.b, for example, we note that the cases of erosion qualified as "minor," according to

the field observations, are, however, usually qualified as "major" erosion events, when using the method of Van Schalkwyk *et al.* (1994). This type of inconsistency is common, in which the erosion class determined by field observations differs from that determined using the methods of Annandale (1995), Van Schalkwyk *et al.* (1994b), and Pells *et al.* (2016). Similarly, some cases deemed non-erosional in the field are qualified as erosional using the Annandale method (Figure 3-1.a).

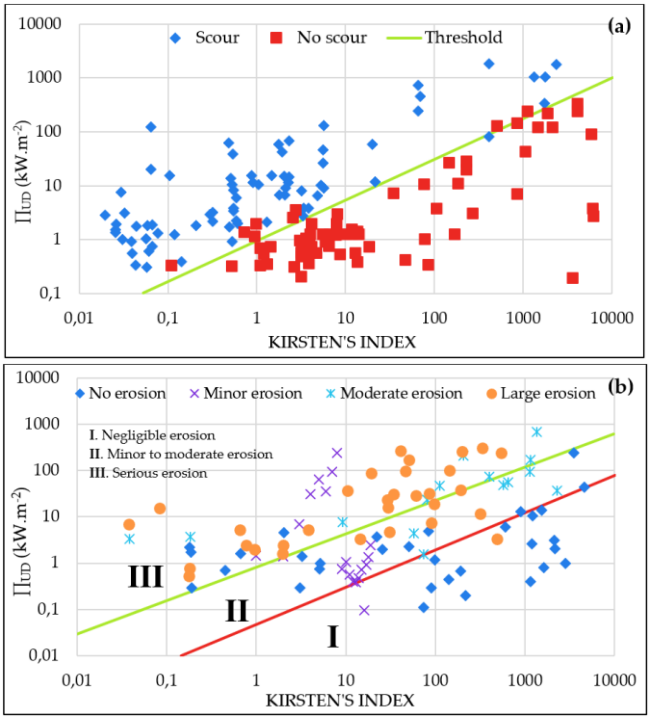

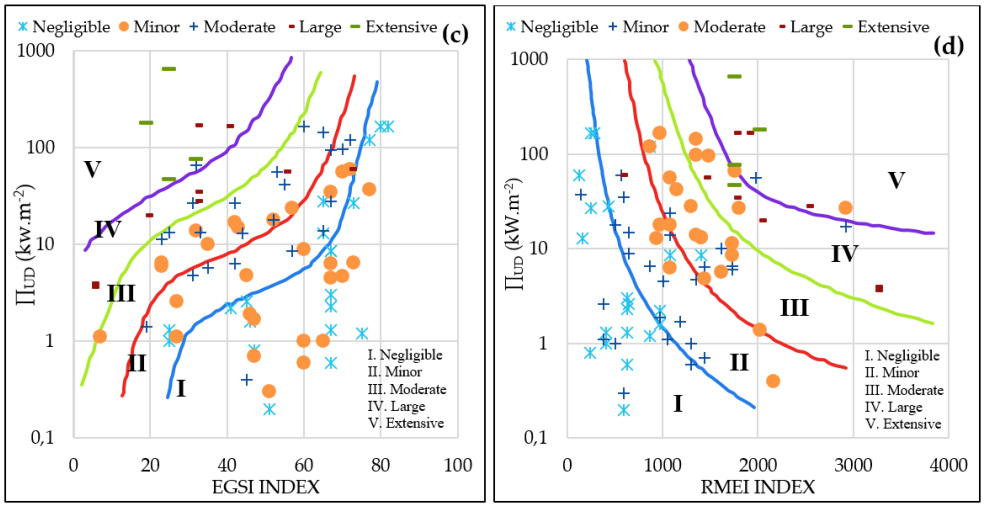

Figure 3-1. Methods for evaluating the hydraulic erodibility of rock mass in the flow channels of spillways, presenting the methods developed by (a) Annandale (1995), (b) Van Schalkwyk *et al.* (1994b), and (c, d) Pells *et al.* (2016).

The causes of these inconsistencies could stem from either the rock mass resistance index (and the rock mass parameters) or the erosive force parameters, which are considered as a hazard parameter. Boumaiza *et al*.(2019) evaluated the representativeness of the various geomechanical parameters used in the resistance indices of the rock mass. They concluded that the various indices rely on some geomechanical parameters that are not relevant to hydraulic erosion for defining the resistance of rock mass. However, other sources of inconsistency could stem from assessments of the water erosive force; this latter source is the focus of this paper.

Apart from the use of energy dissipation in many of the known methods for assessing hydraulic erosion, a number of other parameters or indices are designated to represent the erosive force of water. These indices include the

average velocity of flow ($\bar{u}$ in m.s^{-1}) and the shear stress applied on the bed of a flow channel ($\bar{\tau}_b$ in kPa). For non-uniform flows, Equations *(3-5)* and *(3-6)* provide a first approximation of these indices (Pells 2016a).

$$\bar{\tau}_b = \rho . \mathrm{g} . R_H . S_f \cos\theta, \qquad (3\text{-}5)$$

$$\bar{u} = \frac{1}{n} {R_H}^{2/3} S^{1/2} \; ; \; \text{where } n = \frac{{R_H}^{1/6}}{C} = {R_H}^{1/6} \sqrt{\frac{f}{8\mathrm{g}}} \; , \qquad (3\text{-}6)$$

where n is the resistance coefficient of Manning, R_H is the hydraulic radius (m), S is the slope of the channel equal to dz/dx, x is a distance along the channel (m), z is an elevation above a datum (m), g is the gravity acceleration (m.s^{-2}), θ is the angle of inclination of the channel (°), f is the flow resistance coefficient of Darcy (1845), C is the resistance coefficient of Chezy (1769), and S_f is the total energy gradient.

However, many criticisms of the true representativeness of these indices have discouraged their use in hydraulic erosion assessment methods. The varying estimates of these indices depend on the configuration of the flow channel (Figure 3-2); thus, these estimates are affected by the problem of non-uniqueness in their representation of flow conditions. In Figure 3-2.a and b, the flow velocity is 7 m·s^{-1}, although the hydraulic conditions (flow rate and turbulence) in Figure 3-2.a are five times greater than the flow conditions observed in Figure 3-2.b. Likewise, it is also apparent from Figure 3-2 that a single measure of the average shear

stress or energy dissipation is not associated with a single particular condition of flow rate and hydraulic head (erosive force of the water). For example, the erosive force according to Figure 3-2.c and d may not be equivalent, even when the energy dissipation is constant (Pells 2016a).

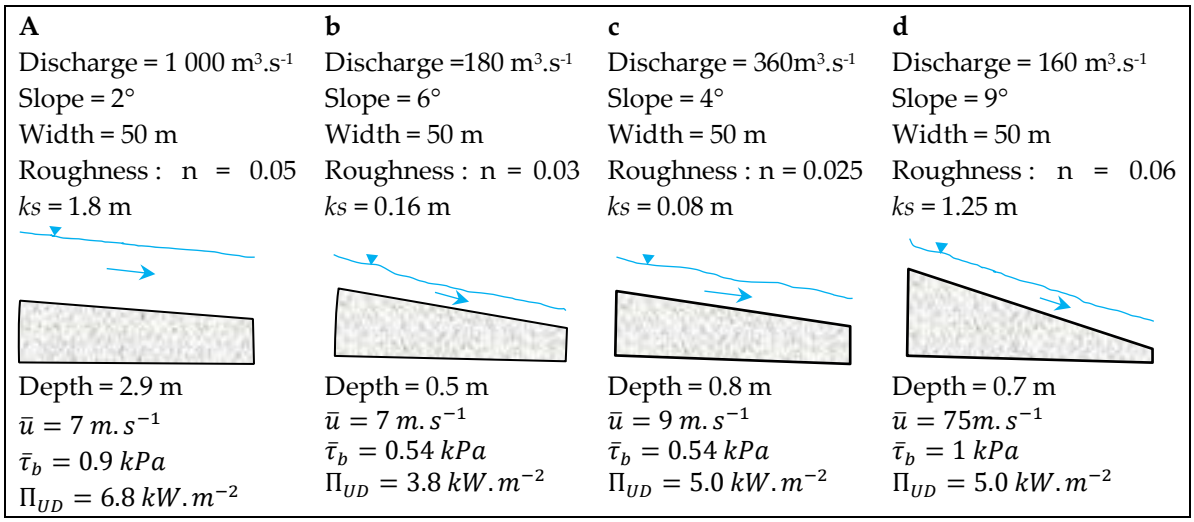

Figure 3-2. Examples of estimates when applying the different indices used to represent the erosive force of water (Pells 2016a).

For a first interpretation, these three indices ($\bar{u}, \bar{\tau}_b$, and Π_{UD}) can be used to represent the erosive force of water in the process of hydraulic erosion; the average flow velocity relates directly to the pressure stagnation points that form in joints and around protrusions. This velocity stagnation induces the creation of differential pressures in the joints of the rock mass, a key process of erosion (Pells 2016a). The index of the average shear stress of the flow channel bed is a physical measurement of the normal stress applied to the bed, also representing a component of the hydraulic erosion process. Energy dissipation, on the other

hand, is also qualified as being representative of the erosive force of water because it is correlated with the turbulence intensity of a flow (Annandale 1995; Kirsten *et al.* 2000). The laboratory studies of Annandale (1995) and Pells (2016) showed a correlation between energy dissipation and the magnitude of pressure fluctuations in a flow field, and this correlation also applies to shear stress and mean flow velocity. Despite these shared points between these indices and the hydraulic power of a flow, an important question remains unresolved: Among these three indices, which index interprets or best represents the erosive force of water as observed in known cases of erosion?

The non-representativeness of average velocity (u_{mean}) is linked to its sensitivity in relation to the problem of "non-uniqueness" in the field of hydraulic erosion. That is, the average shear stress at the bottom surface of the flow channel (τ_b) is designated as being representative of the hazard parameter of the water at the spillways. Van Schalkwyk *et al.* (1994) and Pells *et al.* (2016) demonstrated that the amount of observed erosion is favorably correlated with shear stress. Most researchers believe that erosion caused by the flow of water in the channel stems from the shear stress exerted by the water on the bottom surface of the flow channel. However, Annandale (2006) noted that this notion is only valid for laminar flow; for turbulent flow, the erosion capacity of water depends on the pressure fluctuations exerted by the flowing water rather than shear stress.

Moreover, the effects of shear stress do not explain all probable mechanisms of erosion, including erosion by the dynamic expulsion of blocks recessed in a rock mass or the erosion by fragile fracturing of the rock mass into smaller pieces because of turbulent flow. In addition, the average shear stress in the flow channel is hard to estimate, which can cause considerable uncertainty in estimates of the hydraulic head for different flow conditions within spillways (e.g., hydraulic jumps). These reasons have led to a non-preference of the average shear stress of the bottom of a channel for representing the erosive force of water. The energy dissipation index is the most common means of evaluating hydraulic erosion to represent the erosive force. This index, however, is not always reliable because it does not integrate all the complexities of the erosion process; it is used to calculate the water erosion risk parameter because it is simple to determine, not because of its representativeness. This led Pells (2016) to state that the recommendation for using Π_{UD} is pragmatic and concessional, but not optimal.

At this stage, there is no scientific basis in the literature for choosing the best parameters to represent the erosive force of water. The present justifications for rejecting some parameters such as velocity and shear strength are qualitative. Hence, there is a need to verify the applicability of these different indices used to assess hydraulic erodibility on the basis of actual observed erosion data. In this context, we present a methodology to assess the applicability of the various indices

used in hydraulic erodibility assessments. This paper first describes the algorithm of the method. We then present and discuss the results obtained from its application.

3.2 DESCRIPTION OF THE METHODOLOGY

The methodology developed to determine the relevance of the various indices for evaluating rock mass erosion is presented in Figure 3-3. Each step of this methodology is described in the following subsections.

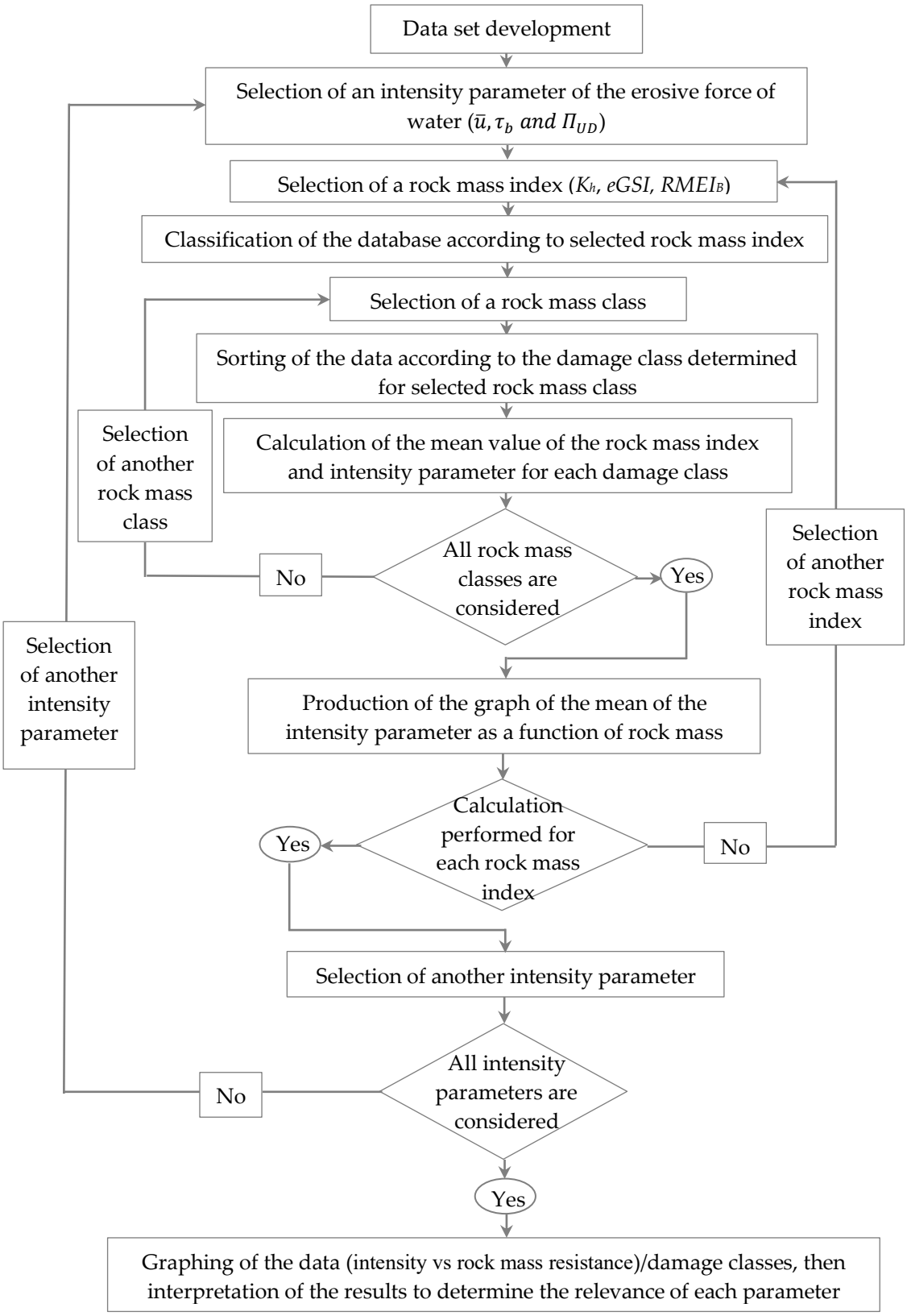

Figure 3-3. Methodology for determining the relevance of the index for the erosive force of water

3.2.1 DATA SET DEVELOPMENT

To evaluate the pertinence and applicability of each method, we used observational data from several dam spillways that have experienced erosion. This data set of erosion cases combines field data collected from more than 100 study cases compiled by Pells *et al.* (2016). We used this data set because it involves case studies carried out on unlined flow channels of spillways of selected dams in Australia and South Africa and contains many relevant parameters useful for this study, including the degree of erosion, various indices representing the intensity of the erosive force of the water (u_{mean}, τ_b and Π_{UD}), and parameters that can be used to determine the resistance of the rock mass via resistance indices that include K_h, *eGSI*, and $RMEI_B$. The rock mass resistance indices are determined according to the guidelines for each index using the geomechanical rock mass characteristics. We determined the erosive force of the water analytically and by using software, including HEC-RAS (Pells 2016a).

3.2.2 SELECTION OF A PARAMETER OF THE EROSIVE FORCE OF WATER (u_{mean}, τ_b and Π_{UD})

To assess the representativeness of the indices used to evaluate the erosive force of water, we applied our method to one intensity index at a time; this index must be then coupled with the resistance indices of the rock mass also one at a time. As the first step, an intensity or erosive force parameter is selected among

u_{mean}, τ_b, or Π_{UD}; each one of these three parameters is analyzed individually, sequentially.

3.2.3 SELECTION OF ROCK MASS INDEX (K_h, *eGSI* and $RMEI_B$)

This step of characterizing of the rock mass consists of selecting a rock mass strength index among K_h, *eGSI*, and $RMEI_B$ to be able to apply the subsequent steps. First, the various geomechanical parameter elements defined by these indices to characterize hydraulic erosion must be determined. Then, according to these hydraulic erosion evaluation methods, the resistance indices break down rock masses into classes on the basis of their resistance. Table 3-2 and Table 3-3 present the rock mass classes defined by Kirsten and by Pells, respectively.

Table 3-2. Class of rock mass in terms of ease of excavation (Kirsten 1982a)

Rock mass class (K_h) in terms of ease of excavation			
1, 2 et 3	Sedimentary rock		0–0.9
4	Rock	Easy	1–9.9
5		Difficult	10–99.9
6		Very difficult	100–999
7		Extremely difficult	1000–9999
8		Explosive	>10 000

Table 3-3. Class of rock mass according to Pells (2016) *eGSI*, derived from the *GSI* of Hoek (Hoek *et al.* 1998)

Rock mass class (*eGSI*)		
1	Very poor	< 20
2	Poor	21–40
3	Moderate	41–60
4	Good	61–80
5	Very good	81–100

Table 3-4 presents a categorization of the rock mass according to the $RMEI_B$ index used for application purposes. This classification was inspired by that of Pells *et al.* 2016 (Figure 3-1.d).

Table 3-4. Class of rock mass according to Pells' $RMEI_B$ index

Rock mass class ($RMEI_B$)		
1	Very poor	< 499
2	Poor	500–999
3	Moderate	1000–1499
4	Moderately good	1500–1999
5	Good	2000–2499
6	Very good	2500–3000
7	Extremely good	>3000

The rock mass classes defined by these indices (Table 3-2, 3-3 and 3-4) generally make it possible to group rock masses of the same resistance; i.e., classified rock masses characterized by the same geomechanical parameters.

3.2.4 CLASSIFICATION OF THE DATA SET ACCORDING TO SELECTED ROCK MASS INDEX

Once the parameters allowing the evaluation of hydraulic erosion are determined, for example $\bar{u}\ vs\ K_h$ or $\tau_b\ vs\ eGSI$, the next step consists of classifying the data set by rock mass class defined by the value of the resistance index. After classifying the data set, the methodology continues by considering the rock mass classes individually.

3.2.5 ORGANIZATION OF THE DATA ACCORDING TO DAMAGE CLASSES FOR THE SELECTED ROCK MASS CLASS

The application of the remaining steps of the methodology by rock mass class requires the use of a third parameter characteristic of hydraulic erosion process, either the degree of damage or the erosion classes of the rock mass. Different classifications are used in the literature for the degree of erosion; erosion is qualified into classes according to the depth of erosion or the volume of eroded rock by 100 m^2. According to Annandale's method (Annandale 1995), the presence of erosion is defined once 2 m of the rock mass is eroded. However, the erosion classes presented by Van Schalkwyk and Pells are more detailed (Van Schalkwyk *et al.* 1994; Pells *et al.* 2016b), as summarized in Table 3-5 and Table 3-6.

Table 3-5. Erosion classes as defined by Van Schalkwyk *et al.* (1994)

Depth of erosion (m)	**Erosion class**
< 0.2	No erosion
0.2 to 0.5	Minor erosion
0.5 to 2	Moderate erosion
> 2	Large erosion

Table 3-6. Erosion classes as defined by Pells *et al.* 2016

Max depth (m)	**General extent m^3 per 100 m^2**	**Class**	**Descriptor**
< 0.3	< 10	I	Negligible
0.3 to 1	10 to 30	II	Minor
1 to 2	30 to 100	III	Moderate
2 to 7	100 to 350	IV	Large
> 7	> 350	V	Extensive

This step consists of treating each resistance class of the rock mass, as defined by the rock mass index, independently. These rock mass classes are in turn sorted according to the degree of damage, ranging from "negligible" to "extensive." For example, in the previous step with *eGSI* as a characteristic index of the rock mass, the second class obtained lies within 21 < *eGSI* < 40, corresponding to a "poor" quality rock mass (Table 3-3). This class is then sorted according to erosion or damage class. When applying this method to the present case, however, the damage classes used to classify each rock mass classes are those of Pells *et al.* 2016 (Table 3-6).

3.2.6 CALCULATION OF THE MEAN VALUE OF THE ROCK MASS INDEX AND INTENSITY PARAMETER FOR EACH DAMAGE CLASS

With the class of rock mass categorized into erosion classes and containing several case studies having different intensities of erosive force, the average value of the erosion force is calculated per erosion class, as is the average value of the resistance index of the rock mass; Equation *(3-7)* presents the method for determining the mean value of each index. Table 3-7 presents a summary of steps 5 to 7 of the methodology, using Class 2 of the *eGSI* index as an example.

$$\overline{In}_{(EC/RMC)} = \frac{\sum(In_1 + In_2 + \ldots\ldots\ldots + In_N)}{N}, \qquad (3\text{-}7)$$

where $\overline{In}_{(EL/RMC)}$ is the mean value of the index (erosive force or resistance of the rock mass) of the erosion class (EC) per rock mass class (RMC), In is the index for each erosion case by erosion class (EC), and N is the total amount of erosion cases per erosion class (see Table 3-7).

Table 3-7. Summary of steps 5 to 7 of the methodology applied to the parameters u_{mean} and *eGSI* parameters, considering only Class 2 of the *eGSI* index.

Rock mass index class *eGSI*		Peak u_{mean} (m/s)	**Chart ID***	Erosion Level	$\overline{eGSI}$	$\bar{u}$
Class 2 21< *eGSI* < 40	25	13.3	Cop.6	Extensive	27	17
	25	21.2	Cop.10	Extensive		
	32	15.5	Cop.5	Extensive		
	32	10.1	Pin.4	Large	34	16
	32	12	Cop.4	Large		
	32	18.8	Cop.9	Large		
	40	25	Bur.4	Large		
	23	6.8	Kli.2	Minor	27	11
	23	7.2	Kli.5	Minor		
	23	12.6	Gar.2	Minor		
	23	15.1	Gar.5	Minor		
	32	9.1	Kam.5	Minor		
	35	12.2	Cop.11	Minor		
	23	8.5	Kli.3	Moderate	31	11
	31	15.6	Goe.2	Moderate		
	31	15.6	Goe.4	Moderate		
	31	12.3	Goe.5	Moderate		
	31	13.2	Hart.2	Moderate		
	31	10	Kam.3	Moderate		
	31	5.1	Pin.2	Moderate		
	32	14.5	Cop.7	Moderate		
	35	6.8	Cop.1	Moderate		
	25	5.2	Gar.1	Negligible	25	6
	25	6.8	Gar.4	Negligible		

* 'Chart ID' represents the name of the dam (Pells 2016a).

Table 3-7 is then prepared for the rock mass classes defined by the index chosen at the outset. Table 3-8 presents a complete summary of the application of the methodology from steps 1 to 7, using u_{mean} and *eGSI* as the pair of indices to assess erosion.

Table 3-8. Summary of steps 1 to 7 of the methodology applied to the paired parameters u_{mean} and *eGSI*.

Rock mass class according to *eGSI*			Erosion class defined (Pells *et al.* 2016b)									
			Negligible		Minor		Moderate		Large		Extensive	
			u_{mean}	*eGSI*	u_{mean}	*eGSI*	u_{mean}	*eGSI*	u_{mean}	*eGSI*	u_{mean}	*eGSI*
1	Very poor	< 20	–	–	–	–	9	9	10	10	20	11
2	Poor	21–40	6	25	11	27	11	31	16	34	17	27
3	Moderate	41–60	4	46	6	51	11	50	10	55	–	–
4	Good	61–80	9	70	11	70	15	69	22	72	–	–
5	Very Good	81–100	–	–	–	–	–	–	–	–	–	–

NB : (–) absence of erosion data for these classes of rock mass.

The representativeness of the water erosive force index can be evaluated after all rock mass resistance indices are considered, and the results can be compared (i.e., repeat step 3, choosing another resistance index, e.g., $RMEI_B$ rather than the *eGSI*, and visualize the behavior of the erosive force index of water in relation to the various resistance indices of the rock mass).

3.2.7 GRAPHICAL REPRESENTATION OF THE EROSIVE FORCE OF WATER VS. RESISTANCE INDICES OF THE ROCK MASS

The data obtained in tabular form (e.g., Table 3-8) are then represented graphically. The graphs constructed for each pair of hydraulic erosion evaluation parameters, e.g., $\bar{u}$ vs K_h, $\bar{u}$ vs $eGSI$, and $\bar{u}$ vs $RMEI_B$, are characterized by curves representing the erosion classes defined in Table 3-6. These various graphs allow evaluating and comparing the pertinence of each erosive force index or intensity, for each rock mass.

3.3 RESULTS AND DISCUSSION

The above-described methodology aims to assess the relevance of the erosive force of water indices for different resistance indices of the rock mass. The aim is to determine the erosive force index best correlated with the degree of damage observed in the field. We consider that this correlation is more reliable when a logical sequence is respected between the intensity of the erosive force and the resistance of the rock mass for each damage class. That is, when applying this methodology, we expect that the regression curves passing through the erosion case studies data will differ in slope, and this slope increases with greater erosion. On the vertical axis, we would expect erosion cases to be ordered from negligible to extensive, as defined by the expected logical sequence in the following sections. We present the results in nine graphs obtained by comparing each of the three selected indices of erosive force with each of the three considered indices of rock mass resistance, three graphs being grouped within the same figure for each index of the intensity of erosive force. These results are represented, interpreted, and discussed in the following subsections.

3.3.1 u_{mean} AS A FUNCTION OF ROCK MASS RESISTANCE INDEX

With the average flow velocity (u_{mean}) representing the erosive force, the observed erosion damage at more than 100 considered sites is plotted against the three

different resistance indices of the rock mass (K_h, *eGSI*,and $RMEI_B$), one index at a time and grouped by class (Figure 3-4).

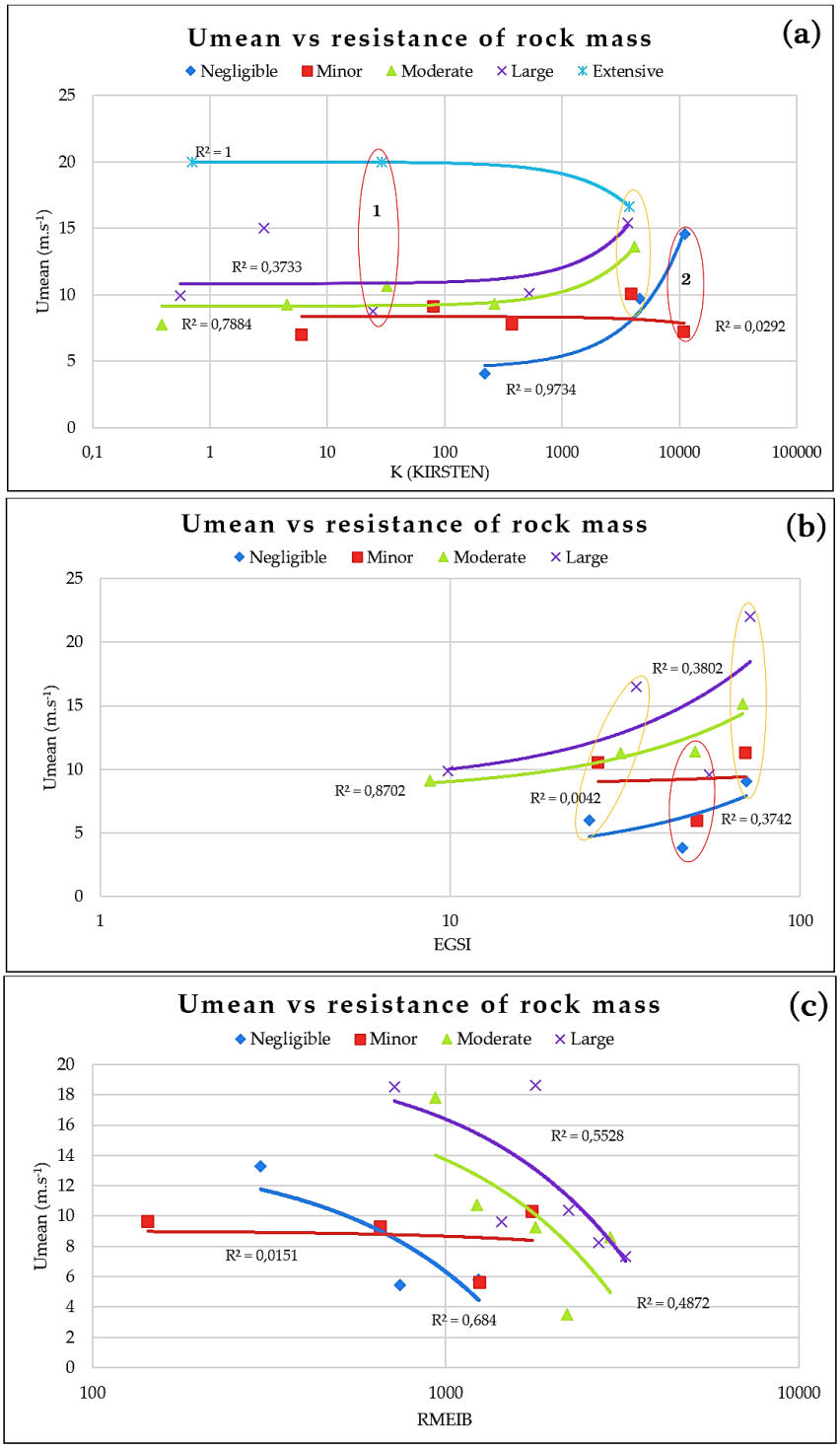

Figure 3-4. Observed erosion damage plotted using u_{mean} as the intensity of the erosive force of water vs. the various resistance indices of the rock mass (K_h, *eGSI*, and $RMEI_B$)

The points within the yellow ellipses in Figure 3-4 respect a logical sequence of erosion classes for the relationship between the resistance of the rock mass and the erosive force of the water. Rock masses of the same class should share similar characteristics and should experience similar erosion levels for a given erosive force intensity. As the erosive force of water increases for a given rock mass resistance, the erosion class should change from "negligible" to "extensive" in a logical sequence (negligible to extensive erosion moving upward along the vertical axis). However, the points within the red ellipses present abnormal sequences. Here, two rock masses of similar resistance show, in one case, negligible erosion while experiencing a high erosive force and, in the second case, minor erosion while experiencing a minor erosive force.

The regression curves on these graphs allow further differentiation of the erosion classes. The regression curves in Figure 3-4.a illustrate that the erosion classes do not always present an expected logical sequence; the negligible, moderate, and large erosional classes follow the expected sequence, whereas the minor and extensive erosion classes do not. A more logical pattern among erosion classes is observed in Figure 3-4.b; ; however, the R^2 values of the corresponding regression curves are generally lower, suggesting a higher variability in the mean flow velocity used to represent the erosive force of water. The erosion case studies do not present any logical sequence in terms of erosion class (Figure 3-4.c); thus,

$RMEI_B$ does not adequately characterize the resistance of the rock mass. With the exception of the "minor" erosion class, the regression curves Figure 3-4.c ($RMEI_B$) are organized in a logical sequence; however, the R^2 of these regression lines is generally lower than observed with the other indices. Therefore, the representativeness of these regression curves is questionable.

3.3.2 τ_b AS A FUNCTION OF ROCK MASS RESISTANCE INDEX

Using the shear stress of the bed of a channel (τ_b) representing the erosive force, we can plot the considered erosion damage classes against three different resistance indices of the rock mass (K_h, *eGSI, and* $RMEI_B$), one index at a time and grouped by rock mass class (Figure 3-5).

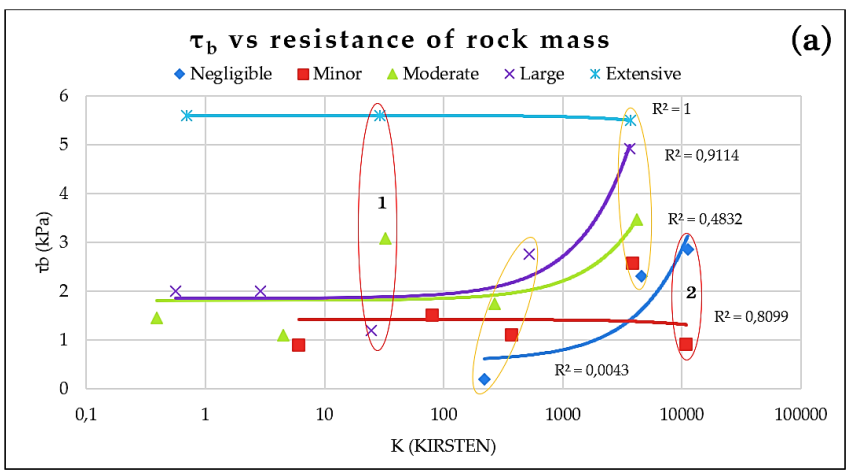

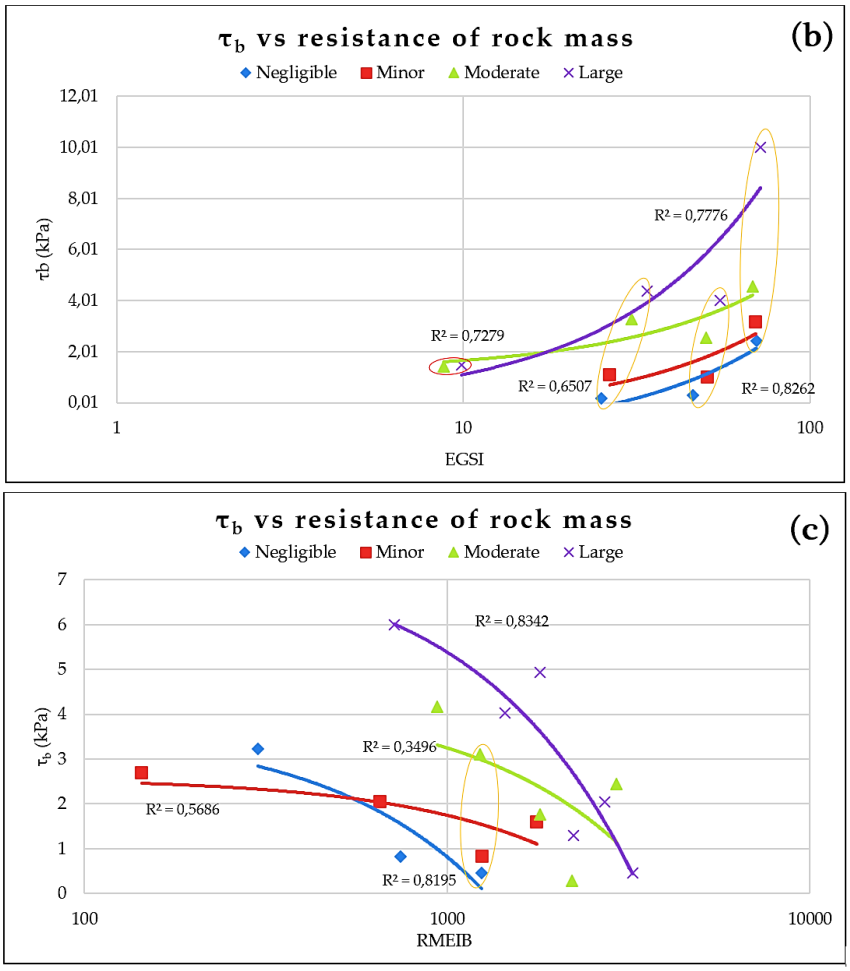

Figure 3-5. Observed erosion damage plotted using τ_b as the intensity of the erosive force of water vs. the various resistance indices of the rock mass (K_h, *eGSI* and $RMEI_B$)

Figure 3-5.a is very similar to that of Figure 3-4.a. The difference is found at the level of the regression curves, as the R^2 of these lines becomes acceptable for most erosion classes (as the value of R^2 gets closer to 1, the more acceptable it is). However, a clear improvement is observed in Figure 3-5.b representing τ_b vs. *eGSI*. In most cases, the distribution of erosion classes follows an expected logical sequence between the erosive force and the resistance of the rock. The obtained regression curves also follow a logical sequence, and the R^2 of these regression curves is generally more representative than the previous abovementioned

values. Hence, shear stress is a better representative index. Figure 3-5.c presents some marked improvements and similar results as to those in Figure 3-4.c. The distribution of some erosion cases follows the expected logical sequence, and the R^2 of the regression curves is much more acceptable; however, the arrangement of these curves is less clear. Comparing Figure 3-4.c and Figure 3-5.c, we note that τ_b best represents the erosive force of the water in assessments of hydraulic erosion.

3.3.3 Π_{UD} AS A FUNCTION OF ROCK MASS RESISTANCE INDEX

With the dissipation of energy (Π_{UD}) to represent the erosive force, we can plot the considered erosion damage classes against the three different resistance indices of the rock mass (K_h, *eGSI, and* $RMEI_B$), one index at a time and then grouped by class (Figure 3-6).

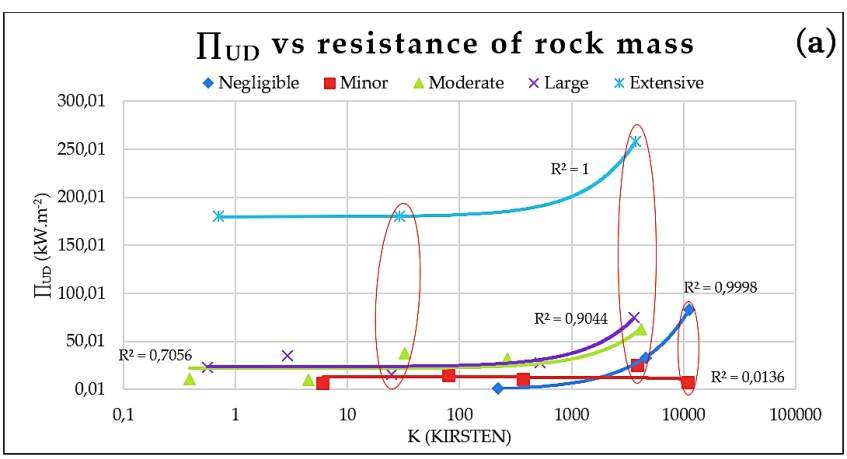

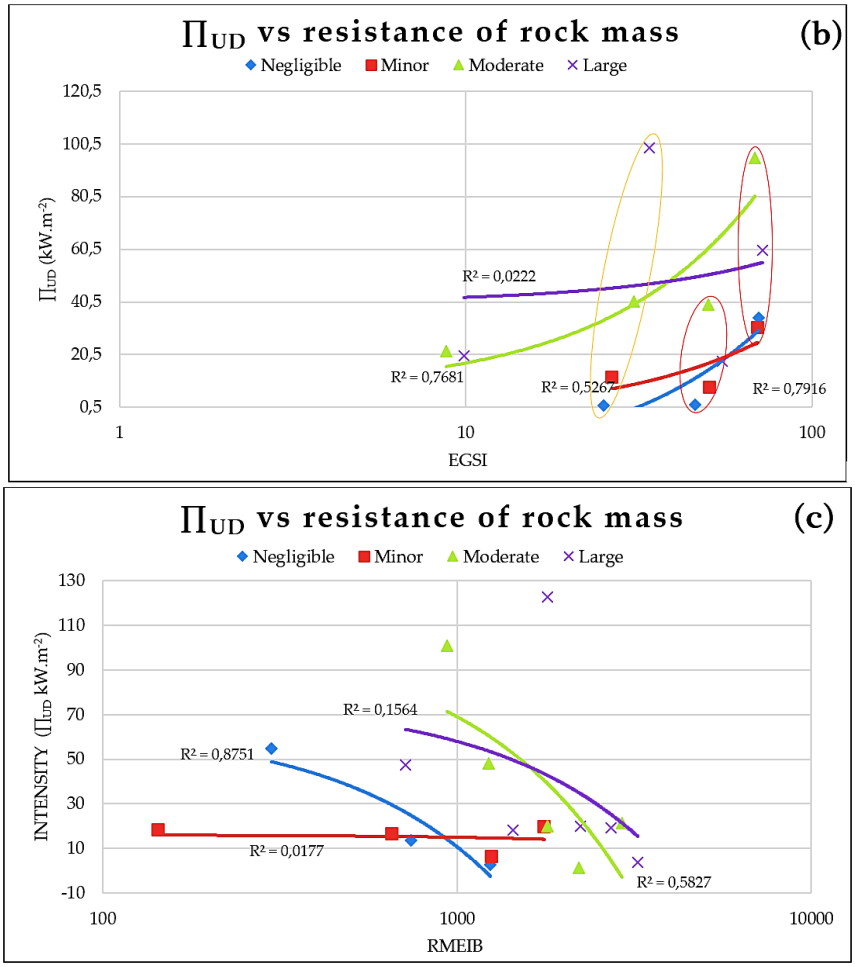

Figure 3-6. Observed erosion damage plotted using Π_{UD} as the intensity of the erosive force of water vs. the various resistance indices of the rock mass (K_h, *eGSI* and $RMEI_B$)

Figure 3-6, with Π_{UD} as the erosive force of water, shows a less clear pattern than the patterns observed in Figure 3-4 and 3-5. In Figure 3-6, the distribution of most erosion cases contains abnormal sequences, and the regression curves of these erosion cases are not ordered logically. With the exception of Figure 3-6.b (Π_{UD} vs *eGSI*), few erosion cases show the expected logical sequence (points within yellow ellipses). In the same figure, a notable grouped logical sequence lies between the regression curves of the erosion classes. A logical sequence is found between the negligible and moderate erosion classes; the minor and large

erosion classes also present a logical sequence. However, when combined, these two groups are not ordered logically. Hence, using energy dissipation to represent the erosive force of water is questionable. With $RMEI_B$ as an index to characterize the resistance of the rock mass and Π_{UD} to represent the erosive of the water (Figure 3-6.c), neither the erosion cases nor the corresponding regression curves are organized logically with respect to erosion class.

To summarize, we can first conclude that our approach makes it possible to visualize the relevance of the different indices used to represent the erosive force of water. Among these indices, energy dissipation is that which presents the least representative results, whereas it is the most commonly used in practice. The most representative index producing relevant results is the shear stress of the bed of a channel; an expected logical sequence is observed for most erosion cases according to erosion class (erosion cases are ordered from negligible to extensive). Results obtained using the mean flow velocity as an erosive force are less representative than using shear stress, and a maximum variability is observed in the distribution of the observed erosion cases.

Average velocity (u_{mean}) can be very sensitive to the problem of "non-uniqueness" in hydraulic erosion studies. Our method for visualizing the relevance of the indices in regard to the erosive force of the water (Figure 3-4) also demonstrates that the average flow velocity is characterized by maximum

variability; thus, the average shear stress at the bottom of the flow channel ($\bar{\tau}_b$) is the most representative index. However, shear stress does not explain all possible erosion mechanisms within spillways (Koulibaly *et al.* 2021), e.g., erosion by the dynamic removal of blocks or erosion by the brittle fracture of large blocks into smaller blocks. These limitations in explaining the erosion mechanisms coupled with these parameters being difficult to estimate explain the non-use of this index in the field. In contrast, energy dissipation as an erosive force is the most commonly used index because of its simplicity in calculation, not because of its representativeness. The latter index is qualified as incomplete, as it does not include all the complexities of the erosion process. Our analyses illustrate that use of energy dissipation as an index of erosive force is not optimal because a strong correlation is not observed between this index and the erosion classes according to rock mass resistance.

Another important point deduced from our method is the representativeness of the resistance indices of the rock mass. The graphs in Figure 3-5 present an expected logical sequence of the distribution of erosion cases only when *eGSI* is used as the resistance index of the rock mass (Figure 3-5.b). And among these three rock mass resistance indices, $RMEI_B$ is the index which presents the least conclusive results. Hence, *eGSI* best defines the resistance of a rock mass relative to other indices of rock mass resistance.

3.4 CONCLUSION

Here, we developed a methodology to assess the relevance of indices used to represent the erosive force of water; our approach is based on observed cases of erosion in spillways and the corresponding rock mass resistance. It appears that the shear stress at the base of the flow channel and the mean flow velocity are better at representing the erosive force of water than the dissipation of energy, with shear stress showing better results than flow velocity. The relevance of shear stress and mean flow velocity can be explained by the direct relationship of these two indices with the pressure exerted on the bottom of the flow channel. However, these indices poorly assess the lifting force of a block because the main force causing erosion by removal of the blocks is the pressure applied to the joints around the blocks. Nevertheless, the equations for determining the shear stress at the base of a flow channel must be improved to be applied to the various known erosion modes.

ACKNOWLEDGMENTS: The authors would like to thank the Natural Sciences and Engineering Research Council of Canada (NSERC) and Hydro-Québec for funding through the CRD program (CRD 537350).

FUNDING: Natural Sciences and Engineering Research Council of Canada (NSERC), Hydro-Québec provided founds through the RDC (RDC 537350) program.

CONFLICTS OF INTEREST / COMPETING INTERESTS: The authors confirm that there are no known conflicts of interest associated with this publication.

AVAILABILITY OF DATA AND HARDWARE: The data used in this article is available in Annexe A, and graphics data sources are presented in Annexe B.

CHAPITRE 4

DÉVELOPPEMENT D'UNE MÉTHODE VECTORIELLE POUR LE CALCUL EXACT DU VOLUME DU BLOC DE ROCHE

Ce chapitre présente un article dont le 1er auteur est l'auteur de ce mémoire. Le chapitre présente le développement d'une nouvelle méthode vectorielle de détermination du volume des blocs in-situ d'un massif rocheux fracturé.

L'article est au stade de la révision avant soumission.

DEVELOPMENT OF A VECTOR METHOD FOR THE EXACT CALCULATION OF THE ROCK BLOCK VOLUME

Aboubacar Sidiki Koulibaly[1], Alireza Shahbazi[1], Ali Saeidi[1*], Alain Rouleau[1], Marco Quirion[2], Romain Chesnaux[1]

[1]Université du Québec à Chicoutimi, 555 boulevard de l'Université, Chicoutimi, Québec G7H 2B1, Canada

[2]Hydro-Québec Production Unité Expertise en barrages, 75 boulevard René-Lévesque Ouest, Montréal, Québec, H2Z 1A4, Canada

Aboubacar Sidiki Koulibaly: aboubacar-sidiki.koulibaly1@uqac.ca

Alireza Shahbazi: alireza.shahbazi1@uqac.ca, orcid: https://orcid.org/0000-0001-9595-8948

*Corresponding author: ali_saeidi@uqac.ca, orcid: https://orcid.org/0000-0001-6954-5453

Alain Rouleau: alain_rouleau@uqac.ca

Marco Quirion: quirion.marco@hydro.qc.ca

Romain Chesnaux: romain_chesnaux@uqac.ca, orcid: https://orcid.org/0000-0002-1722-9499

HIGHLIGHTS

- A new vector method for calculating block volume has been developed for a rock mass consisting of 3 persistent joint sets.
- Previously developed models produce noticeable inconsistencies in calculating block volume.
- The spacings and orientations of the joint sets are the main influential parameters in calculating the volume of the block.

- The inconsistencies of previous methods in calculating block volume has been calculated for a series of field data.

ABSTRACT

The size of rock block is an important parameter not only for stability calculations of underground excavations and slopes in a rock mass, but also in determining the risk of erosion in dam spillways. A new method based on vector operations is developed and compared with existing models for calculation of the volume of the block formed by cross-cutting of joint sets. The rock mass is assumed to include three persistent joint sets with various values of spacing and orientation. The volume of the resulting rock blocks is calculated through the multiplication of the block's edge vector. The results of the developed model are validated with the output of the numerical simulations using 3DEC version 7.0 software. A real database of field data for block volume is compared with the results of the proposed model and previously developed methods and the degree of accuracy for each method is determined.

KEYWORDS

Block volume, Rock mass, Analytical method, Vector multiplication

4.1 INTRODUCTION

Hydraulic erosion of the discharge channels in unlined spillways is one of the present-day concerns of hydropower industries. This phenomenon occurs when the hydraulic power of the water in a spillway is greater than the strength of the rock mass, and the rock mass erodes by the dynamic displacement of rock blocks. The erodibility of the rock mass directly depends on its mechanical properties, most of which are defined by the discontinuity system of the rock mass (Palmström 2001a). The most important geomechanical parameters affecting the rock mass strength are the uniaxial compressive strength (*UCS*), the inter-block shear strength (J_r/J_a), block size (V_b), the opening of the joints (J_o), and the arrangement of the joints in relation to the flow direction (J_s and E_{doa}). In this regard, the block size plays an important role in the stability of underground and surface structures (Palmström 2001a; Palmström 2005; Boumaiza *et al.* 2019a), particularly for erosion, the block size is the main parameter that influence directly the relative displacement of the rock blocks under the effect of the erosion force of the water. Several methods for calculating the block volume have been proposed (Barton *et al.* 1974; Palmström 1982; Palmström 1996; Palmström 2001a; Cai *et al.* 2004b; Palmström 2005; Elci et Turk 2014), and various equations have been developed (Table 4-1). Nevertheless, calculated block volumes mostly deviate from actual field values. For example, based on data from discontinuity survey from 11

limestone quarries in Karaburn Peninsula (Izmir in Turkey), Elci and Turk (Elci et Turk 2014) calculated the block volume (V_b) using the average spacing of the discontinuities (S_a), their real spacing (S), and the number of volumetric joints (J_v). The calculated V_b values showed significant differences with real values of the block volume.

Table 4-1: Methods for calculation of the block volume of a fractured rock mass

Reference	Equation	Parameters	Types of measurement	Method
(Barton *et al.* 1974)	$V_b = RQD/J_n$	RQD: Rock Quality Designator J_n: number of joint sets	1D measurement on the drill core direction	B
(Palmström 1982)	$V_b = \frac{\beta \times J_v^{-3}}{sin\gamma_1 \times sin\gamma_2 \times sin\gamma_3}$	J_v: joint set number β: block shape factor	3D indirect measurement on a rock surface	C
(Palmström 1996)	$V_b = \frac{S_1 \times S_2 \times S_3}{\sin\gamma_1 \times \sin\gamma_2 \times \sin\gamma_3}$	S_i: average spacing of set i γi: angle between a pair of joint sets	3D direct measurement on a rock surface	D
(Palmström 1996)	$V_b = S_a^3$	S_a: average spacing of all joint sets (m)	3D direct measurement on a rock surface	E
(Palmström 1996)	$V_b = \frac{\beta \times wJd^{-3}}{sin\gamma_1 \times sin\gamma_2 \times sin\gamma_3}$	wJd: weighted joint density β: block shape factor	1D or 2D indirect measurement on a rock surface or on drill core	F
(Cai *et al.* 2004a)	$V_b = \frac{S_1 \times S_2 \times S_3}{\sin\gamma_1 \sin\gamma_2 \sin\gamma_3 \sqrt[3]{P_1P_2P_3}}$	S_i: average spacing of set i γi: angle between pair of joint sets P_i: Persistence of joint set i	3D direct measurement on rock surface	G
(Latham *et al.* 2006)	$V_b = 36 \times (S_a/2)^3$	S_a: average spacing of all joint sets (m)	3D direct measurement on a rock surface or 1D in drill cores.	H
(Palmström 1982) (Latham *et al.* 2006)	$V_b = \frac{1}{\sin\gamma_1 \times \sin\gamma_2 \times \sin\gamma_3} \times (S_a/2)^3$	S_a: average spacing of all joint sets (m)	If assumed J_v=2/S 3D indirect measurement on a rock surface	I

Rock mass classification systems, such as Q-system (Barton *et al.* 1974) and excavation index (Kirsten 1982b), include the ratio of RQD/J_n, which represents the

block size. However, the limitation of this quotient in estimating block size has been frequently criticized by Bieniawiski (Bieniawski 1973), Edelbro (Edelbro 2003), Grenon and Hadjigeorgiou (Grenon et Hadjigeorgiou 2003), Palmström (Palmström 2005), and Pells (Pells *et al.* 2017). Hence, this quotient is not considered in this article. Palmström (Palmström 2005) mentioned that the 3D determination of block volume helps characterize the geomechanical behavior of a fractured rock mass. On this basis, he proposed a series of equations to estimate the volume of the block (V_b) and in this regard, Eq. 4-1 is developed as the first equation, as follows:

$$V_b = S_a^3 \,, \qquad (4\text{-}1)$$

where S_a is the average spacing of all joint sets and could be determined by Eq. 4-2, as follows:

$$S_a = \frac{\sum_1^n s_i}{n} \,, \qquad (4\text{-}2)$$

where $\boldsymbol{S_i}$ is the spacing of joint set $\boldsymbol{i}$, and $\boldsymbol{n}$ is the number of joint sets. This equation is only applicable when the average spacing of at least three or more joint sets is known. If the rock mass includes three persistent joint sets and the angle between each pair of sets is known, then the Eq. 4-3, which was developed by Palmström (Palmström 1996), can be used to calculate the block volume:

$$V_b = \frac{s_1 \times s_2 \times s_3}{\sin\gamma_1 \times \sin\gamma_2 \times \sin\gamma_3} \,, \qquad (4\text{-}3)$$

where γ_1, γ_2, and γ_3 are the angles between each pair of joint sets. If all joint sets are perpendicular to one another, Eq. 4-3 is simplified to Eq. 4-4, as follows:

$$V_b = S_1 \times S_2 \times S_3 \,, \qquad (4\text{-}4)$$

Eqs. 4-3 and 4-4 are applicable only if the blocks are formed by the assembly of three joint sets. However, in many cases, either the blocks are formed by random joints or some of the discontinuity sets do not appear in a rock exposure. Such a phenomenon occurs when a rock mass includes less than three joint sets or the joint spacings are large (Palmström 2005). For such cases, Palmström proposed the use of Eqs. 4-5 and 4-6 to empirically calculate the block volume, as follows:

$$V_b \approx S_1 \times 5S_1 \times 5S_1 = 25S_1^3 \qquad \text{if one set is detectable} \qquad (4\text{-}5)$$

$$V_b \approx S_1 \times S_2 \times 5S_1 = 5S_1^2 \times S_2 \qquad \text{if two sets are detectable} \qquad (4\text{-}6)$$

The volumetric joint count (J_v) is also used for block volume calculation. J_v is the number of joints cutting a volume of 1 m^3 of rock and can be calculated by using Eq. 4-7 (Bergh-Christensen 1968), as follows:

$$J_v = \sum_1^n \frac{1}{S_i} \,, \qquad (4\text{-}7)$$

where S_i is the average spacing of set i. To consider the effect of random joints, Palmström (Palmström 1982) modified Eq. 4-7 to Eq. 4-8, as follows:

$$J_V = \frac{1}{s_1} + \frac{1}{s_2} + \frac{1}{s_3} + \cdots + \frac{Nr}{5(\sqrt{A})} \,, \qquad (4\text{-}8)$$

where N_r is the number of random joints that exist in a square meter of the surveying area. Subsequently, the correlation between the volumetric joint count (J_v) and the block volume (V_b) is defined by Eq. 4-9 (Palmström 1995), as follows:

$$V_b = \beta \times J_v^{-3} \frac{1}{\sin\gamma_1 \times \sin\gamma_2 \times \sin\gamma_3}, \qquad (4\text{-}9)$$

where β is the shape factor of blocks and represents the ratio of spacings in a rock mass. In the case of three joint sets, β could be defined by Eq. 4-10, as follows:

$$\beta = \frac{(\alpha_2 + \alpha_2 \times \alpha_3 + \alpha_3)^3}{(\alpha_2 \times \alpha_3)^2}, \qquad (4\text{-}10)$$

where $\alpha_2 = S_2/S_1$ and $\alpha_3 = S_3/S_1$; S_1 is the minimum spacing, whereas S_3 is the maximum spacing of joint sets. For blocks with irregular shapes (more than 6 faces), β can be roughly estimated using Eq. 4-11, as follows:

$$\beta = 20 + 7a_3/a_1, \qquad (4\text{-}11)$$

where a_1 and a_3 represent the longest and shortest dimensions of the block, respectively. In addition, J_v could be measured using other surveying methods, i.e., by borehole or surface scanning and by defining the weighted joint density (*wJd*). *wJd* is a representative index used to illustrate the angle between joint set and surveying direction (core log) or plane (outcrop or ground surveying), and could be estimated by using Eqs. 4-12 and 4-13, as follows:

$$wJd = \frac{1}{\sqrt{A}} \sum f_i \qquad \text{For surface survey,} \qquad (4\text{-}12)$$

$$wJd = \frac{1}{L} \sum f_i \qquad \text{For core logging,} \qquad (4\text{-}13)$$

where A is the surface area of the survey, L is the length of the drill core, and f_i is the interval factor that could be defined by the angle between joint set and core logging direction or the surface area of the survey. The value of the *wJd* is almost equal to the volumetric joint count. According to Latham (Latham *et al.* 2006), *wJd* is an extension of J_v and is used because of its feasibility of the measurements, even if it is potentially less precise than J_v.

The impact of joint persistence on the block volume calculation by Eq. 4-3 was investigated by Cai (Cai *et al.* 2004b). Persistence is a term used to describe the ratio between the size of the discontinuity and rock mass dimension. If l_i is the accumulated joint length of set i in a sampling plan, and L is the characteristic length of the rock mass, then the joint persistence of set i (P_i) can be specified by Eq. 4-14, as follows:

$$P_i = \begin{cases} \frac{\bar{l}_i}{L} & if\ l_i < L \\ 1 & if\ l_i \geq L \end{cases} \qquad (4\text{-}14)$$

Accordingly, the block volume in the case of non-persistent joints could be calculated by using Eq. 4-15, as follows:

$$V_b = \frac{S_1 S_2 S_3}{\sin\gamma_1 \sin\gamma_2 \sin\gamma_3 \sqrt[3]{P_1 P_2 P_3}} \qquad (4\text{-}15)$$

Given that the direction of core logging regarding the joint set orientation is not often recorded in borehole logs, Latham (Latham *et al.* 2006) developed an

approach to estimate the volume of blocks in this case, as shown in the following Eq. 4-16:

$$V_i = 36 \times (S_a/2)^3 \,, \qquad (4\text{-}16)$$

where S_a is the average joint spacing measured along the drill core.

Based on the above-mentioned review of the common methods for block volume calculation, and because the different models are already developed for this purpose, the accuracy and applicability of each model for block volume calculation should be evaluated. Also based on the results of the studies carried out by Elci and Turk (Elci et Turk 2014), according to which the current methods of calculating the volume of the blocks given inaccurate results, the development of a new method to determine the volume of the blocks with precision is still necessary to better characterize the rock mass. For this purpose, a new analytical method to calculate block volume is developed on the basis of vector multiplications and is validated by 3D numerical modeling. This method is named as method "A" in this article. To calculate the volume of the block, the rock mass is assumed to include three persistent joint sets. The volume of the block that is created by the cross of the joint sets is determined by the vector multiplication product of the block's edge vectors. Generally, the block in this case will be a parallelepiped with six faces, and each pair of frontside faces are identical. The block volume calculation with method "A" is fully compatible with the results of the numerical simulation. Also,

the block volume for a series of field data calculated by each method is compared with that calculated by method "A", and the relevant error is evaluated. The previous methods for block volume calculation that have been considered in this article are summarized in Table 4-1. In Section 4.2, the method "A" is developed and validated by numerical simulation. In Section 4.3, the block volume calculations by all models for a specific series of field data are compared.

4.2 DEVELOPMENT OF AN ANALYTICAL MODEL FOR CALCULATION OF THE BLOCK VOLUME

Considering the common methods for block volume calculation reviewed in Section 4-1, and despite that Eq. 4-3 is widely used for this purpose (Palmström 1995; Cai *et al.* 2004b; Palmström 2005), a noticeable difference is found among the results of this model and real data. Thus, the block volume for 10 cases of rock mass that include three joint sets, has been calculated using Eq. 4-3 and compared with the result of 3DEC software in Table 4-2.

Table 4-2: Block volume calculation for a rock mass that includes three joint sets by Eq. 4-3 and 3DEC software

	Dip/dip direction			Spacing			Block volume (m^3)	
	J_1	J_2	J_3	J_1	J_2	J_3	Eq.4-3	3DEC
1	0/20	50/120	10/300	2	1	3	26.54	23.39
2	30/20	10/100	80/300	4	1	0.5	4.14	4.52
3	10/20	50/200	10/300	1	5	0.5	21.7	23.57
4	0/0	30/130	20/27	2	2	7	260.13	167.64
5	39/44	10/130	20/340	1	2	0.5	5.73	3.70
6	0/10	30/45	40/340	1	2	2	20.70	13.73
7	60/10	25/60	55/300	0.5	4	1	57.58	77.65
8	70/20	45/70	40/240	2	3.5	2.5	24.14	25.30
9	0/10	60/100	70/20	1	3	6	23.28	22.46
10	55/60	20/95	90/180	2	3	2	20.57	25.47

Based on Table 4-2, a considerable difference exists between the block volume calculation obtained using a previously developed model (Eq. 4-3) and the output of numerical simulation. As a result, a new model that can be used to calculate the volume of the block created by three persistent joint sets is developed in the following section. Initially, the significant rock mass parameters needed for block volume calculation are identified. Then, a vector model is developed to calculate the block volume in the case of three persistent joint sets. The model is validated by 3D numerical modeling using 3DEC software (Itasca Consulting Group 2021).

4.2.1 SELECTION OF THE SIGNIFICANT PARAMETERS FOR BLOCK SIZE CALCULATION

Rock mass consists of intact rock and a system of discontinuities. In a fractured rock mass, joint set is a family of parallel and evenly spaced planar

discontinuities that can be characterized by dip, dip direction, spacing, and other significant parameters as shown in Figure 4-1. The mechanical properties of a rock mass depend largely on the characteristics of the system of discontinuities and the strength of the intact rock (Palmström 2005).

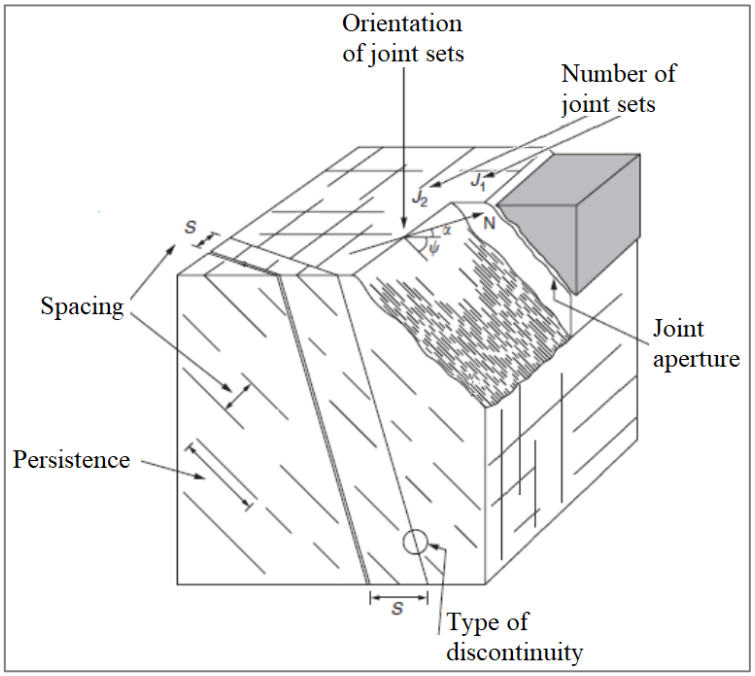

Figure 4-1: The structural characteristics of a rock mass (Wyllie et Mah 2004)

Based on Figure 4-1, a rock mass is an assembly of blocks superimposed on top of one another. Blocks are formed because of the presence of a system of discontinuities in the rock. Block shape and dimensions are defined by geometrical characteristics of joint sets, i.e., number of joint sets, spacing, dip, dip direction, and persistence. However, other geometrical properties of the rock mass, such as aperture and surface profile, do not affect the block size. As an analytical approach is used in this article, the ideal conditions of the discontinuities are assumed for

development of the model. A series of simplifying assumptions are considered, e.g., all joint sets are fully persistent and have fixed values of spacing and orientation. As a result, dip, dip direction, and spacing are assumed to be the only parameters that define block volume. In addition, according to Palmström (Palmström 1995), for a rock mass that includes less than three joint sets, the random joints define the block volume. For more than three joint sets, the block volume could be determined by considering a rock mass with three joint sets instead. Based on this statement and according to Table 4-1, the rock mass is assumed to include three joint sets in order to develop the analytical model.

4.2.2 MODEL DEVELOPMENT

Figure 4-2.a illustrates the rock mass that is created by cross of three joint sets considering the simplifying assumptions described in Section 4.2.1. However, by creating a model, the boundary blocks are mostly cut by the boundaries of the model, and only a couple of inner blocks remained intact, as shown in Figure 4-2.b and c. The outcomes of all previously developed and current models are used to calculate the volume of the intact blocks, i.e., the blocks shown in Figure 4-2.c.

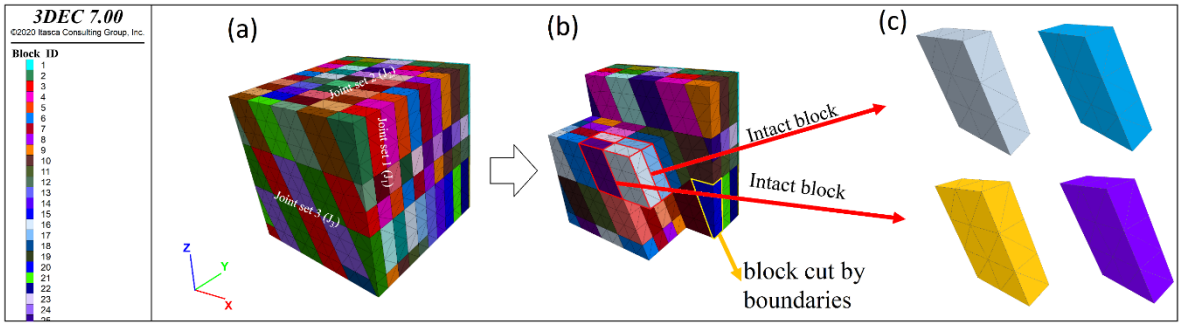

Figure 4-2. The methodology used for the analytical calculation of the block volume. (a) a model comprising three joint sets, (b) blocks that not cut by the boundaries of the model and boundary blocks (c) all the intact blocks are identical in dimension and volume (© A.S Koulibaly et al., 2021)

Except for the boundary blocks, the geometries of the all-other blocks are identical, as illustrated in Figure 4-2.c. To develop the model, one of the intact blocks of Figure 4-2.c is selected and analyzed in Figure 4-3.

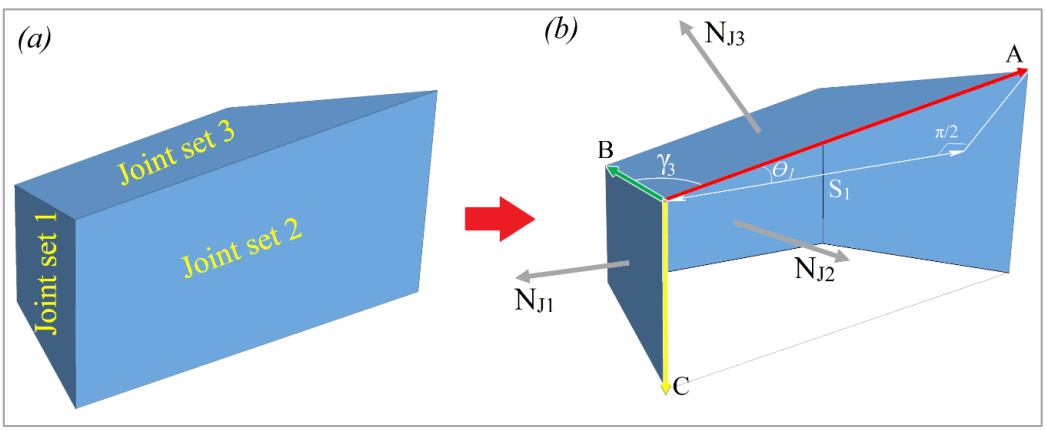

Figure 4-3. Block volume calculation method (a) an intact block that produced by three joint sets. (b) normal to joint set (N_{J1}, N_{J2} and N_{J3}), edge vectors (A, B, and C) and true spacing of joint set 1 (S_1) as well as the angle between edge vector A and S_1 (θ_1) and the angle between joint set 1 and 2 (γ_3) (© A.S Koulibaly et al., 2021)

According to Figure 4-3.a, each couple of parallel sides of the parallelepiped belongs to one joint set. On this basis, the edge vectors (A, B, and C) and normal vectors to joint set planes (N_{J1}, N_{J2}, and N_{J3}) are presented in Figure 4-3.b. The volume of the parallelepiped could be defined by Eq. 4-17, as follows:

$$V_b^A = \left|\left(\vec{A} \times \vec{B}\right).\vec{C}\right|, \qquad (4\text{-}17)$$

where V_b^A is the analytically calculated block volume, and A, B, and C are the block's edge vectors. In this equation, the multiplication sign (×) demonstrates the cross product, and the point (.) shows the inner product of a pair of vectors. Every vector, including an edge vector, have a direction and a magnitude. The direction of a vector can be specified by a unit vector, and for the case of edge vectors, the direction unit vectors could be defined by Eq. 4-18, as follows:

$$\begin{aligned} \overrightarrow{u_A} &= \overrightarrow{N_{J2}} \times \overrightarrow{N_{J3}} \\ \overrightarrow{u_B} &= \overrightarrow{N_{J1}} \times \overrightarrow{N_{J3}}, \qquad (4\text{-}18) \\ \overrightarrow{u_C} &= \overrightarrow{N_{J1}} \times \overrightarrow{N_{J2}} \end{aligned}$$

where N_{J1}, N_{J2}, and N_{J3} are the normal vectors to joint set J_1, J_2, and J_3, and u_A, u_B, and u_C are the unit vectors of A, B, and C, respectively. According to Figure 4-3, the magnitude of edge vectors could be determined by Eq. 4-19, as follows:

$$\begin{aligned} \left|\vec{A}\right| &= \frac{S_1}{\cos\theta_1} \\ \left|\vec{B}\right| &= \frac{S_2}{\cos\theta_2}, \qquad (4\text{-}19) \\ \left|\vec{C}\right| &= \frac{S_3}{\cos\theta_3} \end{aligned}$$

where $|A|$, $|B|$, and $|C|$ are the magnitudes of each edge vectors; S_1, S_2, and S_3 are the true spacing of joint sets 1, 2, and 3, respectively; and θ_1, θ_2, and θ_3 are the angles between normal to joint sets and the direction of the edge vectors. These

parameters are illustrated in Figure 4-3.b. γ (or γ_1 in Figure 4-3.b) is the angle considered by the previous studies (Palmström 1995; Cai *et al.* 2004b; Palmström 2005) for the development of Eq. 4-3.

Based on Eq. 4-19, to specify the magnitude of edge vectors, it is essential to determine θ_i. According to Figure 4-3.b, the angle θ could be defined by considering the inner product of normal to joint set vectors (N_J) and the unit edge vectors (u) according to Eq. 4-20, as follows:

$$\begin{aligned} \overrightarrow{u_A}.\overrightarrow{N_{J1}} &= |\overrightarrow{u_A}| \times |\overrightarrow{N_{J1}}| \times \cos\theta_1 \\ \overrightarrow{u_B}.\overrightarrow{N_{J2}} &= |\overrightarrow{u_B}| \times |\overrightarrow{N_{J2}}| \times \cos\theta_2 \\ \overrightarrow{u_C}.\overrightarrow{N_{J3}} &= |\overrightarrow{u_C}| \times |\overrightarrow{N_{J3}}| \times \cos\theta_3 \end{aligned} \qquad (4\text{-}20)$$

Given that u_A, u_B, and u_C and N_{J1}, N_{J2}, and N_{J3} are unit vectors, their absolute values are equal to 1. Then, by combining Eq. 4-18 and Eq. 4-20 we have:

$$\begin{aligned} \cos\theta_1 &= (\overrightarrow{N_{J2}} \times \overrightarrow{N_{J3}}).\overrightarrow{N_{J1}} \\ \cos\theta_2 &= (\overrightarrow{N_{J1}} \times \overrightarrow{N_{J3}}).\overrightarrow{N_{J2}} \\ \cos\theta_3 &= (\overrightarrow{N_{J1}} \times \overrightarrow{N_{J2}}).\overrightarrow{N_{J3}} \end{aligned} \qquad (4\text{-}21)$$

Considering Eq. 4-18, Eq. 4-19, and Eq. 4-21, the vectors A, B, and C could be determined by Eq. 4-22, as follows:

$$\vec{A} = \left|\vec{A}\right| \times \overrightarrow{u_A} = \frac{S_1}{\left(\overrightarrow{N_{J2}} \times \overrightarrow{N_{J3}}\right).\overrightarrow{N_{J1}}} \times \left(\overrightarrow{N_{J2}} \times \overrightarrow{N_{J3}}\right)$$

$$\vec{B} = \left|\vec{B}\right| \times \overrightarrow{u_B} = \frac{S_2}{\left(\overrightarrow{N_{J1}} \times \overrightarrow{N_{J3}}\right).\overrightarrow{N_{J2}}} \times \left(\overrightarrow{N_{J1}} \times \overrightarrow{N_{J3}}\right) \qquad (4\text{-}22)$$

$$\vec{C} = \left|\vec{C}\right| \times \overrightarrow{u_C} = \frac{S_3}{\left(\overrightarrow{N_{J1}} \times \overrightarrow{N_{J2}}\right).\overrightarrow{N_{J3}}} \times \left(\overrightarrow{N_{J1}} \times \overrightarrow{N_{J2}}\right)$$

The normal vector to joint sets (N_{J1}, N_{J2}, and N_{J3}) could be defined by Eq. 4-23, as follows:

$$\overrightarrow{N_{J1}} = (\sin DD_1 . \sin D_1)\vec{\imath}, (\cos DD_1 . \sin D_1)\vec{\jmath}, (-\cos D_1)\vec{k}$$

$$\overrightarrow{N_{J2}} = (\sin DD_2 . \sin D_2)\vec{\imath}, (\cos DD_2 . \sin D_2)\vec{\jmath}, (-\cos D_2)\vec{k}\ , \qquad (4\text{-}23)$$

$$\overrightarrow{N_{J3}} = (\sin DD_3 . \sin D_3)\vec{\imath}, (\cos DD_3 . \sin D_3)\vec{\jmath}, (-\cos D_3)\vec{k}$$

where DD_1, DD_2, and DD_3 are dip directions, and D_1, D_2, and D_3 are dip of the joint sets 1, 2 and 3, respectively. Finally, block volume could be specified through the incorporation of Eq. 4-23 and Eq. 4-22 into Eq. 4-17. By obtaining the information on the dip, dip direction, and true spacing of the three joint sets, the volume of the intact blocks could be determined by Eq. 4-17. For easier use of Eq. 4-17, an excel spreadsheet for calculating the block volume has been attached to this article.

4.2.3 MODEL VALIDATION

The result of the proposed method for the calculation of the block volume with Eq. 4-17 is compared with the output of the numerical simulations using 3DEC version 7 software (Itasca Consulting Group 2021). A series of 13 cases with

various arrangements of dip, dip direction, and spacing are considered. Accordingly, the results of each method are listed in Table 4-3. The volume calculated in Table 4-2 and Table 4-3 belongs to the intact block, as shown in Figure 4-2.b and c.

Table 4-3: Discontinuity's characteristics used for comparison of block volume calculation by analytical and numerical methods

	Joint set 1			Joint set 2			Joint set 3			Block volume (m^3)	
Case	DIP 1	DD 1	Spacing 1 (m)	DIP 2	DD 2	Spacing 2 (m)	DIP 3	DD 3	Spacing 3 (m)	3DEC	Eq.4-17
1	23	30	0.34	20	10	2.05	27	320	0.14	15.14	15.14
2	90	350	0.39	20	352	0.14	90	10	0.39	0.07	0.07
3	73	25	0.35	61	352	0.35	84	8	5.91	4.60	4.60
4	22	25	0.34	90	350	0.98	60	0	0.35	3.65	3.65
5	90	350	0.39	90	10	0.39	32	50	2.05	1.08	1.08
6	90	350	5.91	90	70	0.14	90	30	5.2	N/A	N/A
7	20	350	0.34	22	25	1.37	61	354	5.2	17.02	17.02
8	54	65	0.34	90	350	0.98	90	30	0.35	0.31	0.31
9	80	0	5.91	90	70	0.14	66	292	0.34	1.04	1.04
10	60	0	3.46	67	340	5.2	90	30	0.87	85.36	85.35
11	90	30	3.46	54	295	1.37	80	0	3.94	124.94	124.90
12	90	70	0.34	43	300	1.37	73	25	5.2	7.09	7.09
13	43	60	0.14	73	335	5.2	90	10	0.39	0.51	0.51

To numerically calculate the volume of the intact block with 3DEC software, a FISH function is embedded in the command lines to define the maximum block size of the model. For this purpose, the numerical model should be large enough to contain at least one intact block. The maximum block size did not change with further increase of the model size.

In addition, according to Table 4-2, in most of the cases, a major difference exists among the results of the previously developed model (Palmström 1995) and

the output of the numerical simulations. However, the calculation of the block volume with the developed model in this article is completely in accordance with the results of 3DEC, as shown in Table 4-3. Furthermore, in case number 6 of Table 4-3, the block volume is defined to be unlimited by numerical simulations and by Eq. 4-17. However, Eq. 4-3 specifies a real value for the block volume that is calculated by this method (10.57 m^3).

A series of analytical models are already developed to calculate the volume of blocks formed by the intersection of three joint sets in a rock mass, as listed in Table 4-1. In the models, all joint sets can be assumed to be persistent, and the orientations and spacing of the discontinuities are constant. As the results of these methods are not sufficiently accurate, a more efficient model is developed in the current study. This developed method calculates the block volume by determining the dip, dip direction, and spacing of the joint sets.

Based on Eq. 4-17, the block volume is defined by inner and cross products of parallelepiped edge vectors. If all edge vectors (A, B, and C) are perpendicular to each other, the volume of the formed block is equal to multiply of the edge's values. This case is correctly calculated by considering $\theta_1 = \theta_2 = \theta_3 = \pi/2$ in Eq. 4-21 and Eq. 4-22. Accordingly, the block volume is defined by $V_b^A = |A|\times|B|\times|C|$. However, the volume of the case number 6 in Table 4-3 is defined as 10.57 m^3 by

Eq. 4-3 despite the fact that Eq. 4-17 and the numerical model calculate the infinite block volume for this case. For better comprehension of the case, a 3D model of case number 6 with different values of spacing is illustrated in Figure 4-4. The spacing is selected to be different from case number 6 for better visualization of the formed block. However, it does not affect the whole issue.

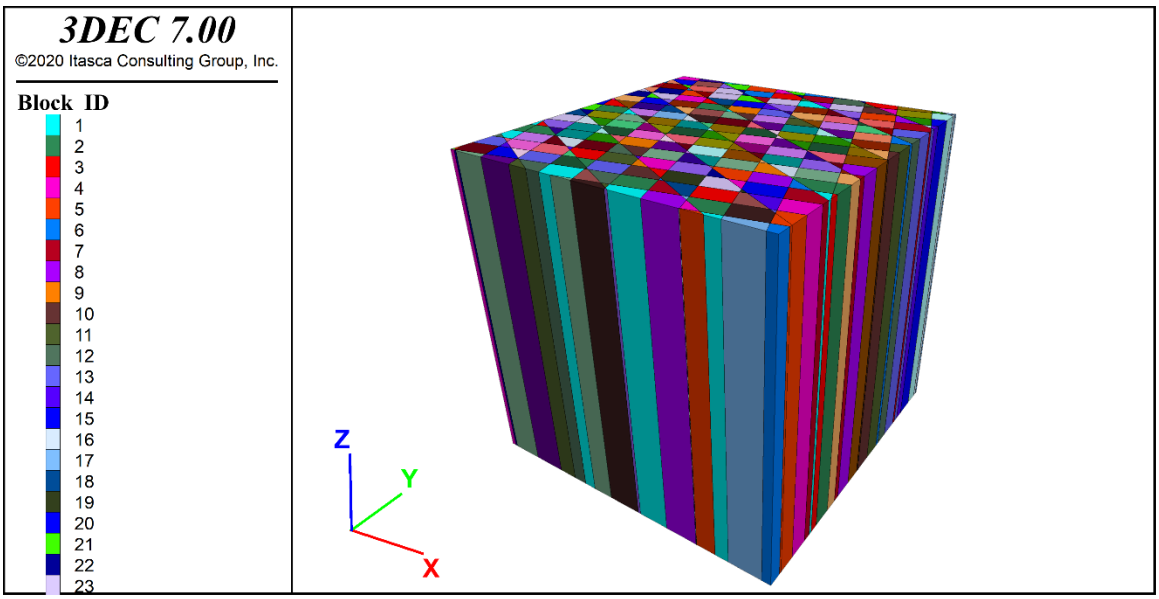

Figure 4-4. A 20x20 m rock mass that includes three joint sets with dip/dip direction according to case number 6 of Table 4-3, but with different spacings (2, 3, and 4 meters for joint sets 1, 2, and 3, respectively) (© A.S Koulibaly et al., 2021).

According to Figure 4-4, all formed blocks are stretched vertically. Hence, by increasing the size of the numerical model, the blocks expand in an unlimited manner. The output obtained using the developed model is in accordance with the results of the numerical simulations, and both are in conflict with the results that obtained from the previously developed model (Eq. 4-3).

4.3 COMPARISON OF THE METHODS FOR BLOCK VOLUME CALCULATION

4.3.1 PREPARATION OF THE DATABASE

The Pells database (Pells 2016b) was used to compare previously developed models with the one presented in this article (method "A") for calculation of the block volume. This database was made up of field data collected from more than 100 real case studies conducted on the uncoated flow channels of the spillways in Australia and South Africa. In addition, it summarizes all the relevant geomechanical parameters, i.e., dip, dip direction of joints, and spacings. To adjust the compatibility between this database and the methods listed in Table 4-1, the cases that include only three persistent joint sets and do not comprise columnar blocks, as shown in Figure 4-4, are selected in this study and listed in Table 4-4.

Table 4-4: Characteristic data of the database summarizing the case studies of Pells (Pells 2016b)

	Dip/Dip direction			Joint spacing (m)				Angle between joint sets (°)			
	Joint Set 1	Joint Set 2	Joint Set 3	Joint Set 1	Joint Set 2	Joint Set 3	Average (S_a)	Angle 1-2	Angle 1-3	Angle 2-3	Average
1	25/110	30/230	20/220	0.75	1	1.5	1.08	47	36	11	31
2	10/50	90/192	90/50	0.35	2.5	6	2.95	97	80	142	106
3	05/50	35/50	90/120	0.35	6	4	3.45	30	88	78	65
4	10/50	80/130	90/65	1.5	4.5	0.06	2.02	78	80	65	74
5	10/50	30/350	90/50	1.2	0.75	10	3.98	26	80	75	60
6	05/50	90/140	90/80	1.75	0.4	0.7	0.95	90	85	60	78
7	5/200	80/250	80/225	1.5	1.75	10	4.42	76	75	24	58
8	5/200	80/250	80/225	1.5	3	10	4.83	76	75	24	58
9	5/200	80/225	80/140	0.65	6.5	0.65	2.60	75	77	83	78
10	5/200	80/225	80/140	0.65	6.5	0.65	2.60	75	77	83	78
11	57/150	80/243	19/165	0.4	1.1	1.35	0.95	87	38	76	67
12	57/150	80/243	19/165	0.4	1.1	1.35	0.95	87	38	76	67
13	57/150	80/243	19/165	0.4	1.1	1.35	0.95	87	38	76	67
14	70/77	80/335	35/335	0.22	0.3	0.4	0.31	97	80	45	74
15	20/74	80/335	80/290	0.8	0.55	1.6	0.98	83	96	44	74
16	20/63	80/316	75/5	0.8	0.55	0.55	0.63	86	65	48	66
17	41/193	72/244	80/337	0.8	0.8	0.8	0.80	51	113	89	84
18	85/280	76/51	27/208	0.65	1.5	0.8	0.98	128	77	101	102
19	90/98	90/192	0/100	0.7	0.7	0.5	0.63	94	90	90	91
20	50/160	90/255	35/155	0.9	0.4	1.15	0.82	71	15	79	55
21	9/105	90/237	90/170	0.4	8	20	9.47	96	86	67	83
22	9/105	90/237	90/170	0.4	8	20	9.47	96	86	67	83
23	9/105	90/237	90/170	0.4	8	15	7.80	96	86	67	83
24	9/105	90/237	90/170	0.4	8	15	7.80	96	86	67	83
25	0/150	90/75	90/202	0.6	0.075	0.2	0.29	90	90	127	102
26	12/150	90/75	90/202	0.6	0.075	0.2	0.29	87	82	127	99
27	10/65	62/75	90/310	0.35	1	0.5	0.62	52	94	120	89
28	35/200	90/202	90/310	0.35	0.2	0.5	0.35	55	101	108	88
29	22/228	75/172	77/246	0.15	0.1	0.15	0.13	64	56	71	64
30	80/278	80/130	35/280	10	0.3	0.55	3.62	142	45	110	99
31	75/278	80/130	58/200	10	1	0.4	3.80	101	56	67	75
32	90/220	86/103	9/133	0.8	3	0.45	1.42	116	89	78	94
33	80/231	65/162	15/250	1.25	0.2	0.45	0.63	66	65	65	65
34	62/243	83/144	34/130	0.19	0.45	0.45	0.36	94	78	50	74
35	25/150	35/340	85/250	0.4	2	0.4	0.93	59	89	86	78
36	25/150	35/340	85/250	0.4	2	0.4	0.93	59	89	86	78
37	65/250	85/190	55/350	0.4	0.13	0.4	0.31	60	83	135	93
38	65/250	85/190	55/350	0.4	0.06	0.4	0.29	60	83	135	93
39	25/110	90/90	90/0	0.4	1.3	1.3	1.00	66	98	90	85
40	25/110	90/90	90/0	0.4	1.3	1.3	1.00	66	98	90	85
41	25/110	90/90	90/0	0.4	1.3	1.3	1.00	66	98	90	85
42	25/110	90/90	60/0	0.4	1.3	1.3	1.00	66	70	90	75
43	25/110	90/90	60/0	0.4	1.3	1.3	1.00	66	70	90	75
44	45/55	57/235	75/0	0.06	0.06	0.06	0.06	102	55	109	89
45	45/55	57/235	75/0	0.06	0.06	0.06	0.06	102	55	109	89
46	45/55	57/235	75/0	0.06	0.06	0.06	0.06	102	55	109	89
47	45/55	57/235	75/0	0.06	0.06	0.06	0.06	102	55	109	89
48	25/0	60/220	63/145	0.4	0.06	1.3	0.59	80	84	64	76
49	25/0	60/220	63/145	0.4	1.3	1.3	1.00	80	84	64	76
50	25/0	60/220	63/145	0.4	1.3	1.3	1.00	80	84	64	76
51	20/270	72/180	85/0	1.3	1.3	1.3	1.30	73	85	157	105
52	20/270	72/180	85/0	1.3	1.3	1.3	1.30	73	85	157	105
53	20/270	72/180	85/0	0.4	0.4	0.4	0.40	73	85	157	105
54	20/270	72/180	85/0	0.4	0.4	0.4	0.40	73	85	157	105
55	20/270	72/180	85/0	0.4	0.13	0.4	0.31	73	85	157	105
56	15/150	80/250	80/90	1.3	1.3	0.4	1.00	82	72	151	102
57	15/150	80/250	80/90	1.3	1.3	0.4	1.00	82	72	151	102
58	15/150	80/250	80/90	1.3	1.3	0.4	1.00	82	72	151	102
59	15/150	80/250	80/90	1.3	1.3	0.4	1.00	82	72	151	102
60	15/150	80/250	80/90	1.3	1.3	0.4	1.00	82	72	151	102
61	0/0	90/10	80/290	1.3	1.3	1.3	1.30	90	80	80	83
62	0/0	90/10	80/290	0.4	1.3	0.4	0.70	90	80	80	83
63	0/0	90/10	80/290	1.3	1.3	1.3	1.30	90	80	80	83
64	0/0	90/10	80/290	1.3	1.3	1.3	1.30	90	80	80	83
65	0/0	90/10	80/290	0.4	0.4	0.4	0.40	90	80	80	83
66	0/0	90/10	80/290	1.3	1.3	1.3	1.30	90	80	80	83
67	0/0	90/10	80/290	0.4	0.4	0.4	0.40	90	80	80	83
68	30/12	90/105	80/195	0.4	0.4	0.13	0.31	91	110	90	97
69	30/12	90/105	80/195	0.4	0.4	0.13	0.31	91	110	90	97
70	30/12	90/105	80/195	0.4	0.4	0.13	0.31	91	110	90	97
71	30/12	90/105	80/195	0.4	0.4	0.13	0.31	91	110	90	97
72	30/12	90/105	80/195	0.4	0.4	0.13	0.31	91	110	90	97

4.3.2 BLOCK VOLUME CALCULATION

The block volume for 72 cases of joint sets that listed in Table 4-4, is calculated using the previously developed methods listed in Table 4-1 and the method developed in this study (Eq. 4-17- method "A"), and the results are presented in Figure 4-5.

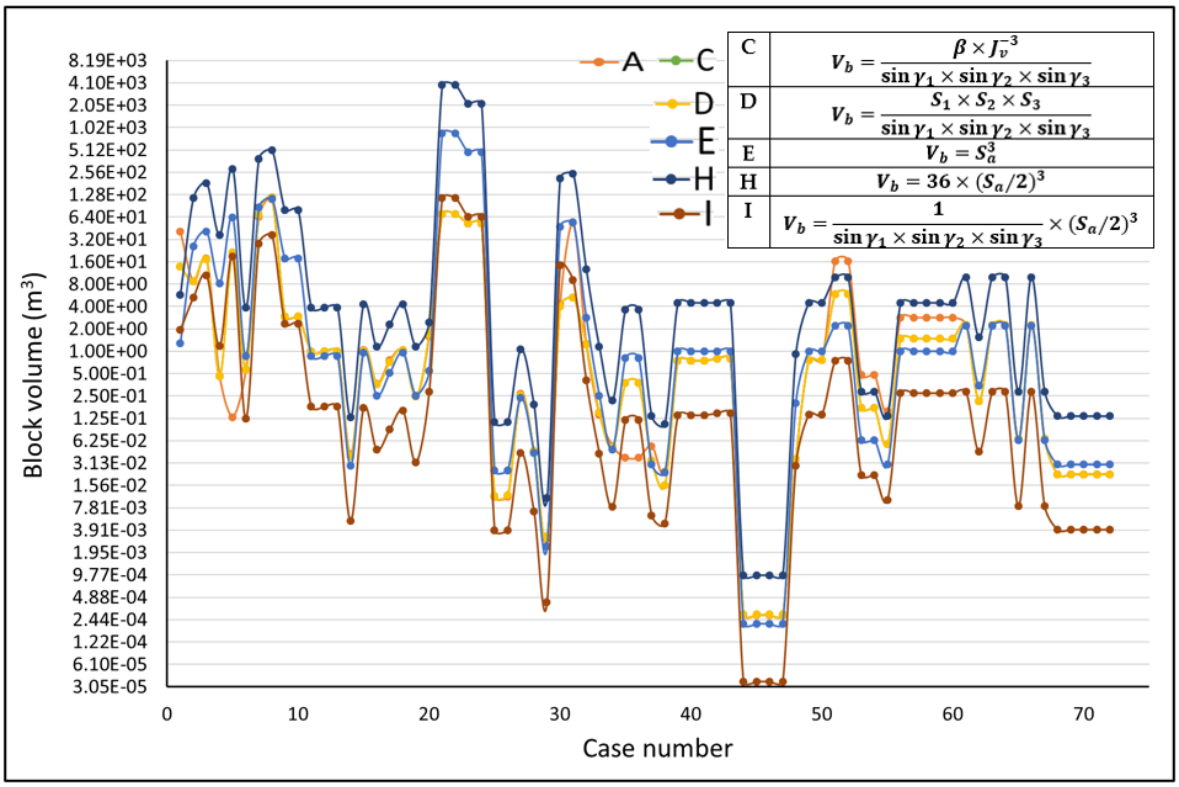

Figure 4-5. Graphical representation of the block volumes for the cases presented in Table 4-4, that are calculated by models of Table 4-1 and the method that is developed in this article (method "A"). NB: method C and D give the same results, which is why curve C is visible. (© A.S Koulibaly et al., 2021)

According to Figure 4-5, the results of the models are compatible with each other in some ranges and incompatible in other ranges. Most of the differences exist in the range of case numbers 1 to 11, 20 to 25, 29 to 32, 44 to 47, and 67 to 72. Method *A* (Eq. 4-17) can calculate the block volume accurately. Thus, whether the

method overestimates or underestimates the block volume was determined. Comparison result of the graphs of other methods with method *A* shows that methods C, D, E and I mostly underestimate, whereas method H greatly overestimates block volume for the data of Table 4-4.

From Figure 4-5 and according to Elci and Turk (Elci et Turk 2014), a noticeable difference exists between the actual value of the block volume and that obtained using previously developed methods. To better evaluate the differences, the Root Mean Square Error (RMSE) of the existing methods for block volume calculation for the cases of Figure 4-5 is explained in detail in Section 4.3.3.

4.3.3 ROOT MEAN SQUARE ERROR (RMSE) CALCULATION

RMSE measures the difference between the actual and expected values of a specific parameter. The lower the RMSE value, the more accuracy is expected. For block volume calculation, RMSE is defined by comparing results that obtained using the previously developed models with method *A* (Eq. 4-17), as the accuracy of this method is already validated in Section 4.2.3. The RMSE values of each method are listed in Table 4-5.

Table 4-5: RMSE of block volume calculation results obtained by previously developed methods compared with the method developed in this study (Eq. 4-17-Method "A") for the cases of Figure 4-5

Method	Equation	Reference value	RMSE
C	$V_b = \frac{\beta \times J_v^{-3}}{\sin\gamma_1 \times \sin\gamma_2 \times \sin\gamma_3}$	$V_b^A = \lvert(\vec{A} \times \vec{B}).\vec{C}\rvert$	7
D	$V_b = \frac{S_1 \times S_2 \times S_3}{\sin\gamma_1 \times \sin\gamma_2 \times \sin\gamma_3}$		7
E	$V_b = S_a^3$		148
H	$V_b = 36 \times (S_a/2)^3$		20
I	$V_b = \frac{1}{\sin\gamma_1 \times \sin\gamma_2 \times \sin\gamma_3} \times (S_a/2)^3$		15

Based on Table 4-5, the accuracy of most of the previously developed models is questioned. The RMSE varies from 7 to 148 and shows a noticeable deviation between the actual and the calculated values of the block volume. The source of the error is discussed in Section 4.4 in order to identify the block characteristics that affect the accuracy of block size values.

4.4 DISCUSSION

Geomechanical and geometrical characteristics of the joints have an indisputable impact on the mechanical properties of the rock mass. The block volume is a geometrical parameter that has a significant impact on the mechanical properties of the fractured rock mass. Commonly used methods for calculating block size in a fractured rock mass were developed based on measurements of spacings and the orientation of the joint sets. For better discussion of the various

methods, all joint sets in a rock mass are assumed to be persistent. Eq. 4-3 is one of the most widely used equations and comprises the spacings of the joint sets and the angle between them. This equation comprises 3 parts ($S_i/sin\gamma_i$), and as a result, the author estimated $sin\gamma_i$ by $cos\ \theta_i$; i.e., $sin\gamma_i \approx cos\theta_i$, where θ_i is the angle between apparent and true spacing of joint sets, as illustrated in Figure 4-3. Therefore, $S_i/sin\gamma_i \approx Sp_i$, where Sp_i is the apparent spacing of joint set i. By these assumptions, Eq. 4-3 calculates the block volume by the multiplication of three apparent spacings. Almost the same logic is behind the development of the other equations for the calculation of the block volume. However, two major criticisms of the utilization of these methods exist. First of all, approximation of the volume of a parallelepiped block by multiplication of the apparent spacings by itself is accompanied with error; it is a reminder of the right method for calculation of the parallelepiped volume. The second source of the error belongs to the estimation of the apparent spacings by true spacing and the angle between joint sets. The apparent spacing is accurately calculated using the $Sp_i = S_i/cos\theta_i$ relation. However, approximation of $sin\gamma_i$ by $cos\theta_i$ is fundamentally accompanied by the error in calculation of the block volume. This phenomenon occurs despite the fact that the angle θ_i is considered for the development of Eq. 4-17. Table 4-5 lists the errors produced by each method compared with the block volume calculated by Eq. 4-17. However, the error values differ from one model to another. At first glance, the

accuracy of the method that has the least difference with method *A*, i.e., methods D and C in Table 4-5, is more than that of the other models. However, the type of data and geometrical characteristics of the rock mass that are used to determine the error has a direct impact on the error value. To systematically evaluate the error of each method for calculation of the block volume, the error function should be specified in the range of variation of the effective parameters. By doing this, specifying the ranges of reliability for each model becomes possible. However, the error values listed in Table 4-5 are a sample of the field data for calculation of the block volume and could represent the overall accuracy of each model.

4.5 CONCLUSION

An analytical model based on vector product has been developed to calculate the block volume for the case of three persistent joint sets with constant values of spacing and orientation. The accuracy of the model is validated by the numerical simulation. The results of the developed model are more reliable than those of the previously developed ones. The method could be applied using the vector product (an excel spreadsheet is attached to this article) by knowing dip, dip direction, and spacings of joint sets.

The accuracy of previously developed methods in block volume calculation is evaluated using a series of field data in Table 4-5. Despite that the error values

differ from one model to another, a range of variation for each parameter could be specified, so that the accuracy level of the model can be acceptable.

4.6 DECLARATIONS

FUNDING

Natural Sciences and Engineering Research Council of Canada (NSERC) and Hydro-Québec provide the funding through the CRD (CRD 537350) program.

DECLARATION OF COMPETING INTEREST

The authors declare that there is no conflict of interest associated with this publication.

CODE AVAILABILITY

The Itasca 3DEC version 7.0 software with license number 215-001-0266-00001 under the IEP loan program has been used in this research.

ACKNOWLEDGMENT

The authors would like to thank the Natural Sciences and Engineering Research Council of Canada (NSERC) and Hydro-Québec for funding through the RDC (RDC 537350) program. Furthermore, the authors want to deeply thank Itasca Consulting Group in Minneapolis for the IEP Research Program, especially Jim Hazzard, for his valuable technical help and advice.

CHAPITRE 5

CONCEPTION D'UN MODÈLE PHYSIQUE RÉDUIT D'ÉVACUATEUR DE CRUES POUR L'ÉVALUATION DE L'ÉRODABILITÉ HYDRAULIQUE D'UN MASSIF ROCHEUX FRACTURÉ

Ce chapitre reprend un article dont le 1er auteur est l'auteur de ce mémoire. Le chapitre présente la conception d'un modèle physique réduit d'évacuateur ainsi quelques résultats issus du test d'écoulement sur le modèle.

L'article est au stade de la révision avant soumission.

DESIGN OF A REDUCED-SCALE PHYSICAL MODEL OF A SPILLWAY TO EVALUATE THE HYDRAULIC ERODIBILITY OF FRACTURED ROCK MASS

Aboubacar Sidiki Koulibaly[1*], Ali Saeidi[1], Alain Rouleau[1], Marco Quirion[2]

[1] Université du Québec à Chicoutimi, 555 boulevard de l'Université, Chicoutimi, Québec, G7H 2B1; ali_saeidi@uqac.ca ; alain_rouleau@uqac.ca

[2] Hydro-Québec Production Unité Expertise en barrages, 75 boulevard René-Lévesque Ouest, Québec, H2Z 1A4, Canada; quirion.marco@hydro.qc.ca

[*]Correspondance : Aboubacar-sidiki.koulibaly1@uqac.ca ; Tel.: +1-581-235-1247

ABSTRACT

Hydraulic erosion of the rock mass at the dam spillway is an important phenomenon considered in assessing the stability of dam infrastructures. As it is clearly resulting from the interaction between water and the rock mass of the spillways, the methods commonly used to assess this phenomenon use the notion of a threshold line, a correlation between the erosive force of the water and the resistance of the rock mass against erosion. These methods are empirical or semi-empirical in nature, and they have been developed based on a limited amount of available data from dam sites, and on data from other rock engineering domains such as excavability. The effect of each parameter of the rock mass on the erosion processes have not been determined due to the limitation of existing data. The laboratory-scale physical model that is presented in this paper has been developed to determine the effects of rock mass parameters on erosion. This model is designed for considering and measuring the effect of several parameters on the

rock mass erosion, such as joint opening, block size, joint shear strength and the nature of potentially erodible surface.

ARTICLE HIGHLIGHTS

- ✓ Design of a reduced physical model of a spillway.
- ✓ Identification of various rock mass parameters controlling the resistance of bedrock against the erosive force of water.
- ✓ Identification of the various characteristic parameters of the hydraulic load at the spillways.
- ✓ Variation of the erosive force of the water according to the various geomechanical parameters of the rock mass.

KEYWORDS

Erosive force, Hydraulic erosion, Hydraulic pressure, Rock mass, Physical model, Spillway.

5.1 INTRODUCTION

Water retention structures such as dams are equipped with spillway to discharge excess water arriving at the dam during high-flow periods to ensure the stability of the dams. These structures are provided with either a flow channel or a plunge pool excavated in the rock. Sometimes the bedrock is covered with concrete if it is assessed to be not resistant enough against the erosive force of the water. In most cases, though, the bedrock is not lined, as it is considered as capable to resist the erosive force of water, but a number of cases of important erosion has been

observed over time. In February 2017, a large cavity was observed in the spillway of Oroville dam in California following a water discharge. Another example is given by the 113 m high Copeton embankment dam in Australia where a 20 m deep gorge was observed in the rocky mass of the spillway (Pells 2016a) after operation. Several methods are proposed to assess the hydraulic erosion of rock mass downstream of dam spillways. Some of these methods are currently used in the spillway design phase (Moore *et al.* 1994; Pells 2016a). In these methods, the hydraulic conditions are assessed, by considering an erosive force called dissipation of the hydraulic power of the water and the quality of the rock mass by way of an index developed by a number of researchers. Most of these methods are empirical in nature and based mainly on the results of a few small-scale prototypes in the laboratory (Annandale 2006a). Hence important questions are yet unanswered concerning effectiveness of the methods that are used for predicting hydraulic erosion of rock mass. All of these methods use the notion of a "threshold line", obtained by the correlation between the erosive force of the water and the resistance of the rock mass. The methods commonly cited in the literature are summarized in Table 5-1.

Table 5-1. Methods currently used to assess hydraulic erosion of rock mass.

Methods	**Correlation function**		**Types of methods**	**Considered parameters**
(Moore *et al.* 1994)	Energy dissipation Vs. Kirsten's index	$\Pi_{UD} = f(K_h)$	Empirical to semi-empirical methods	$\Pi_{UD} = \rho.g.q\frac{dE}{dx}$ $K_h = M_S \cdot K_b \cdot K_d \cdot Js$ $eGSI = GSI + E_{doa}$ $RMEI_B = (RF_{P1}.LF_{P1}).(RF_{P2}.LF_{P2}).[(RF_{P3}.LF_{P3}) + (RF_{P4}.LF_{P4}) + (RF_{P5}.LF_{P5})]$ $K_{I,in} = (0{,}105\ to\ 0{,}132)T + (0{,}054\sigma_c) + 0{,}53$ $K_{I,in} = (0{,}008\ to\ 0{,}010)UCS + (0{,}054\sigma_c) + 0{,}42$ $K_I = 0{,}8.P_{max}.F.\sqrt{\pi.L_f}$
(Van Schalkwyk *et al.* 1994)				
(Annandale 1995)				
(Kirsten *et al.* 2000)				
(Pells *et al.* 2016b)	Energy dissipation Vs. Geological strength index for erodibility	Π_{UD} Vs. *eGSI*		
	Energy dissipation Vs. Rock mass erodibility index	Π_{UD} Vs. *RMEI*		
(Bollaert et Schleiss 2002; Bollaert 2004; Bollaert et Schleiss 2005)	Stress applied to the rock mass Vs. In-situ resistance of a rock mass	K_I Vs. $K_{I\text{-}in}$	Semi-analytical methods	

A number of indices have been developed to determine the resistance to erosion using different parameters of the intact rock and the rock mass.

- The Kirsten index (K_h) is based on the confined compressive strength of the intact rock (M_s), the shear strength of the rock joints (K_d), the size of the rock blocks (K_b), the relative structure of the blocks (J_s), which considers the effect of the shape and orientation of the blocks with respect to the flow direction of water in the canal.
- The Geological Strength index for erodibility (*eGSI*) is based on the *Geological Strength Index* (*GSI*), a classification index of the rock mass developed by Hoek (Hoek *et al.* 1998) and the relative structure of the blocks (E_{doa}), which considers the effect of the shape and orientation of the blocks with respect to the flow direction of water in the channel.
- The Rock Mass Erodibility Index ($RMEI_B$) is based on the relative importance factor (*RF*) and the likelihood (*LF*) of 5 geomechanical parameters (*P1* to *P5)*, representing *P1* the viable mechanisms at kinematic separation of the blocks, *P2* the nature of the potentially eroded surface, *P3* the nature of the joints contained in the rock mass, *P4* the spacing between the joints, and *P5* the shape of the blocks.

- The In-situ resistance indices ($K_{I,in}$) is based on the tensile strength of the rock (T), the unconfined compressive strength (UCS in MPa) and the horizontal confinement in situ stress (σ_c in MPa).

Concerning the erosive force of water, two different indices or hydraulic parameters are most often considered.

- The Dissipation of energy (Π_{UD} in kW.m^{-2}) include the density of water (ρ in kg.m^{-3}), the gravity acceleration (g in m.s^{-2}), the flow rate per unit length of channel width $\left(q = Q/B_f\text{, in m}^2.\text{s}^{-1}\right)$ where B_f is the channel width (m) and Q is the water flow rate (m^3.s^{-1}), and the energy loss during flow $\left(\frac{dE}{dx}\right)$.
- The Stress applied to the rock mass (K_I in MPa.m$^{1/2}$) include the maximum instantaneous dynamic pressure in the diving pool (P_{max}), the correction factor depending on the types of the joint when it is persistent (F) and the total length of a joint (L_f in m).

The application of these methods on some dams suggests that no strong erosion should occur, but the observations made after the dams have been put into operation indicate the opposite. The empirical nature of these methods makes it difficult to identify the conditions for which the method does not allow a correct prediction, in particular it is impossible to study the combined effects of several geomechanical parameters on erosion using these methods. Also all of these

methods have been developed based on erosion results observed on a few dams in Australia, the United States and South Africa. These results are limited and do not cover all the geomechanical and hydraulic conditions observed at spillways around the world. In this context, the use of laboratory-scale prototypes is a very effective option for determining the effects of several parameters controlling erosion process.

A number of physical models have been developed to study hydraulic erosion process. These reduced-scale models are designed either to study the hydraulic characteristics of the flow, or the phenomena of erosion in granular materials or in rock mass, or to validate the hypotheses which are the basis for the establishment of some erosion evaluation methods. These models generally allow the acquisition of data from tests on different configurations of spillways and different types of rock mass.

In general, these reduced models can be classified into two categories, namely models which only study the hydraulic parameters and models also including the study of the geomechanical parameters of the rock mass of erosion. The first category of physical model focuses in particular on the study of hydraulic parameters affecting erosion such as the slope of the channel, the flow rate, and the roughness of the surface on the hydraulic parameter like pressure and energy

(Withers 1991; Manso et Schleiss 2006; Lesleighter *et al.* 2016; Gu *et al.* 2017; Kote et Nangare 2019). Some models in this first category aim to study different solutions for reducing hydraulic power downstream of spillways and others serve at simulating water flow or spillway erosion downstream in specific situations (Sawadogo 2010; Tuna 2012; Wilkinson *et al.* 2018).

The second category of models study the effects of geomechanical parameters of the rock mass on the hydraulic erosion process. These models make it possible to evaluate the distribution of the pressure applied by the flow on instrumented blocks; the configuration of these blocks is intrinsically linked to a few geomechanical parameters including the orientation of the joints, as well as the shape and the protrusion of the blocks. The type of water flow that is considered is either a plunging jet or an open flow channel (Table 5-2). This table summarize information that characterizes these models, whether they represent a reproduction of a real spillway, the hydraulic parameters used (flow rate or velocity), the geomechanical that evaluated, and their mode of quantification of these parameters; either quantitative if measurements are carried out or qualitative if the parameter is characterized by simple comparison.

Table 5-2. Summary of reduced physical models of spillways developed to study the effects of the geomechanical parameters of the rock mass on erosion.

Authors	**Model types**	**Configuration**	**Maximum flow or velocity**	**Analysis method of measured parameters**
(Montgomery 1984)	Horizontal flow channel	**Variable:** Vertical orientation of blocks Opening the joints **Fix:** Size and shape of blocks	250 L/s	**Quantitative** Pressure measurements on the faces of a block
(Reinius 1986)	Horizontal flow channel	**Variable:** Vertical orientation of blocks **Fix:** Opening the joints Size and shape of blocks	311 L/s	**Quantitative** Pressure measurements on the faces of a block
(Annandale *et al.* 1998)	Jet plunging into a pool	**Fix:** Disposition of Block Jet characteristics	3400 L/s	**Quantitative** Pressure measurements in the joints
(Liu *et al.* 1998)	1: 100 scale model of a plunging jet type evacuator	**Variable:** Size of blocks Jet characteristics **Fix:** Orientation and opening of joints	87 L/s	**Quantitative** Pressure measured under the block
(Bollaert et Schleiss 2002)	Vertical jet in a basin	**Variable:** Jet characteristics Types of joints **Fixe :** Joints orientation	120 L/s	**Quantitative** Pressures measured in the joints and at the surface of the basin
(Wang et Jiang 2010)	Flow channel and 1: 100 scale model of a spillway Inclination : 1.44-2.62%	**Variable:** Inclination of the spillway **Fixe:** Geometric configuration and discharge	38 m / s	**Quantitative** Channel: Pressure drop Model: Flow velocity
(George *et al.* 2015)	Tetrahedral block placed in a flow channel inclined at 21°	**Variable:** Orientation of block **Fixe:** Inclination of the channel Block size and shape	300 L/s	**Quantitative** Block movement and ejection speed
(Pells 2016a)	Cubic block placed in the center of a flow channel inclined at 4.6° to 11.1°	**Variable:** Orientation and protrusion of the block Flow characteristics **Fixe:** Opening the joints	350 L/s	**Quantitative** Pressure and force measurements on the faces of the block

Some of the physical models of this category make it possible to relate the hydraulic parameters to some geomechanical parameters. To assess hydraulic erosion, these models considered different geomechanical parameters individually in relation to hydraulic pressure. A more comprehensive approach would be to evaluate also possible interactions between these geomechanical parameters, and their combined effects on the erosion process, because most of the geomechanical parameters are interrelated.

Boumaiza et al. (2019) have proposed a hierarchy of the most important rock mass parameters affecting the erosion process in a spillway. The physicals models present in Table 5-2 can be further classified according to their applicability to study the effect of each one of the identified geomechanical parameters on the erosion process (Table 5-3).

Table 5-3. Summary of the parameters evaluated by the existing scale model

Type of flows	**Model**	**Orientation parameter**	J_o	V_b	K_d	*NPES*	**Protrusion**
Plunging jet	(Annandale *et al.* 1998)						
	(Liu *et al.* 1998)			X			
	(Bollaert et Schleiss 2002)		X				
Open channel	(Montgomery 1984)	X	X				X
	(Reinius 1986)	X					X
	(Wang et Jiang 2010)					X	
	(George *et al.* 2015)	X					X
	(Pells 2016a)	X					X

Note : ***NPES*** corresponds to the nature of the potentially erodible surface.

It appears that some parameters are studied much more than others, such as the orientation of the joints and the protrusion of the blocks. Most of the other parameters are very little investigated. For example, the shear strength of joints was not studied although this parameter is identified as having an important role in the erosion of rock mass. Thus, these physical models only allow a partial evaluation of the hydraulic erosion process. Also, a major problem associated with the existing physical models is the representativeness of the characteristic parameters of the erosion phenomenon. Often problems encountered in a number of cases include the following: the shape of the models does not reflect reality, the flow rates that are used are very low compared to the flow rates in spillways, and also the non-representativeness of the rock mass. For example, the use of a single block instrumented with concealed joints to represent the rock mass (Montgomery 1984; Reinius 1986; Pells 2016a). Other problems include using several blocks that do not allow the quantification of geomechanical parameters (Annandale *et al.* 1998; Sawadogo 2010), or, using steel blocks with slot, which is not representative of a rock mass (Bollaert et Schleiss 2002). A more appropriate physical model should permit to study the effect of individual parameters, as well as their interaction to better characterize the hydraulic erosion process. This paper describes the design of a physical model of a spillway with an inclined flow channel. This Reduced-Scale Physical Model (RSPM) permit to study the various

hydraulic and geomechanical parameters affecting the erosion phenomenon, and also examine the interactions between these parameters.

5.2 DESIGN METHODOLOGY

We developed a methodology to design this RSPM of a spillway to study the important characteristic elements of hydraulic erosion (Figure 5-1). Spillways can be classified according to the energy dissipation process associated with the flow of water. The energy is dissipated either in the flow channel or in the plunge pool at the downstream end of the spillway structure. In the first case, different configurations can be applied depending on the geometry of the channel, including flow parallel to the channel bed, hydraulic jumps and knickpoint flows caused by changes in the angle of the channel. For the second mode of energy dissipation, the main flow mode is a jet plunging into a dissipation pool. In addition, these two modes of energy dissipation are carried out directly on unlined rock masses in the majority of field cases and the spillways with flow channels are the most widespread in the world (Khatsuria 2004). These are the reasons why, the RSPM is designed to represents a flow channel spillway.

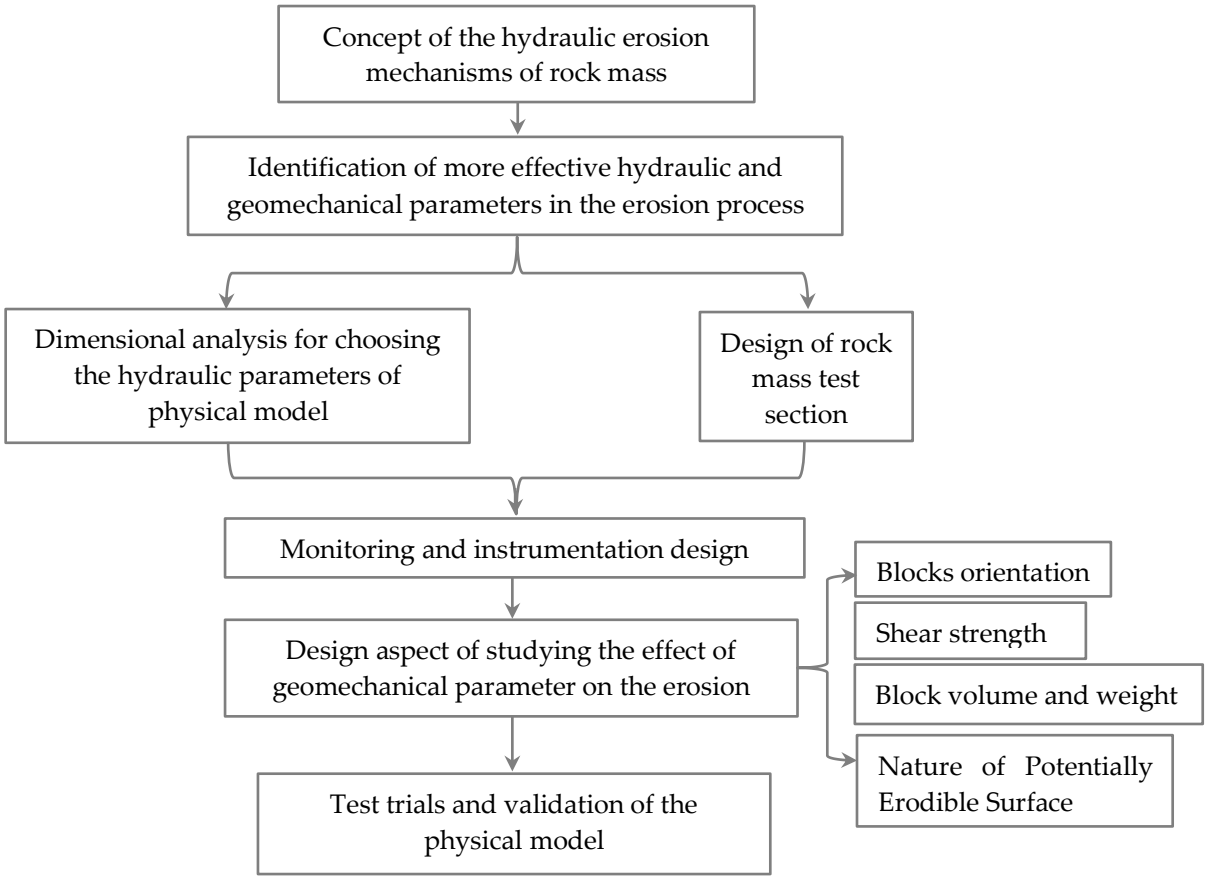

Figure 5-1. The design stages of the physical model

5.2.1 MECHANISSME OF ROCK MASS HYDRAULIQUE EROSION

Hydraulic erosion may proceed by tree different mechanisms; 1) erosion by instantaneous brittle fracturing, 2) continuous brittle fracturing of the rock mass, and 3) dynamic removal of rock blocks from the rock mass (Bollaert et Schleiss 2002; Annandale 2006b; Bollaert 2010). Erosion of the rock mass by the instantaneous brittle fracturing, occurs when the intensity of the induced fluctuating pressure in the joints is larger than the resistance of the rock, and

hence, the rock mass erodes into small pieces, and easily transported by the flowing water (Figure 5-2).

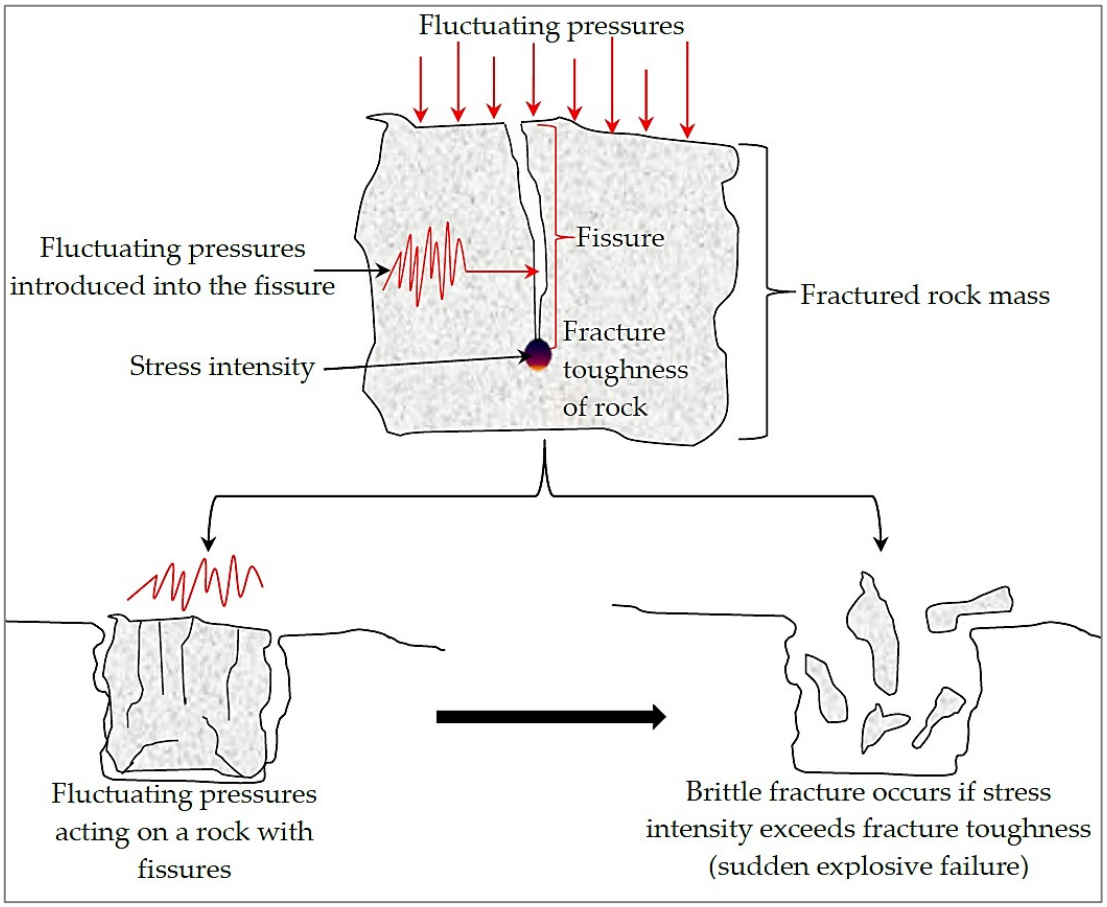

Figure 5-2. Erosion by instantaneous brittle fracture (Annandale 2006b).

The second mechanism is continuous fracturing or fatigue failure mode, which takes place if an instantaneous brittle fracture of rock mass is not possible. That fatigue failure occurs when the intensity of the stress in the joints does not exceed the resistance of the rock mass. However, the rock mass is broken by continuous loads of water pressure present in the joints, an erosion mechanism that is highly time-dependent (Figure 5-3).

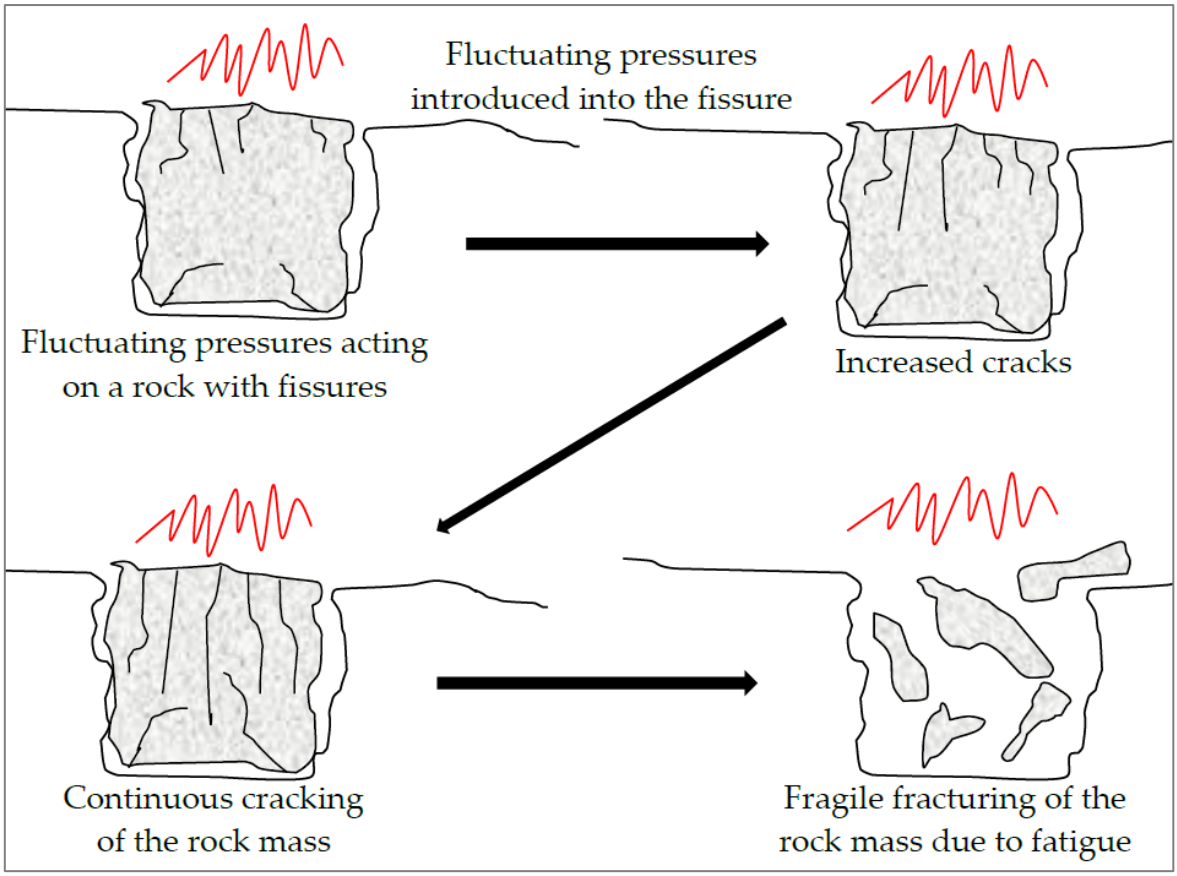

Figure 5-3. Erosion by continuous fragile fracturing of rock mass or hydrofracturing by fatigue (Annandale 2006b).

The third mechanism of erosion is the removal of blocks, a process depending on the water pressure in the joints of fractured rock mass. The amplitude of the fluctuating pressure changes with time during a turbulent flow, and the pressure applied inside rock joints can cause an increase in pressure directly below the blocks. In addition, the rock mass is eroded by dynamic expulsion of the blocks when the lifting pressure under the block exceeds the load resistance of the block in the rock mass (Figure 5-4). The load as a resistance component includes the submerged weight of the block (G_b), the pressure forces on top of the block (F_o), and the shear resistance forces along the sides of the block (F_{sh}).

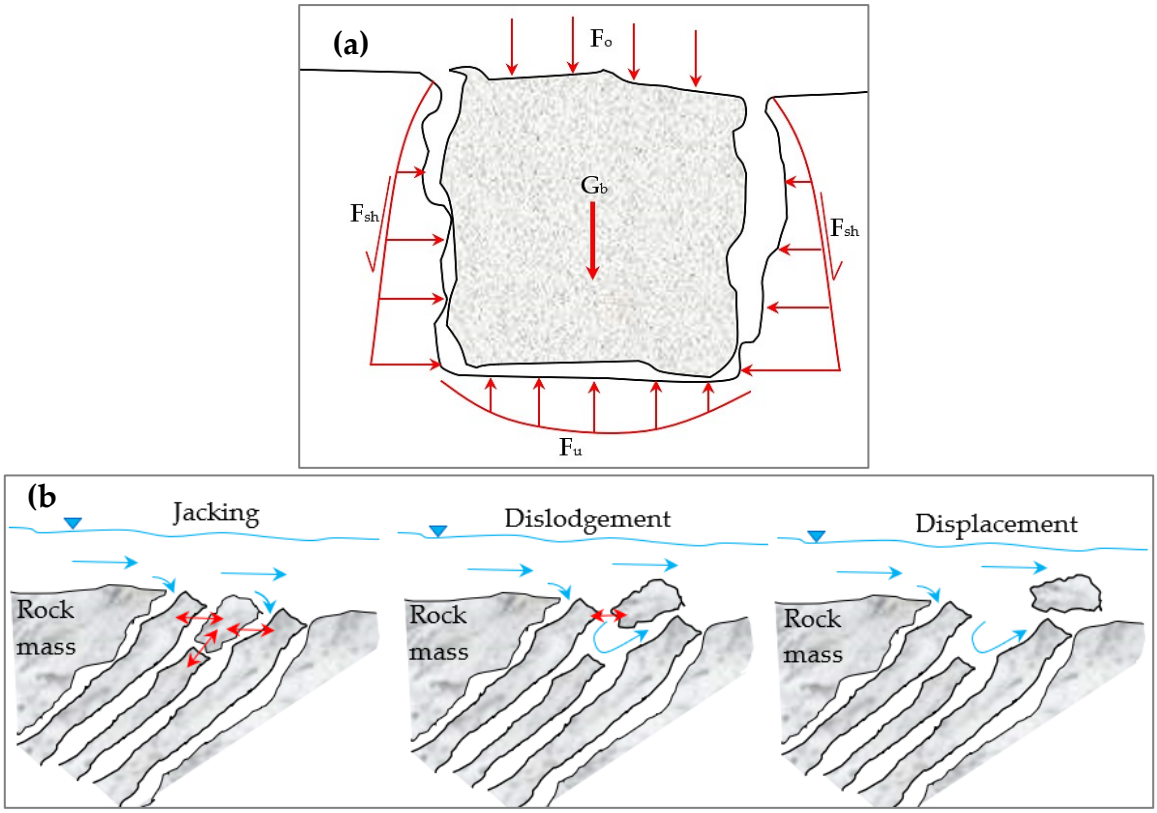

Figure 5-4. Erosion by block removal called dynamic block impulses, (a) erosion by removal of blocks in a plunging stream (Bollaert et Schleiss 2002; Annandale 2006b), and (b) erosion by removal of blocks in a flow parallel to the bottom of the flow channel (Annandale 1995).

Of these three erosion mechanisms, dynamic block removal seems to be the most common erosion mechanism of the fractured rock mass in spillways specially in the crystalline rock masses which are classified as very high strength rocks. This remark is justified by observations made in several field studies carried out around the world (Boumaiza *et al.* 2019b).

5.2.2 IDENTIFICATION OF THE RELEVANT PARAMETERS IN THE EROSION PROCESS

As mentioned above, the forces involved in the hydraulic erosion process are the erosive force of the water and the resistance force of the rock mass. Regarding

the resistance of the rock mass, it emerges from the various erosion mechanisms and resistance indices, that this resistance depends on several geomechanical parameters including the *UCS*, K_b, K_d, V_b, J_o, E_{dao}, J_s and *NPES* (Table 5-1). The effect of each one of these parameters on rock mass erosion have been investigated. It has been qualified, some of these parameters have no significant effect on the rock mass erosion and others doesn't properly reflect the considered rock mass parameters. For example, the irrelevance of the block size (K_b) is linked to the limited performance of the *RQD* in the characterization of a rock mass (Palmström 2001b; Palmstrom 2005; Pells *et al.* 2016b). It is also recognized that *UCS* is not suitable for evaluating the resistance of the rock mass to erodibility, because high values of this parameters are observed at most dam sites. In reality, in the majority of cases, *UCS* value are higher than the compressive strength of concrete used lined spillways. That is the case of the Mokolo dam in South Africa, where high erosion rate has been observed on strong rocks based on *UCS* values.

In reality the rock mass resistance to erosive forces depends mainly on the discontinuities present in a rock mass, and related parameters such as spacing, persistence, and the roughness of the joints of the joint sets (Bieniawski 1989). Boumaiza *et al.* (2019) developed a methodology for determining the most important parameters on the erosion process based on the rock mass parameters and observed erosion data of 110 dam sites in the world. They concluded that the

most relevant parameters for erodibility are the shear strength of the joints (K_d or F_{sh}), the opening of the joints (J_o), the volume of the rock blocks (V_b), the shape and orientation of the blocks in relation to the direction of water flow (E_{doa}) and the nature of the surface potentially erodible (*NPES*).

Regarding the erosive force of water, indices that are commonly used are the rate of energy dissipation (Π_{UD} in kW m^{-2}), the average flow velocity ($\bar{u}$ in m s^{-1}) and the average shear stress on the bottom surface of flow channel ($\bar{\tau}_b$ in kPa). Koulibaly *et al.* (2021) have noted no good agreement on the representativeness of these indices. Most studies have shown that the indices depending mainly on the pressure (P_r) are most relevant to represent the erosive force of water. Also, when considering the different erosion mechanisms (Figure 5-2 to 5-4), it appears that the hydraulic pressure represents the main force in the brittle fracturing of the rock and the block uplifting.

An interesting application of the reduced-scale physical model (RSPM) is to study the water flow to have a good representation of the erosive force of the water, and its interaction with the rock mass. In this paper we focus on the design of the RSPM for studying the hydraulic erosion process, especially the effects of relevant geomechanical parameters on the erosive process (K_d, J_o, V_b, E_{doa} and *NPES*).

5.2.3 DIMENSIONAL ANALYSIS FOR CHOOSING THE HYDRAULIC PARAMETERS OF PHYSICAL MODEL

In the domain of fluid mechanics, laboratory-scale models are generally developed to study phenomena that are difficult or impossible to study on a larger field scale. A dimensional analysis is required to ensure the representativeness of hydraulic parameters at different scales. The three aspects to consider in this analysis are the geometric, the kinematic and the dynamic similarities. The geometric similarity, suggesting that the reduced model should have the same geometric shape as the real model, perform using scaling. Kinematic similarity, mean that the flow velocity at any point in the reduced model must be proportional to the velocity at the corresponding point in the real system. The dynamic similarity is obtained when all the forces of the reduced model flow are proportional to the corresponding forces in the real model flow.

It is common practice in the hydroelectric dam industry to predefine hydraulic parameters to reduce the effects of the erosive force of the water. The velocity of the water leaving the reservoir and in the flow channel must be between 15 and 30 $m.s^{-1}$ depending on the nature of the rock mass. The RSPM described below is designed according to filed data from the Romaine- IV dam spillway (Hydro-Quebec; Figure 5-5).

Figure 5-5. Spillway of Romaine IV dam (Hydro-Québec)

The similarity conditions are met by using appropriate values, including the characteristic of the real model, the scale factor, and the dimensionless number allowing transposing the geometric dimensions and the hydraulic parameters. The selected scale factor (*Fe*) is 1/40; this value is based on the available laboratory space and the allocated budget, and it is considered as ensuring an adequate representativeness of the RSPM. For two dimensionless numbers that are used are 1) the Froude number (*Fr*) in order to respect the similarity conditions, and 2) the Reynolds number (*Re*) to check the invariance of the hydraulic conditions at the two scales. Equation 5-1 is used to determine the characteristic dimensions of the RSPM as a function of the dimensions of the real model.

$$Fr_{RM} = \frac{u_{Pro}}{\sqrt{g.l_{Pr}}} = Fr_{RSPM} = \frac{u_M}{\sqrt{g.l_M}}, \qquad (5\text{-}1)$$

where Fr_{RM} is the Froude number on the scale of the real model (*RM*), and Fr_{RSPM} at the scale of the reduced-scale physical model (*RSPM*), u is the flow velocity at both scales, l represents the dimensions in meters at both scales, and g is the gravitational acceleration. The dimensions obtained for RSPM with Eq. 5-1 are summarized in Table 5-4.

Table 5-4. Summary of the dimensional parameters of the real model and the RSPM

RM (RO-4) (m)		**Ratio factor**	**RSPM (m)**	
L	166,4	$Fe = {}^{1}/_{40}$	L	4,2
W_1	27,2		W_1	0,68
W_2	35		W_2	0,87
H_p	22,3		H_m	0,56
BH_1	30		BH_1	0,75
BH_2	30		BH_1	0,75
Q_{RM}	2950	$Fe^{5/2} = {}^{1}/_{10\,119,19}$	Q_{RSPM}	0,292m^3/s
V_{RM}	20	$Fe^{1/2} = {}^{1}/_{6,325}$	V_{RSPM}	3,162 m/s
θ_{RM}	15% ≈ 9°	-	θ_{RSPM}	15% ≈ 9°

Note : **RO-4** = Romaine -4 dam spillway, **RM** = real model, **RSPM** = reduced-scale physical model, $\boldsymbol{L}$ = length of the flow channel selected, $\boldsymbol{W}$ = width of the channel at upstream and downstream, $\boldsymbol{H}$ = height of the spillway in relation to the reference surface, $\boldsymbol{BH}$ = height of the banks of the flow channel at upstream and downstream, $\boldsymbol{Q}$ = flow rate, $\boldsymbol{V}$ = velocity, and $\boldsymbol{\theta}$ = slope of the flow channel.

The Reynolds number then serves to determine the flow conditions in the RSPM using Equation 5-2, and then compared with the flow condition of the RM.

$$Re_{RM} = \frac{u.L}{\nu} = \frac{20 \times 3,66}{1,002.10^{-6}} = 73,05.10^{6} > 2\,000 \implies \text{turbulent flow}$$

$$Re_{RSPM} = \frac{u.L}{\nu} = \frac{3,162 \times 0,092}{1,002.10^{-6}} = 2,90.10^{5} > 2\,000 \implies \text{turbulent flow} \qquad (5\text{-}2)$$

Where u is the flow velocity upstream of the spillway, ν is the kinematic viscosity of water at 20° C ($1{,}002.10^{-6}$ $m^2.s^{-1}$) (Cengel 2014), L is the characteristic length corresponding to the hydraulic radius of the channel, the *RM* designate the real model (RO-4), and *RSPM* designate the reduced-scale physical model. Calculations performed with R_e numbers give the same flow conditions at both scales, hence the dimensional analysis is accepted.

5.2.4 DESIGN OF ROCK MASS TEST SECTION

Rock mass erosion generally begins at as specific location in a spillway, depending on the characteristic of the rock mas and the flow patterns that are encountered (Kirsten *et al.* 2000). For inclined channel spillways, erosion often begins in the downstream area, where there may be a sudden change in the flow regime. An example is given by the erosion at the Copeton dam in Australia (Figure 5-6). Therefore, the place of the rock mass in the test section of the RSPM is located in the downstream area, but this location could be changed eventually.

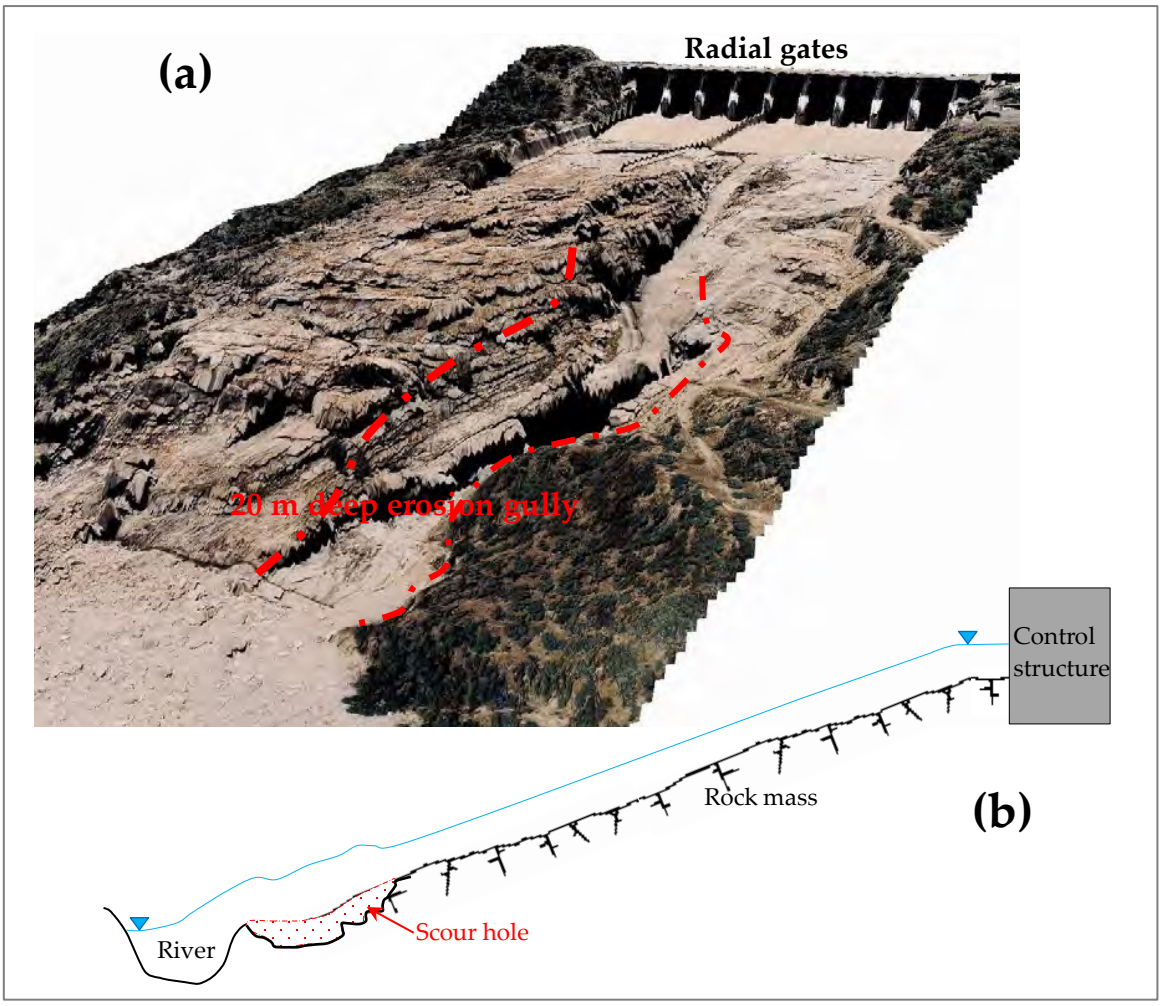

Figure 5-6. Location of areas subject to erosion on an inclined spillway, a) downstream erosion at the Copeton dam in Australia (Pells 2016a), and b) area sensitive to erosion an inclined flow channel (Kirsten 2000).

The test section the RSPM (Figure 5-7 and 5-8) is designed using the data in Table 5-4. This test section (reduced spillway) is integrated within a water recirculation system (Figure 5-9) to maintaining stable and continuous test conditions, using pump, and the two water reservoirs.

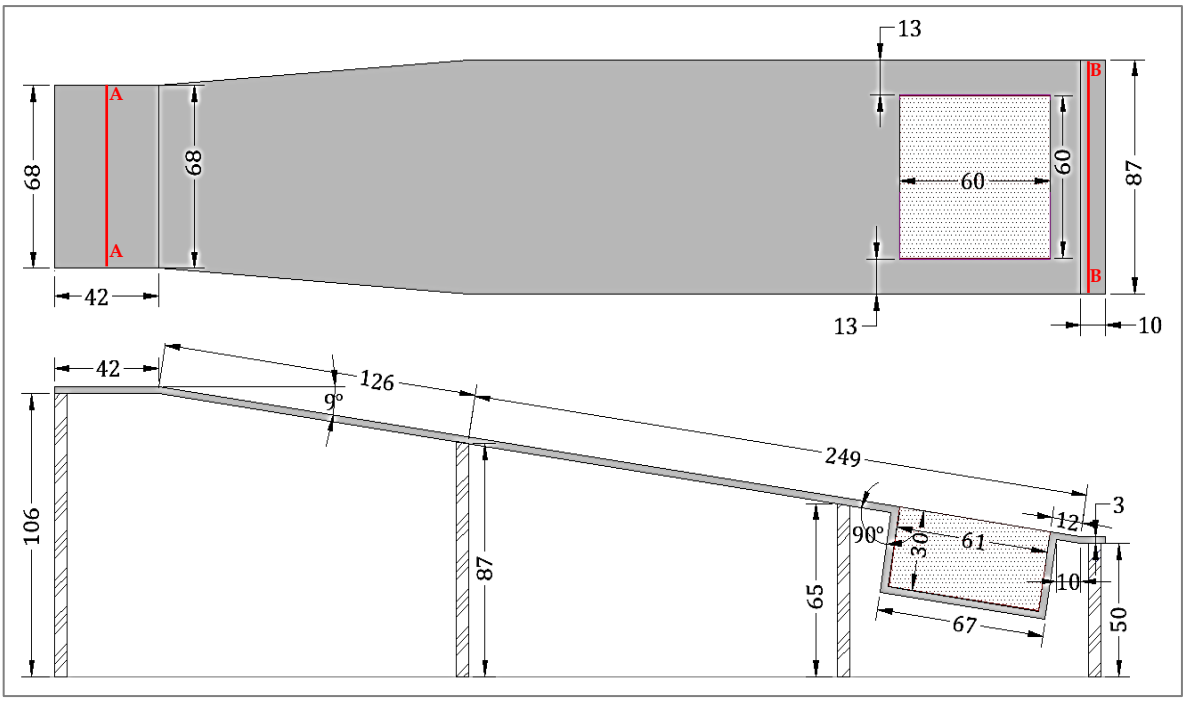

Figure 5-7. Plan of the test section of the RSPM (dimension in centimeters) (© A.S Koulibaly, 2021)

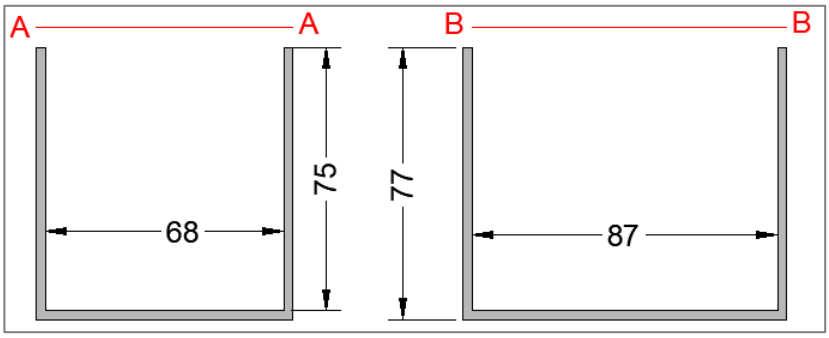

Figure 5-8. Cross-section of the test section of the RSPM at upstream (A-A) and downstream (B-B) location along flume (dimension in centimeters) (© A.S Koulibaly, 2021).

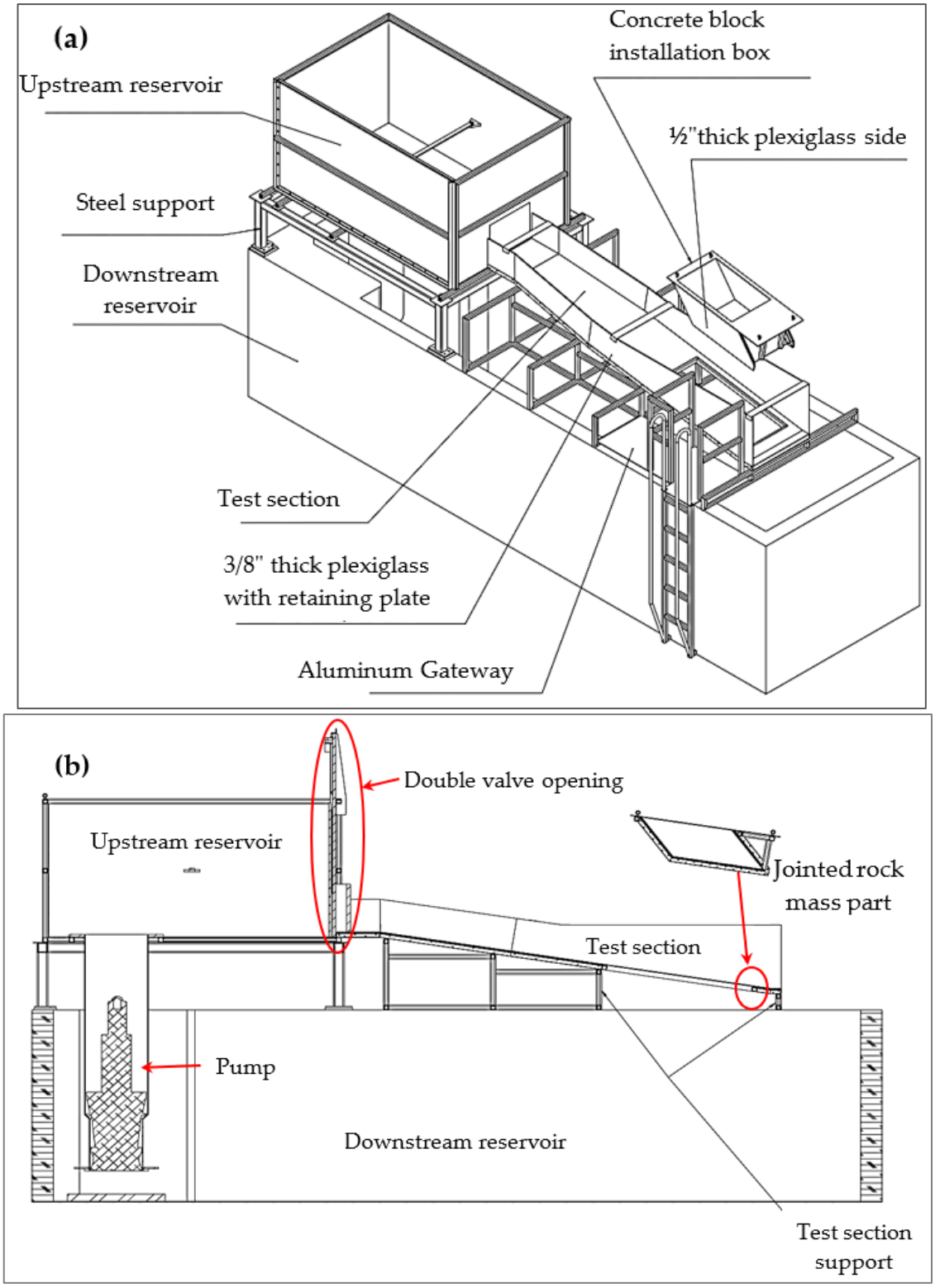

Figure 5-9. The designed RSPM of the spillway. (a) 3D view, and (b) sectional view of the system (© A.S Koulibaly, 2021).

The closed-circuit physical model (Figure 5-9) is made up of four parts, the concrete basin includes a downstream reservoir and a centrifugal pump. The purpose of this pump is to provide water at a controlled rate from the concrete basin constituting the downstream reservoir to the upstream aluminum reservoir connected to the test section. The selected pump yields a maximum flow rate of 400 L/s. The volume of water circulating through a downstream reservoir is 24 000 liters. A double valve opening system is used to control the flow rate and velocity entering the test section, and to assess the effect of asymmetric flow on the rock mass (Figure 5-10).

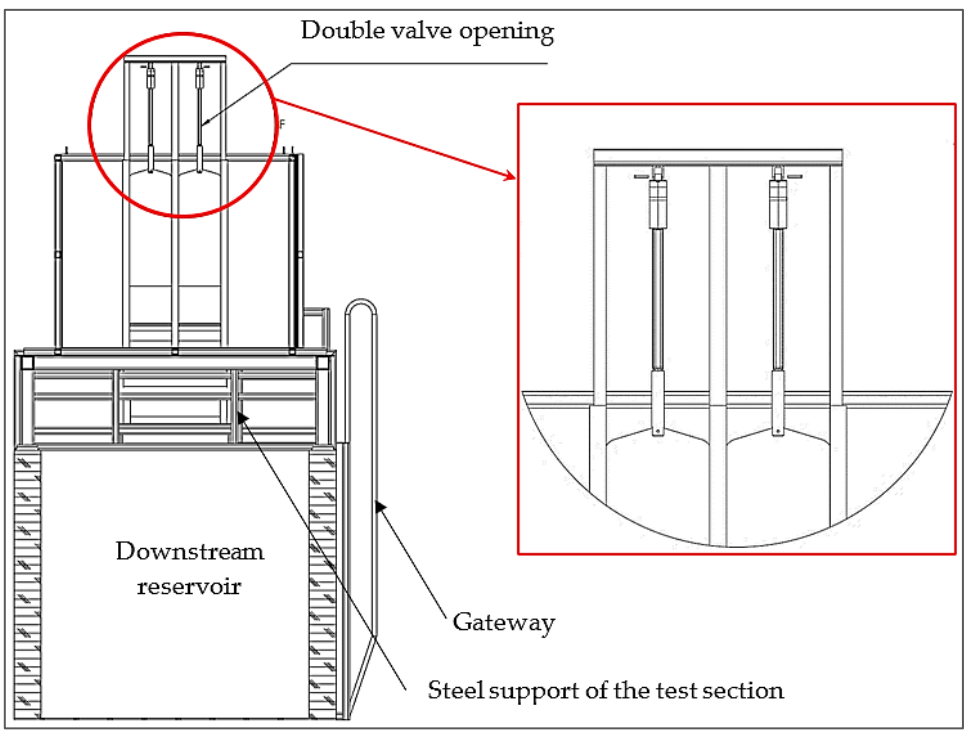

Figure 5-10. View of the double valve system in model (© A.S Koulibaly, 2021)

The RSPM is also equipped with a velocity sensor to measure the velocity in the channel, and their specification are presented in Table 5-5.

Once of the most important factors of RSPM is the representativeness of the rock mass test section. A cavity located in the downstream part of the test section is designed to receive concrete blocks that are specially designed and equipped to monitor and investigate the behavior of rock mass against water flow (Figure 5-7 and Figure 5-11). Nine concrete blocks and two casing with various dimensions and arrangements are planned to evaluate different geomechanical parameters of the rock mass.

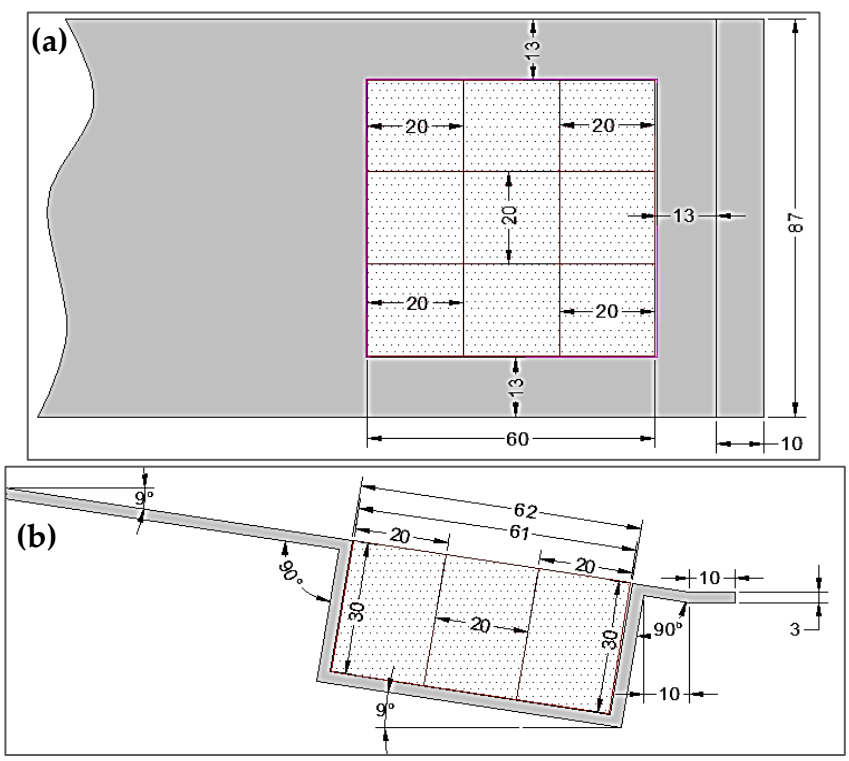

Figure 5-11. Schematic view of the initial configuration of casing of concrete blocks. (a) Plan view of concrete blocks and (b) Longitudinal profile of concrete blocks (dimension in centimeters) (© A.S Koulibaly, 2021).

5.2.5 MONITORING AND INSTRUMENTATION DESIGN

To investigate the reaction of some rock mass parameters against the water erosive forces, three of nine blocks in the casing have been instrumented by eight pressure sensors to measure the water pressure apply on each side of the block (Figure 5-12; Table 5-5). On each side of the block, we have two holes for inlets water (red arrow), and points of outlets water (green arrow) on the top side, which are connecting to pressure sensors. The holes in the block contain ¼" diameter copper tubing and are effective in reducing pressure loss; and Figure 5-13 shows the conception materials and an example of a test block fitted with a pressure sensor. An accelerometer is placed on the topside of each instrumented block to study the geomechanical parameters which control the relative displacement of the block under the effect of the pressure.

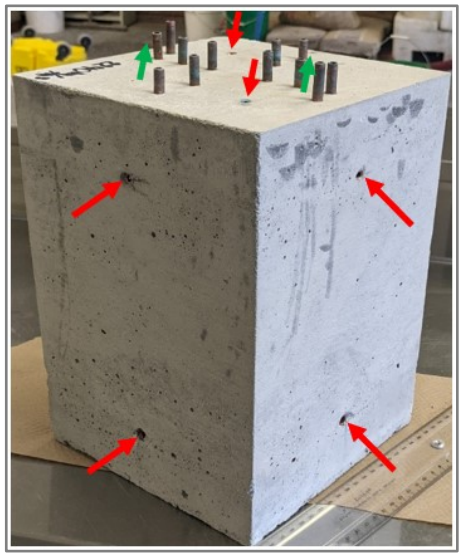

Figure 5-12. Example of concrete block instrumented to measure the water pressure on each side (© A.S Koulibaly, 2021).

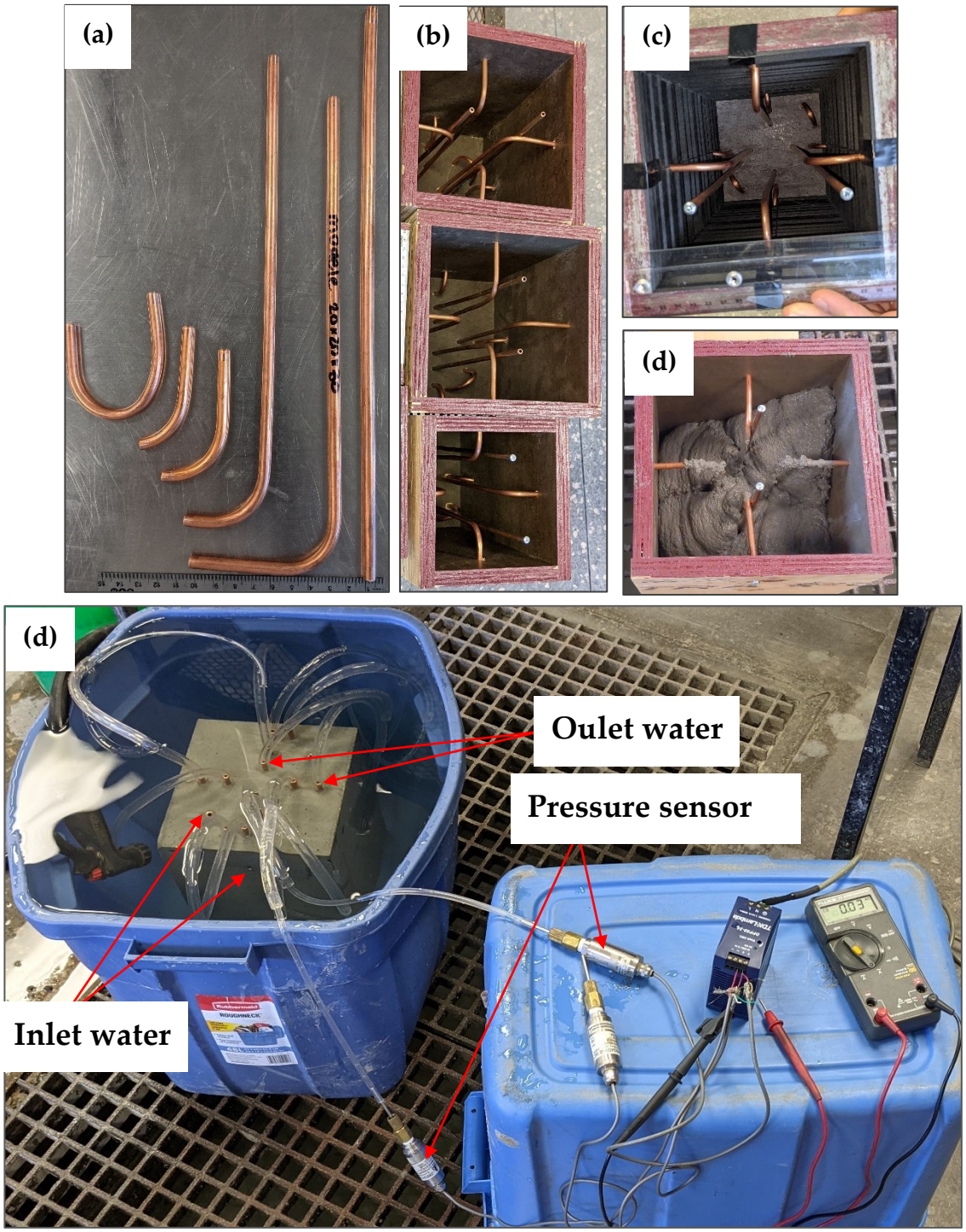

Figure 5-13. a) ¼" diameter copper pipes, of different shapes depending on the pressure measurement points, b) Wooden mold with copper pipes installed on each face of the block, mold for blocks with smooth surface, c) Wooden mold with 3D printing of a rough profile, mold for blocks with a rough surface, d) Pouring a concrete block, and e) Pressure sensor installed on a concrete block for a pressure measurement for validation test on each face of the block (© A.S Koulibaly, 2021).

Table 5-5. Characteristics of measuring instruments

Item	Description
Pump	CAD01100; KSB type Amacan PA4 600-350/256UAG1; Vertical Electric Pump; Motor 37HP, 575V / 3 Ph / 60 Hz; Maximum flow rate of 400 liters/s.
Flowmeters	GLOBAL WATER FP111, Flow Probe 3.7′ – 6′.
Velocity sensor	Heavy-Duty Displacement Sensor/Position Sensor/Motion Sensor; LDI-128-450-A010A
Pressure sensor	Dwyer 623-07-GH-P-1-E4-S1, Pressure-Transmitter, 0-15 Psi with 1.0% accuracy and general-purpose housing.
Data acquisition system (Ni 3080 card + Computer)	USB-6343 Series data acquisition box X (32 analog inputs, 48 E/S digital, 4 analog outputs).

5.2.6 TEST DESIGN FOR STUDYING THE EFFECT OF GEOMECHANICAL PARAMETER

The aim of this RSPM is the evaluation of the interaction between the water forces and rock mass parameters. The representativeness of the model requires that the set of concrete blocks are characterized by geomechanical parameters including K_d, J_o, V_b, E_{doa} and *NPES*.

5.2.6.1 Design for evaluating the effect of blocks orientation on the erosion

The block orientation represents a very important parameter in the hydraulic erosion process. It is increasingly easy to move the blocks under the effect of the erosive force of water when the dip of these blocks is in the same direction as the flow. In contrast, these blocks are more resistant to flow when their dip is opposite to the direction of flow (Kirsten *et al.* 2000). Two parameters are known to

characterize the effect of the orientation of the blocks, J_s and E_{doa}. However, J_s is qualified by some authors as not representative for erosion (Pells *et al.* 2016b; Boumaiza *et al.* 2019b), thus, E_{doa} serves as a basis to define three dip values for block orientation. Initially the blocks are arranged at 90°, -45° and 45° to the direction of water flow (Figure 5-14).

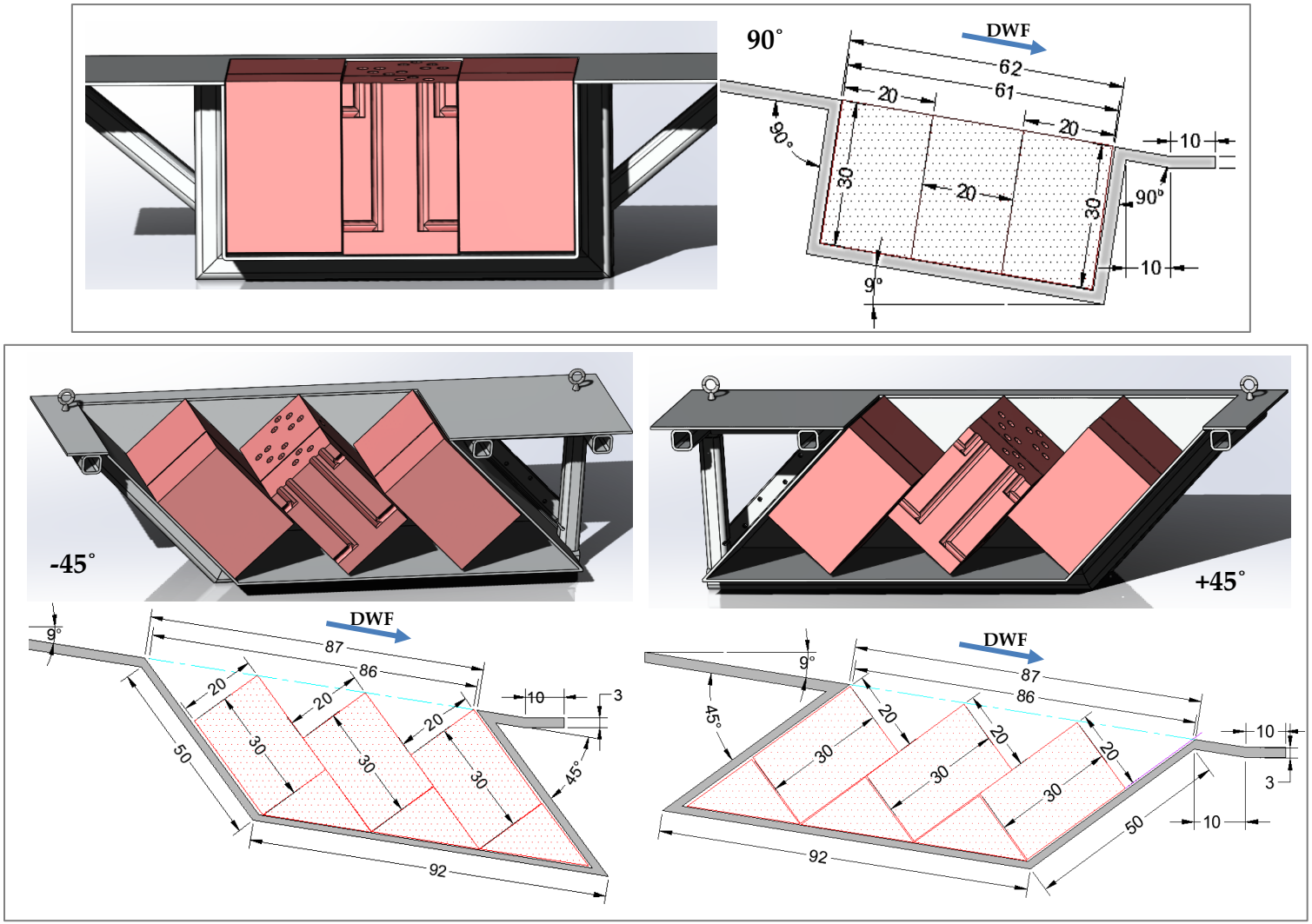

Figure 5-14. Arrangement of the blocks with respect to the direction of water flow (DWF) (distance in centimeters) (© A.S Koulibaly, 2021).

5.2.6.2 Design for evaluating the effect of joint shear strength on erosion

In a rock mass classification, the shear strength (F_{sh}) of the joints is usually related to the ratio between the joints roughness (J_r) and the degree of alteration of the joints face (J_a) (Kirsten *et al.* 2000). However, during the course of erosion, the alteration zones or the filling materials of joints are leached and eroded in an initial phase of the process (Figure 5-15). Consequently, the important parameters to characterize the shear strength of joints submitted to erosion are joints opening (J_o), as well as joint surface irregularities capture by the Joint Roughness Coefficient (JRC) parameter. In this RSPM, the configuration of the casing and the concrete blocks allows to study the effect of the joint opening on rock mass erosion. For the joint roughness, different JRC profiles (smooth to very rough) are obtained using 3D printing; an example of a block with smooth surface and another with rough surfaces is show in Figure 5-16.

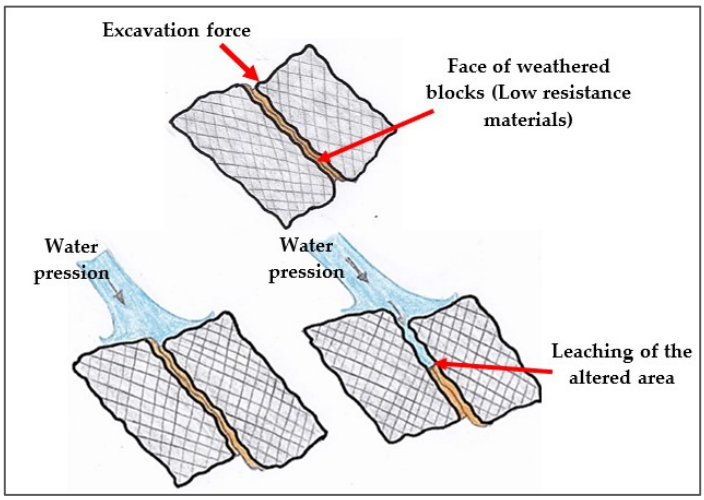

Figure 5-15. Altered joint behavior of a rock mass under the effect of forces of different nature (© A.S Koulibaly, 2021)

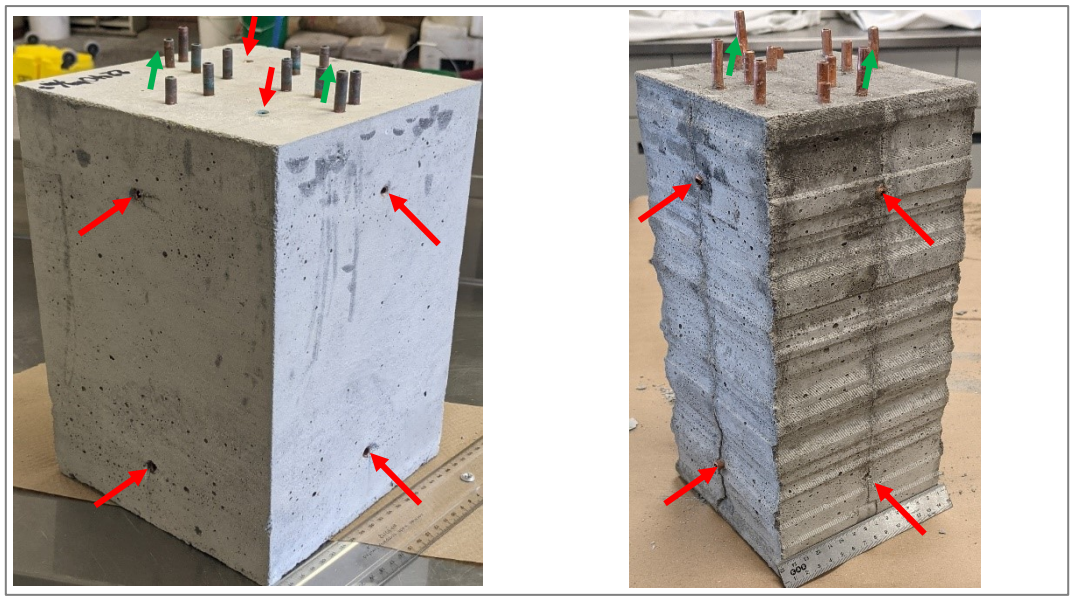

Figure 5-16. Smooth and rough faces of concrete blocks, water inlet in red and water outlet in green (© A.S Koulibaly, 2021)

5.2.6.3 Design for evaluating the effect of block volume (V_b) and weight (G_b)

The volume of the blocks is a very important parameter to evaluate rock mass erosion, since it is intrinsically linked to the weight which greatly influences the pressure required to uplift the blocks. In this RSPM, two sets of blocks with different volume and density are designed to study the effect of block volume and weight on the lifting pressure. Blocks of 12 000 cm³ (20cm*230cm*20cm) and 6 750 cm³ (15cm*230cm*15cm) are designed, and the density values are 1 275, 1 290, 1 785, 1 820 and 2 240 kg/m³ (Figure 5-17). These block size value are determined using the rock mass data from more than 100 dam spillways (Pells 2016a). Blocks of different volume and density are used, in order to determine at what density the blocks may be susceptible to displacement under the effect of known uplift pressure. For this reason, accelerometers and high-definition cameras are installed

above and on one side of the test section to visualize the relative movement of the blocks.

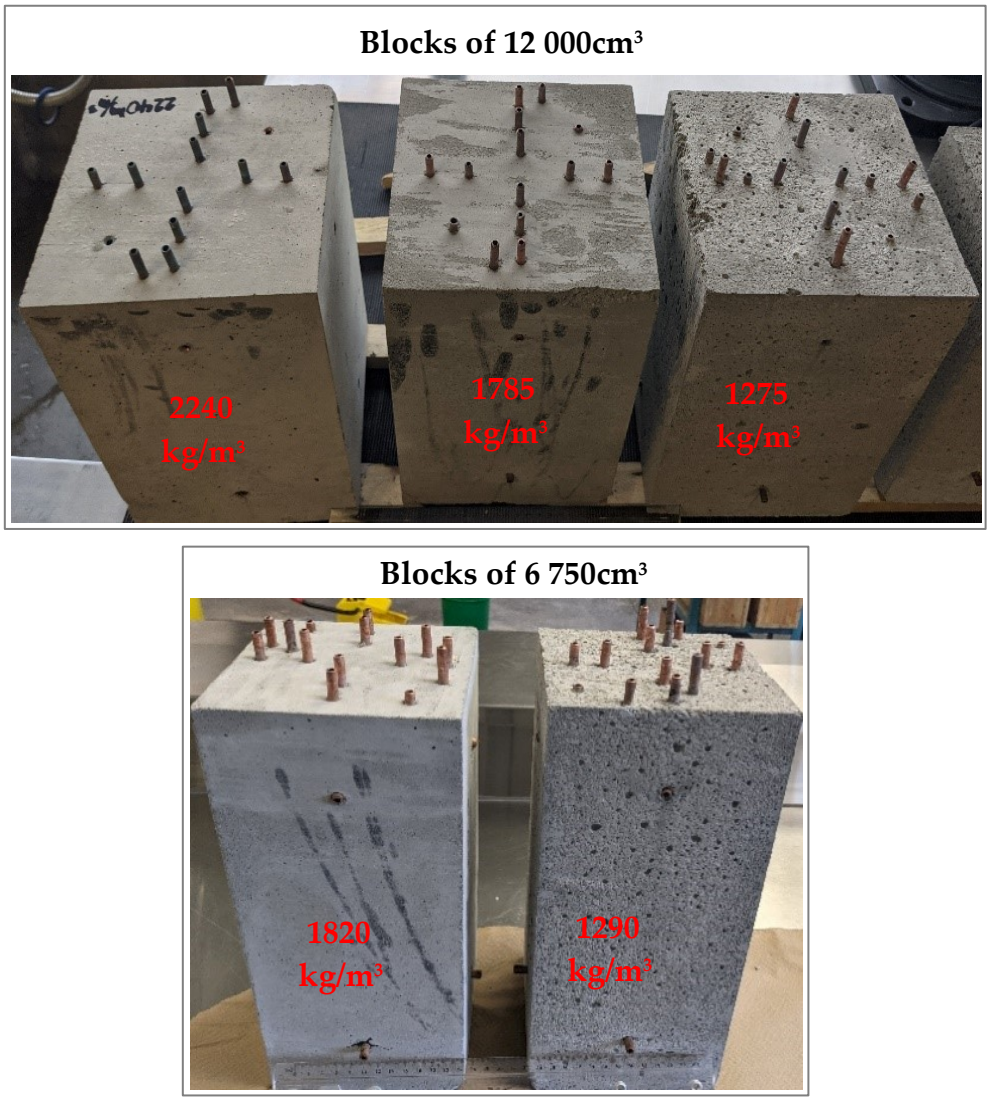

Figure 5-17. Different size and density of the concrete blocks (© A.S Koulibaly, 2021)

5.2.6.4 Design for studying the Nature of Potentially Erodible Surface (*NPES*)

The degree of the flow turbulence is greatly depending on the nature of the flow channel, such as its shape and the roughness of its floor. The flow channels of spillways are often highly irregular due to the presence of protrusions and open joints. These irregularities increase the flow turbulence, creating high differential

pressure valuers in the joints. A channel with high protrusion is more susceptible to erosion by block removal. Conversely, smooth surface flow channels are less susceptible to erosion, as the likelihood of high-pressure build-up around the rock block is low (Pells 2016a). Figure 5-18 shows some cases of rock block protrusion in a flow channel, which are the most commonly encountered in the *NPES* parameter (Pells 2016a) and also according the results obtained by Reinius (1986) in his experimental study on a RSPM.

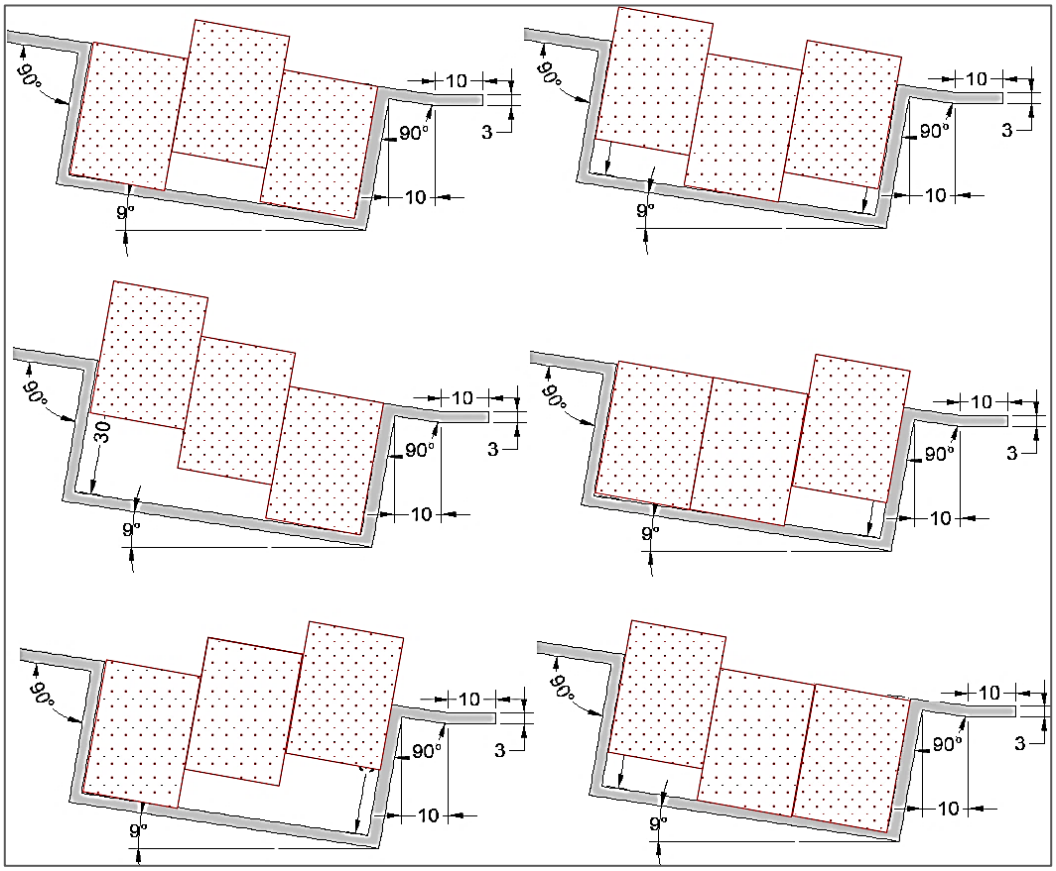

Figure 5-18. Some examples of the arrangement of concrete blocks with different protrusion (© A.S Koulibaly, 2021)

5.3 RESULTS FROM THE VALIDATION TESTS OF THE REDUCE PHYSICAL MODEL

The pressure associated with the water flow should be sensitive to variation in the flow rate, the channel geometry as well as various geomechanical as described in the following list of expected results.

- The pressure (*Pr*) associated with the flow should increase as a function of the flow velocity (*V*) in the test section,
- The uplift pressure (*Pr-u*) should increase as the spacing between the blocks increases (*Jo*),
- The uplift pressure should be higher when the inclination of the blocks is in the same direction as the direction of flow,
- The relative displacement of the blocks should follow the variation of the uplift pressure, but still depends on the joints opening, the volume and the roughness of faces of the blocks,
- The pressure associated with the flow should increase as a function of the degree of flow turbulence which is mainly dependent on the inclination of the test section and the nature of the potentially erodible surface (*NPES*), i.e., the irregularity of the area of the test section.

Regarding of these expected results, flow tests were carried out with some parameters to validate the representativeness of the RSPM. In the following

subsections, the values of the pressure measured correspond to the total pressure, which equal to the sum of dynamic and static pressure.

5.3.1 THE EFFECTS OF THE INFLOW RATE ON THE WATER PRESSURE

To evaluate the effect of the flow rate on the water pressure, different conditions 0.233, 0.566 and 0.666 $m^3.s^{-1}$ are used. The rock mass is represented by a concrete block with 25 mm protrusion and spacing between block (Figure 5-19). The result obtained from this condition test is the variation of pressure on the first side of the block perpendicular (face C) to flow circulation (Figure 5-20).

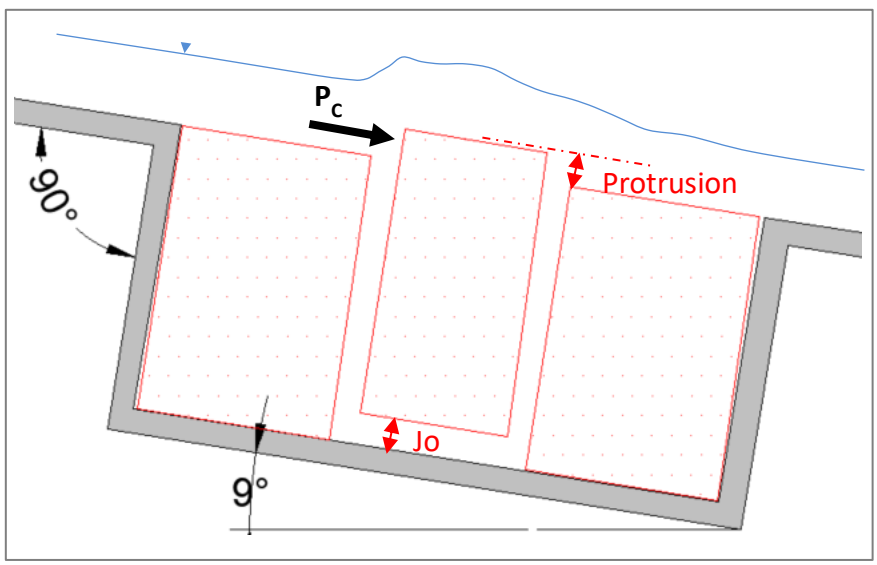

Figure 5-19. Condition tests to evaluate the effect of the inflow rate on the pressure (© A.S Koulibaly, 2021)

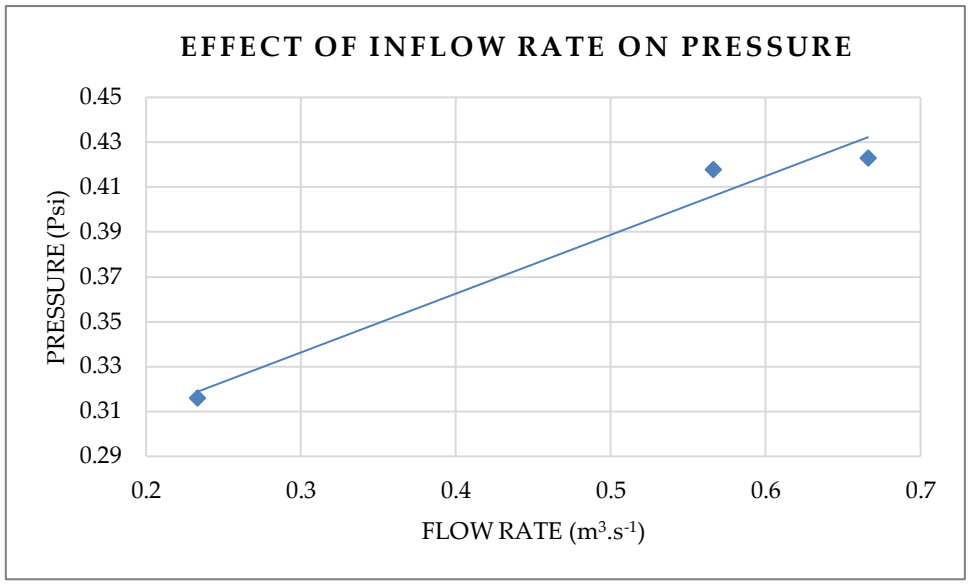

Figure 5-20. Effect of flow water inflow rate on the apply pressure on the rock mass (© A.S Koulibaly, 2021)

Figure 5-20 shows that the pressure applies on the block increase with the increase of the inflow rate. This result is relevant because it's corresponding to expected results.

5.3.2 THE EFFECT OF THE OPENING JOINT (J_o) UNDER THE BLOCK AND PROTRUSION (*NPES*) ON THE PRESSURE

Figure 5-21 represent the test condition to evaluate the effect of J_o and NPES on the water pressure apply on the topside and the underside of rock blocks. The rock mass is characterized by 25 mm spacing between block, 15, 25 and 53 mm of spacing under the test block which inversely related to the protrusion. The result obtained from this test concord with the expected result, the increase of the uplift pressure, and that applies to the topside of the block depending on the J_o and *NPES* (Figure 5-22).

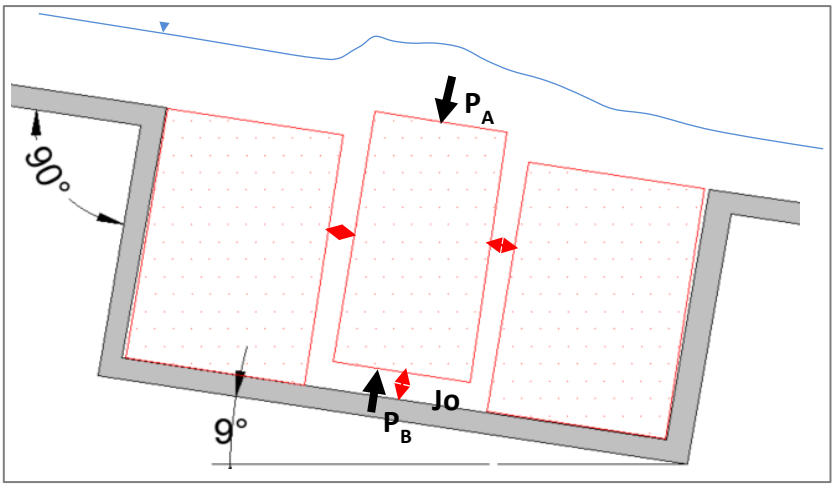

Figure 5-21. Condition tests to evaluate the effect of the spacing under the rock block and the protrusion on the apply pressure under and on it (© A.S Koulibaly, 2021)

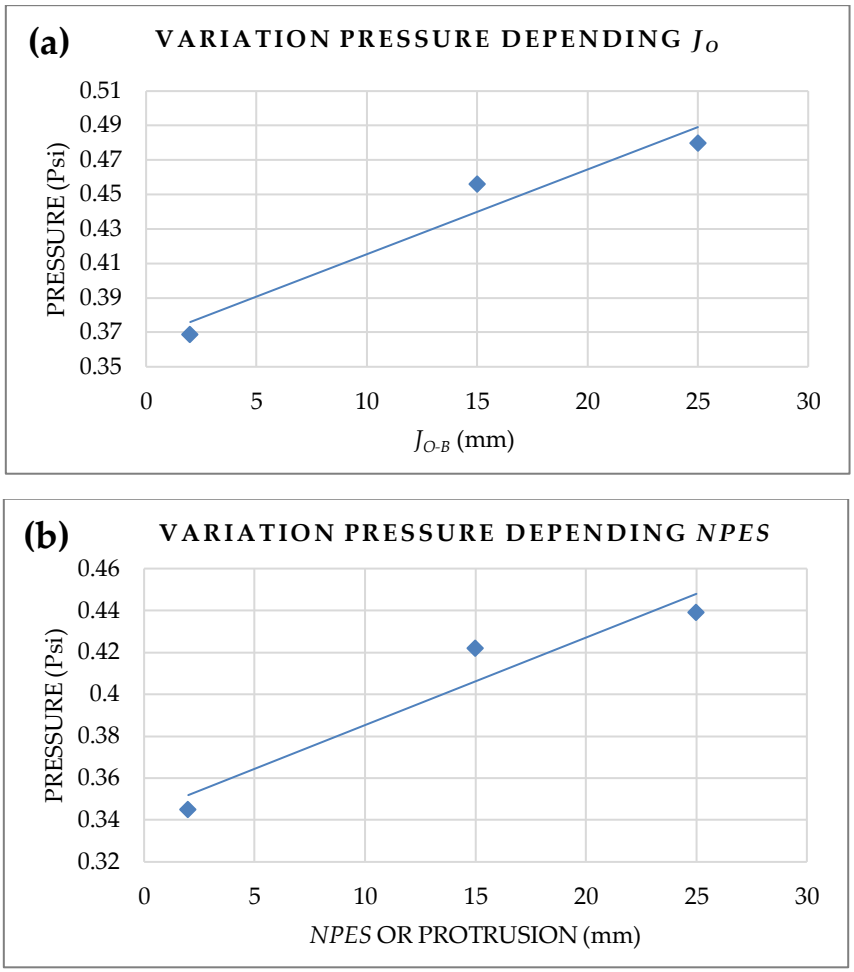

Figure 5-22. a) Effect of the variation of J_o under the block on the uplift pressure, and b) effect of the protrusion (NPES) on the apply on the block (© A.S Koulibaly, 2021)

The pressure related to the water flow in an open channel is mostly affected by the degree of the turbulence in the flow, which depends on the nature of the surface of the channel. As well as, the surface of the flow channel is characterized by high protrusions (high irregularity), the turbulence in the water flow will the same and the pressure that related to it (Figure 5-22.b). Furthermore, the uplift pressure increasing pending on the variation of the spacing below the rock block is totally normal (Figure 5-22.a) because the infiltration of water below the block is directly linked to this opening.

5.3.3 THE EFFECT OF THE OPENING JOINT (J_o) ON THE PRESSURE

Figure 5-23 represent the test condition for evaluation of the effect of J_o around the block on the uplift pressure and pressure around the block.

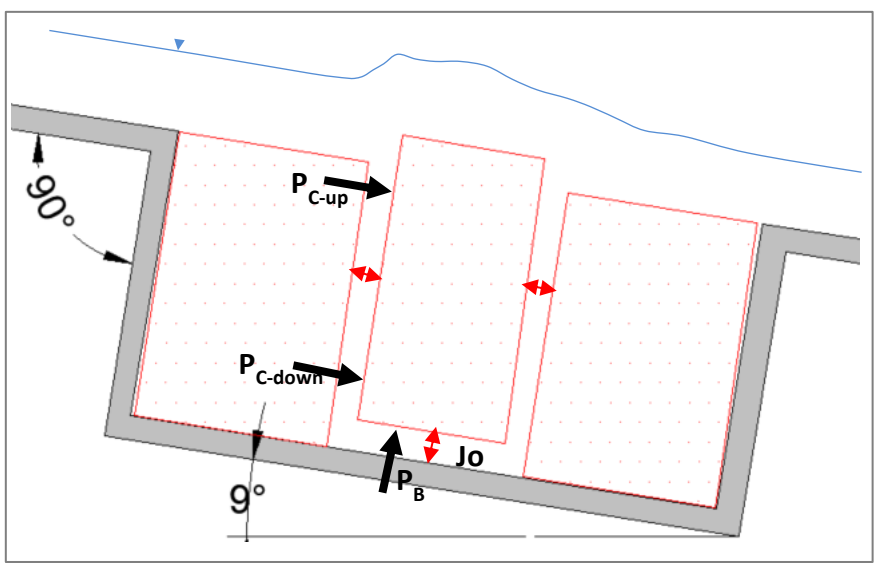

Figure 5-23. Condition tests to evaluate the effect of the spacing around the rock block on the apply pressure (© A.S Koulibaly, 2021)

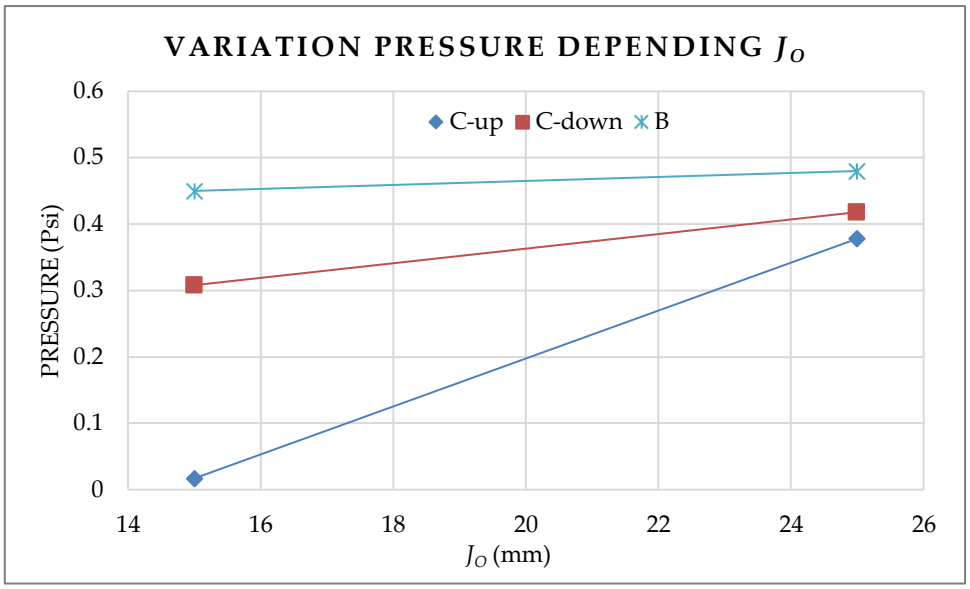

Figure 5-24. Effect of the variation of *Jo* around the block on the pressure (© A.S Koulibaly, 2021)

We expect that the applied pressure in the joint increase with increasing opening joints. The curve C_{-up} and C_{-down} of Figure 5-24, show here that the pressure applied to the side C increase with increasing of J_o. We also notice that the uplift pressure of the block increase with J_o around the block; and the pressure at the top of the block less than down pressure. This variation is perfectly normal, because total pressure in the turbulent flow is equal to the sum of the static and dynamic. Depending on the water height differential between point P_B, $P_{C\text{-down}}$ and $P_{C\text{-up}}$, the static pressure at point P_B must be greater than that of $P_{C\text{-down}}$, and $P_{C\text{-down}}$ greater than $P_{C\text{-up}}$. The contribution of the static pressure in our measurements is quite remarkable in Figure 5-24, which is useful to validate the representativeness of the total pressures measured during the validation tests of the RSPM.

5.4 DISCUSSIONS, RECOMMENDATIONS AND RESEARCH PERSPECTIVE

The prediction of hydraulic erosion of the rock mass in the dam spillway represents a real challenge, because the parameters that characterize this phenomenon are not well quantified. The rock mass resistance index and that of the erosive force of the water, used to evaluate the hydraulic erosion process, are based on some parameters which are not relevant for this process (Koulibaly *et al.*, 2021; Boumaiza *et al.*, 2019). This RSPM is designed to resolve this problem, because this RSPM allow evaluating interaction between erosive force of water and the geomechanical parameters which characterize rock mass. Most of the important parameters that are qualified to be relevant for hydraulic erosion process are considered by this RSPM, such as the flow rate, flow velocity, turbulence of the flow, inclination of the flow channel and the rock mass geomechanical parameters (J_o, E_{doa}, V_b, $NPES$, G_b and K_d). The representativeness of this RSPM to evaluate the interaction between the geomechanical parameters of the rock mass and the erosive force of the water is validated by test trials. The results obtained from different test trials correspond well to expect results.

With this RSPM, there are many study perspectives. First, the real identification and quantification of the relevant hydraulic and geomechanical

parameters, as well as the evaluation of the interaction between these parameters to better characterize hydraulic erosion.

Other long-term study perspectives are also possible with this RSPM. It could serve as a prototype to predict the behavior of flows in the flow channels of spillways and also predict the risk of erosion of future hydroelectric dams. An innovative solution that UQAC could develop, and which could be of great use to Hydro-Québec and other companies in controlling the possible risk of hydraulic erosion of dam spillways.

5.5 CONCLUSION

We designed and developed an innovative physical model for studying the rock mass processes in dam spillways that named RSPM. This RSPM includes the most important hydraulic and geomechanical parameters that interact in the hydraulic erosion process. The water pressure appears as the most important hydraulic parameter to be evaluated in relation with relevant geomechanical parameters of a rock mass such as J_o, E_{doa}, V_b, J_r, *NPES*, G_b and K_d. The test section of the RSPM is equipped with a set of concrete blocks with pressure measurement points on each face. By changing the arrangement of these concrete blocks, different geomechanical parameters are represented and the pressure can be evaluated according to these different configurations of the rock mass in the test section. Thus, this RSPM allow a relatively complete evaluation of the process of hydraulic erosion of the rock mass of the outflow channels of the spillways.

CHAPITRE 6 CONCLUSION

Malgré l'existence et l'utilisation de différentes méthodes d'évaluation ou de prédiction de l'érodabilité hydraulique des massifs rocheux des évacuateurs de crue des barrages hydroélectriques, il a été constaté dans de nombreux cas, et ce dès après la construction de ces ouvrages, que des massifs rocheux évalués comme résistants subissent une érosion notable remettant en cause la capacité de ces méthodes à prédire correctement l'intensité de l'érosion des massifs rocheux. Ces méthodes utilisant la notion de la ligne seuil, c'est-à-dire la corrélation entre la force érosive de l'eau et la résistance du massif rocheux. Il est évident que les insuffisances montrées par ces méthodes sont liées soit à la détermination de la force érosive de l'eau, soit à celle de la résistance des massifs rocheux, voire à l'utilisation de certains paramètres hydrauliques et géomécaniques non pertinents dans cette situation. Par ailleurs, il n'y a pas de consensus quant à la viabilité d'un couple d'indices pour représenter les deux forces en cause dans le processus d'érosion hydraulique. Une revue de littérature générale présentée dans ce mémoire démontre que le processus d'érosion hydraulique n'est que partiellement investigué par les études de laboratoire à travers des modèles physiques réduits. Ces études de laboratoire ne concernaient que l'évaluation des paramètres hydrauliques dans la plupart des cas et de quelques paramètres géomécaniques dans de rares cas. Dans ce mémoire, de nouvelles méthodes sont élaborées dans le

but de pouvoir mieux étudier le processus d'érosion hydraulique. Des outils ont été mis en place pour identifier et évaluer l'applicabilité des paramètres hydrauliques pertinents dans le processus d'érosion. Une méthode plus exacte de détermination du volume des blocs de roche dans un massif rocheux a également été développée. Par ailleurs, les différents paramètres hydrauliques et géomécaniques considérés comme pertinents dans les processus d'érosion hydraulique sont minutieusement étudiés dans le but de pouvoir les représenter à une échelle plus réduite. Les résultats obtenus sont résumés en des chapitres suivants.

6.1 IDENTIFICATION DES PARAMÈTRES HYDRAULIQUES INFLUANTS L'ÉRODABILITÉ HYDRAULIQUE

De la revue des travaux antérieurs sur l'érodabilité hydraulique, il ressort que le facteur commun lié aux indices utilisés pour représenter la force érosive de l'eau est la pression appliquée à la surface et dans les discontinuités du massif rocheux. Parmi les mécanismes d'érosion connus, celui par enlèvement dynamique des blocs de roche semble être le plus courant dans les massifs rocheux fracturés des évacuateurs de crue. Cela souligne que les différents modes d'écoulement observés aux évacuateurs de crue sont caractérisés par la même dynamique d'érosion et donc, l'indice d'expulsion dynamique des blocs semble être le plus adapté par rapport à la dissipation de l'énergie, la vitesse moyenne d'écoulement et la

contrainte de cisaillement moyenne du lit d'un canal. Cependant, l'indice d'expulsion dynamique doit être fondamentalement amélioré, car il néglige certains paramètres importants, dont la résistance au cisaillement des joints et l'ouverture des joints. De plus, la forme de l'indice connu n'est applicable qu'aux jets plongeants. Pour améliorer cet indice, il faudrait caractériser la variation de la pression dynamique dépendamment des différents paramètres géomécaniques pour différents modes d'écoulements rencontrés aux évacuateurs de crues. Il faut donc, pour une meilleure caractérisation, étudier à l'aide d'un modèle physique réduit d'évacuateur de crue les points suivants :

- La variation de pression en fonction de la forme ou de la taille des blocs,
- La variation de pression en fonction de l'ouverture des joints,
- La variation de la pression selon la disposition des joints par rapport au sens d'écoulement de l'eau,
- La variation de pression selon la nature de la surface potentiellement érodable (saillie principalement),
- L'évaluation du déplacement relatif des blocs en fonction de la force de résistance liée à la rugosité de la face des joints sous l'effet de la pression.

6.2 QUELLE EST L'APPLICABILITÉ DES INDICES REPRÉSENTANT LA FORCE ÉROSIVE DE L'EAU?

La méthode développée permet de visualiser l'applicabilité des indices utilisés pour représenter la force érosive de l'eau, qui sont la dissipation de l'énergie, la contrainte de cisaillement et la vitesse moyenne d'écoulement. Parmi ces trois indices, la dissipation de l'énergie représente l'indice le plus utilisé par les méthodes connues d'évaluation de l'érodabilité des massifs rocheux. En revanche, il ressort de l'application de cette nouvelle méthode que la contrainte de cisaillement moyenne du lit d'un canal représente mieux la force érosive de l'eau par rapport à la dissipation d'énergie, suivie de la vitesse moyenne d'écoulement. La pertinence de ces indices par rapport à la dissipation de l'énergie peut être définie par le lien direct entre ces indices et la pression exercée sur le lit d'un canal. Néanmoins, ces indices ne permettent pas d'interpréter comme il faut la force de soulèvement d'un bloc, car la principale force provoquant l'érosion par enlèvement des blocs est la pression appliquée dans les joints autour des blocs. Cependant, des recherches supplémentaires sont nécessaires pour améliorer les équations de détermination de la contrainte de cisaillement d'un canal d'écoulement pour qu'elle soit applicable aux différents processus d'érosion connus.

6.3. DÉVELOPPEMENT D'UNE MÉTHODE VECTORIELLE POUR LE CALCUL EXACT DU VOLUME DES BLOCS DE ROCHE

Le volume des blocs étant l'un des paramètres géomécaniques important dans la détermination de la résistance d'un massif rocheux, cette nouvelle méthode analytique basée sur le produit vectoriel est développée pour calculer le volume des blocs dans le cas de trois ensembles de joints persistants avec des valeurs constantes d'espacement et d'orientation. La précision de cette méthode est validée par la simulation numérique et les résultats obtenus par cette nouvelle méthode sont plus fiables que ceux des méthodes existantes. Pour appliquer cette méthode de produit vectoriel, il faut connaitre le pendage, la direction du pendage et les espacements des ensembles de joints. Une feuille de calcul Excel est programmée pour des fins d'applications de cette méthode. De plus, la précision des méthodes existantes dans le calcul du volume des blocs est évaluée à l'aide d'une série de données de terrain sur la base de cette nouvelle méthode.

6.4. CONCEPTION D'UN MODÈLE PHYSIQUE RÉDUIT D'ÉVACUATEUR DE CRUE POUR L'ÉVALUATION DU PROCESSUS D'ÉROSION HYDRAULIQUE

Le processus d'érosion hydraulique s'effectuant à grande échelle, cela rend la compréhension de ce phénomène complexe. Pour pallier à cette difficulté des modèles numériques et des modèles physiques réduits sont conçus en laboratoire

pour étudier ces phénomènes se produisant à grande échelle. Cependant, l'un des problèmes souvent mal résolus dans les modèles physiques réduits est leur représentativité, c'est-à-dire l'invariance des paramètres à l'étude à des échelles différentes. Parmi les autres problèmes rencontrés mentionnons des cas où le modèle réduit n'est pas du tout identique aux prototypes et/ou ne tient pas compte de l'ensemble des paramètres qui caractérisent le phénomène à l'étude. Le modèle physique réduit conçu dans notre projet pour des fins d'évaluation du processus d'érosion hydraulique représente un modèle relativement complet. Le modèle inclut tous les paramètres hydrauliques et géomécaniques qualifiés de pertinents afin de pouvoir les évaluer. Le modèle est conçu de façon à être adapté à différentes conditions d'écoulements (débit, vitesse et inclinaison du canal variable) et à pouvoir varier les différents paramètres géomécaniques dépendamment de l'emplacement et de la configuration du massif rocheux voulu.

Ainsi, avec ce modèle physique réduit, il sera possible d'identifier et quantifier les paramètres hydrauliques et géomécaniques, ainsi que l'évaluation de l'interaction entre ces paramètres pour mieux caractériser l'érosion hydraulique.

À plus long terme, ce modèle physique réduit peut servir de prototype pour prédire le comportement des écoulements dans les canaux d'écoulement et aussi prédire le risque d'érosion des futurs évacuateurs de crue des barrages

hydroélectriques. Une solution innovante que l'UQAC pourrait développer et qui pourrait être d'une grande utilité à Hydro-Québec et à d'autres entreprises pour contrôler le risque éventuel cas d'érosion hydraulique des canaux d'écoulement des évacuateurs de crue.

RÉFÉRENCES

Annandale G. 1995. Erodibility. Journal Of Hydraulic Research, 33 : 471-494.

Annandale G, Wittler R, Ruff J et Lewis T. 1998. Prototype validation of erodibility index for scour in fractured rock media. Water Resources Engineering'98 : 1096-1101.

Annandale GW. 2006a. Scour technology. McGraw-Hill.

Annandale GW. 2006b. Current Technology to Predict Scour of Rock. Golden Rocks 2006, The 41st US Symposium on Rock Mechanics (USRMS), 2006/1/1/, Golden, Colorado.

Barton N, Lien R et Lunde J. 1974. Engineering classification of rock masses for the design of tunnel support. Rock mechanics, 6 : 189-236.

Bergh-Christensen J. 1968. On the blastability of rocks. Technical University of Norway, Trondheim, Norway, 320 p.

Bieniawski ZT. 1973. Engineering classification of jointed rock masses. Civil Engineer in South Africa, 15 : 11.

Bieniawski ZT. 1989. Engineering rock mass classifications: a complete manual for engineers and geologists in mining, civil, and petroleum engineering. John Wiley & Sons.

Bollaert E. 2004. A comprehensive model to evaluate scour formation in plunge pools. International Journal on Hydropower & Dams, 11 : 94-101.

Bollaert E. The comprehensive scour model: Theory and feedback from practice. Dans : 5th International Conference on Scour and Erosion, San Francisco, 2010.

Bollaert E et Schleiss A. 2002. Transient water pressures in joints and formation of rock scour due to high-velocity jet impact. EPFL-LCH.

Bollaert E, Duarte R, Pfister M, Schleiss A et Mazvidza D. 2012. Physical and numerical model study investigating plunge pool scour at Kariba Dam. Journal of Hydraulic Engineering : 241-248-241-248.

Bollaert EF et Schleiss AJ. 2005. Physically based model for evaluation of rock scour due to high-velocity jet impact. Journal of Hydraulic Engineering, 131 : 153-165.

Boumaiza L, Saeidi A et Quirion M. 2019a. A method to determine relevant geomechanical parameters for evaluating the hydraulic erodibility of rock. Journal of Rock Mechanics and Geotechnical Engineering, 11 : 1004-1018.

Boumaiza L, Saeidi A et Quirion M. 2019b. A method to determine relevant geomechanical parameters for evaluating the hydraulic erodibility of rock. Journal of Rock Mechanics and Geotechnical Engineering.

Bray DI. 1979. Estimating average velocity in gravel-bed rivers. Journal of the Hydraulics Division, 105 : 1103-1122.

Cai M, Kaiser P, Uno H, Tasaka Y et Minami M. 2004a. Estimation of rock mass deformation modulus and strength of jointed hard rock masses using the GSI system. International Journal of Rock Mechanics and Mining Sciences, 41 : 3-19.

Cai M, Kaiser PK, Uno H, Tasaka Y et Minami M. 2004b. Estimation of rock mass deformation modulus and strength of jointed hard rock masses using the GSI system. International Journal of Rock Mechanics and Mining Sciences, 41 : 3-19.

Cengel Y. 2014. Heat and mass transfer: fundamentals and applications. McGraw-Hill Higher Education.

Churchill SW. 1973. Empirical expressions for the shear stress in turbulent flow in commercial pipe. AIChE Journal, 19 : 375-376.

Deere DU et Deere DW. 1989. Rock Quality Designation (RQD) after Twenty Years.

Edelbro C. 2003. Rock mass strength : a review. Luleå tekniska universitet, Luleå, 92 p.

Elci H et Turk N. 2014. Block Volume Estimation from the Discontinuity Spacing Measurements of Mesozoic Limestone Quarries, Karaburun Peninsula, Turkey. The Scientific World Journal, 2014 : 363572.

George M, Sitar N et Sklar L. 2015. Experimental evaluation of rock erosion in spillway channels. 49th US Rock Mechanics / Geomechanics Symposium 2015.

Graf WH et Altinakar MS. 2000. Hydraulique fluviale: écoulement et phénomènes de transport dans les canaux à géométrie simple. PPUR presses polytechniques.

Grenon M et Hadjigeorgiou J. 2003. Open stope stability using 3D joint networks. Rock Mechanics and Rock Engineering, 36 : 26.

Gu S, Liqun R, Xing W, Hongwei X, Yuefei H, Jiahua W et Songdong S. 2017. SPHysics Simulation of Experimental Spillway Hydraulics. Water, 9. doi : 10.3390/w9120973.

Guo J et Julien PY. 2005. Shear stress in smooth rectangular open-channel flows. Journal of Hydraulic Engineering, 131 : 30-37.

Henderson FM. 1966. Open channel flow.

Hoek E, Marinos P et Benissi M. 1998. Applicability of the Geological Strength Index (GSI) classification for very weak and sheared rock masses. The case of the Athens Schist Formation. Bulletin of Engineering Geology and the Environment, 57 : 151-160.

Itasca Consulting Group I. 2021. 3DEC — Three-Dimensional Distinct Element Code. Itasca, Minneapolis.

Keaton JR. 2013. Estimating erodible rock durability and geotechnical parameters for scour analysis. Environmental & Engineering Geoscience, 19 : 319-343.

Khatsuria RM. 2004. Hydraulics of spillways and energy dissipators. CRC Press.

Khodashenas SR, Abderrezzak KEK et Paquier A. 2008. Boundary shear stress in open channel flow: A comparison among six methods. Journal of Hydraulic Research, 46 : 598-609.

Kirsten H. 1982a. A classification system for excavating in natural materials. Civil Engineering= Siviele Ingenieurswese, 24 : 293-308.

Kirsten HA, Moore JS, Kirsten LH et Temple DM. 2000. Erodibility criterion for auxiliary spillways of dams. International journal of sediment research, 15 : 93-107.

Kirsten HAD. 1982b. A classification system for excavating in natural materials. Civil Engineering = Siviele Ingenieurswese, 24 : 293-308.

Kote AS et Nangare PB. 2019. Hydraulic Model Investigation on Stepped Spillway's Plain and Slotted Roller Bucket. Engineering, Technology & Applied Science Research, 9.

Koulibaly AS, Saeidi A, Rouleau A et Quirion M. 2021. Identification of Hydraulic Parameters Influencing the Hydraulic Erodibility of Spillway Flow Channels. Water, 13 : 2950.

Latham J-P, Van Meulen J et Dupray S. 2006. Prediction of in-situ block size distributions with reference to armourstone for breakwaters. Engineering Geology, 86 : 18-36.

Lesleighter EJ, Bollaert EFR, McPherson BL et Scriven DC. 2016. Spillway Rock Scour Analysis - Composite of Physical & Numerical Modelling, Paradise Dam, Australia. 6th IAHR International Symposium on Hydraulic Structures, 27-30 june, Portland.

Liu PQ, Dong JR et Yu C. 1998. Experimental investigation of fluctuation uplift on rock blocks at the bottom of the scour pool downstream of Three-Gorges spillway. Journal of Hydraulic Research, 36 : 55-68.

Lowe J, Chao P et Luecker A. 1979. Tarbela service spillway plunge pool development. Water Power and Dam Construction, 31 : 85-90.

Manso PFdA et Schleiss A. 2006. The influence of pool geometry and induced flow patterns in rock scour by high-velocity plunging jets. EPFL (Lausanne).

Montgomery RA. 1984. Investigations into rock erosion by high velocity water flows. Royal Institute of Technology, Stockholm.

Moore JS, Temple DM et Kirsten HAD. 1994. Headcut advance threshold in earth spillways. Bulletin of the Association of Engineering Geologists.

Nezu I et Rodi W. 1986. Open-channel Flow Measurements with a Laser Doppler Anemometer. Journal of Hydraulic Engineering, 112 : 335-355.

Palmstrom A. 2005. Measurements of and correlations between block size and rock quality designation (RQD). Tunnelling and Underground Space Technology, 20 : 362-377.

Palmström A. The volumetric joint count—a useful and simple measure of the degree of rock mass jointing. Dans : International Association of Engineering Geology International congress, India / Netherlands, 1982. A.A. Balkema, p. 221-228.

Palmström A. 1995. RMi-a rock mass characterization system for rock engineering purposes. University of Oslo.

Palmström A. 1996. The Rock Mass Index (RMi) applied in rock mechanics and rock engineering. Joumal of Rock Mechanics and Tunnelling Technology, 2 : 40.

Palmström A. 2001a. Measurement and characterization of rock mass jointing. Dans : Sharma VM et Saxena KR éds. In-situ characterization of rocks. A.A. BalkemaA Publishers, India, p. 1-40.

Palmström A. 2001b. Measurement and characterization of rock mass jointing. In-situ characterization of rocks : 49-97.

Palmström A. 2005. Measurements of and correlations between block size and rock quality designation (RQD). Tunnelling and Underground Space Technology, 20 : 362-377.

Pells P, Pells S et van Schalkwyk A. A tale of two spillways. Dans : Proceedings of the International Symposium on “Appropriate Technology to Ensure Proper Development, Operation and Maintenance of Dams in Developing Countries”, SANCOLD, 2016a.

Pells PJ, Bieniawski ZT, Hencher SR et Pells SE. 2017. Rock quality designation (RQD): time to rest in peace. Canadian Geotechnical Journal, 54 : 10.

Pells S. 2016a. Erosion of rock in spillways. School of Civil and Environmental Engineering, University of New SouthWales.

Pells S. 2016b. Erosion of rock in spillways. University of New South Wales, Australia, 1982 p.

Pells SE, Pells PJ, Peirson WL, Douglas K et Fell R. 2015. Erosion of unlined spillways in rock–does a "scour threshold" exist? Contemporary Challenges for Dams Proceedings of the Annual Australian National Committee on Large Dams Conference, ANCOLD, 4.

Pells SE, Pells PJ, Peirson WL, Douglas K et Fell R. 2016b. Erosion of rock in spillways. University of New South Wales.

Ramana Prasad B et Russell Manson J. 2002. Discussion of a geometrical method for computing the distribution of boundary shear stress across irregular straight open channels. Journal of Hydraulic Research, 40 : 537-539.

Reinius E. 1986. Rock erosion. International Water Power and Dam Construction, 38 : 43-48.

Rouse H. 1965. Critical analysis of open-channel resistance. Journal of the Hydraulics Division, 91 : 1-23.

Sawadogo O. 2010. Scour of Unlined Dam Spillways. Stellenbosch University, Stellenbosch University, 166 p.

Schlichting H. 1979. Boundary Layer Theory, McGraw-Hill, New York, 1979. FIGURE CAPTIONS solid curve displays the exact solution The difference between the exact solution and the eighth QLM iteration for all t in the figure is less than : 10-10.

Seckin G, Seckin N et Yurtal R. 2006. Boundary shear stress analysis in smooth rectangular channels. Canadian Journal of Civil Engineering, 33 : 336-342.

Severy A et Felder S. Flow Properties and Shear Stress on a Flat-Sloped Spillway. Dans : Proceedings of the 37th IAHR World Congress, August, 2017.

Streeter V, Wylie B et Bedford K. 1998. External flows. Fluid Mechanics 9th ed New York: McGraw-Hill : 327-328.

Tuna MC. 2012. Effect of offtake channel base angle of stepped spillway on scour hole. Iranian Journal of Science and Technology Transactions of Civil Engineering, 36 : 239-251.

Van Schalkwyk A, Jordaan J et Dooge N. 1994. Erosion of rock in unlined spillways. International Commission on Large Dams, 71 : 555-571.

Wang Y-k et Jiang C-b. 2010. Experimental study of drag reduction in flumes and spillway tunnels. Water Science and Engineering, 3 : 200-207. doi : 10.3882/j.issn.1674-2370.2010.02.008.

Wilkinson C, Harbor DJ, Helgans E et Kuehner JP. 2018. Plucking phenomena in nonuniform flow. Geosphere, 14.

Withers WJ. 1991. Pressure fluctuations in the plunge pool of an impinging jet spillway. University of Glasgow, Glasgow, 357 p.

Wyllie DC et Mah C. 2004. Rock slope engineering. CRC Press.

Yang S-Q et Lim S-Y. 2005. Boundary shear stress distributions in trapezoidal channels. Journal of Hydraulic Research, 43 : 98-102.

Yen BC. 2002. Open channel flow resistance. Journal of Hydraulic Engineering, 128 : 20-39.

Yen BC et Akan AO. 1999. Hydraulic design of urban drainage systems. McGraw-Hill: New York, NY, USA.

ANNEXES

Annexe A. Hydraulic and geomechanical data used in chapter 3 (Pells 2016a)

HEC-RAS Estimates					Rock mass indices			**Chart ID**	Erosion Level
Peak q (m^2/s)	S_f	Peak u_{mean} (m/s)	Peak $\tau_{b\text{-}mean}$ (kPa)	Peak $\prod_{UD}$ (kW/m^2)	**K** Kirsten index	**eGSI** Pells index	**RMEI$_B$** Pells index		
1,4	0,124	3,3	0,45	1,7	868	47	1188	Ant. 1	Minor
2,7	0,031	2,6	0,29	0,8	575	47	243	Ant. 2	Negligeable
3,7	0,02	2,5	0,24	0,7	868	47	1440	Ant. 3	Minor
1	0,676	4,4	1,3	6,3	1903	42	1080	Ant. 4	Moderate
22,9	0,019	6,1	0,75	4,2	3721	67	1440	Bro.1	Minor
22,4	0,082	9,6	2,33	18	2756	67	1296	Bro.2	Moderate
22,4	0,082	9,6	3,49	18	2233	55	1152	Bro.3	Moderate
22,4	0,082	9,6	4,02	18	2233	53	1080	Bro.4	Moderate
22,4	0,082	9,6	2,33	18	5629	65	432	Bro.5	Negligeable
22,4	0,082	9,6	2,68	18	7003	77	144	Bro.6	Minor
22,4	0,082	9,6	4,02	18	2425	55	1440	Bro.7	Large
38	0,443	25	5,4	165	11417	82	252	Bur.1	Negligeable
38	0,443	25	5,4	165	7848	80	288	Bur.2	Negligeable
38	0,443	25	5,4	165	6089	60	972	Bur.3	Moderate
38	0,443	25	5,4	165	3653	40	1890	Bur.4	Large
7	0,874	22	10	60	3706	72	567	Cat.1	Minor
7	0,874	22	10	60	3706	72	126	Cat.2	Negligeable
7	0,874	22	10	60	3706	72	567	Cat.3	Large
6	0,097	6,8	0,83	5,7	724	35	1620	Cop.1	Moderate
15,9	0,222	12	2,8	34,7	3721	32	1755	Cop.4	Large
20,5	0,378	15,5	4,8	76,1	3721	32	1755	Cop.5	Extensive
22	0,218	13,3	3,4	47,1	3721	25	1755	Cop.6	Extensive
32,5	0,207	14,5	4,1	66,1	3721	32	1755	Cop.7	Moderate
40	0,428	18,8	6,6	168	3721	32	1755	Cop.9	Large
140	0,473	21,2	8,3	650	3721	25	1755	Cop.10	Extensive
19	0,054	12,2	0,8	10	724	35	1620	Cop.11	Minor
25	0,396	15,5	3,8	97	8372	70	1350	Cop.12	Moderate
29	0,51	19,5	7	145	8372	65	1350	Cop.13	Moderate
1,3	1,411	12,5	2	18	4515	52	504	Dar.1	Minor
1,3	1,411	12,5	2	18	4515	52	1080	Dar.2	Moderate
1,3	1,411	12,5	2	18	4515	52	972	Dar.3	Moderate
1,3	1,411	12,5	2	18	0,22	10	1980	Dar.4	Moderate
1	0,917	7	1	9	4535	60	648	Dar.5	Minor
2,3	0,155	5,2	0,69	3,5	4651		2700	Dar.6	Large
3,2	0,271	6,8	1,3	8,5	0,22	7	1980	Dar.7	Moderate
5,8	0,011	3,4	0,13	0,6	1757	60	1296	Har.1	Minor
5,8	0,018	5,1	0,2	1	2283	65	1296	Har.2	Minor
5,8	0,016	5,1	0,2	1	4269	60	504	Har.3	Minor
8,9	0,646	14,9	3,8	56	5024	70	1980	Har.4	Minor
60,3	0,059	15	2	35	6038	67	594	Kun.1	Minor
60,3	0,059	15	2	35	2,9	12	864	Kun.2	Large
2	0,013	2,1	0,04	0,3	110	51	594	Moo.1	Minor
0,8	0,02	1,4	0,02	0,2	110	51	594	Moo.2	Negligeable
3,7	0,744	9,7	2,8	27	110	42	2925	Moo.3	Moderate
2	0,91	7,9	2,22	17	110	42	2925	Moo.4	Minor
2,5	1,06	9,5	2,7	26	0,42	17	2925	Moo.5	Large
1	1,631	7,5	2,1	16	0,42	17	2925	Moo.6	Moderate
3,6	0,135	5,1	0,9	4,8	310	45	1440	Pin.1	Minor
3,6	0,135	5,1	0,9	4,8	157	31	1440	Pin.2	Moderate
5,6	0,007	2,4	0,14	0,4	558	45	2160	Pin.3	Moderate
13,5	0,211	10,1	2,75	28	523	32	2520	Pin.4	Large

HEC-RAS Estimates					Rock mass indices				
Peak q (m^2/s)	S_f	Peak u_{mean} (m/s)	Peak $\tau_{b\text{-}mean}$ (kPa)	Peak $\prod_{UD}$ (kW/m^2)	**K** Kirsten index	**eGSI** Pells index	**RMEI$_B$** Pells index	**Chart ID**	Erosion Level
7,9	1,556	16	5,1	120	2664	72	864	Spl.1	Moderate
7,9	1,556	16	5,1	120	4729	77	864	Spl.2	Negligeable
7,9	0,311	9,7	2,5	24	359	57	1080	Spl.3	Minor
8,5	0,033	5,8	0,46	2,8	6089	67	1080	Way.1	Negligeable
8,5	0,033	5,8	0,46	2,8	4871	67	1404	Way.2	Negligeable
8,5	0,033	5,8	0,46	2,8	1282	57	1728	Way.3	Moderate
32,5	0,07	11,9	1,82	22	44	2		Way.4	Moderate
15	0,018	7,1	0,3	2,6	206	45	648	**App.1**	Negligeable
10,9	0,142	8,5	1,72	15	206	43	648	App.2	Minor
41	0,298	22,5	4	120	5495	43		Flo.1	Moderate
41	0,298	22,5	4	120	100	13		Flo.2	Moderate
1,9	0,054	5,2	0,17	1	106	25	405	Gar.1	Negligeable
2,1	0,68	12,6	1,1	14	106	23		Gar.2	Minor
2	0,459	10	0,7	9	2,9	3		Gar.3	Moderate
4,3	0,031	6,8	0,18	1,3	106	25	405	Gar.4	Negligeable
5,1	0,39	15,1	1,3	20	106	23		Gar.5	Minor
9,3	0,986	15,6	7,5	90	2934	69		Goe.1	Minor
5	1,835	15,6	7,5	90	26	31		Goe.2	Moderate
21,9	0,233	12,5	3,6	50	2934	69		Goe.3	Negligeable
9,3	0,986	15,6	7,5	90	26	31		Goe.4	Moderate
15	0,152	12,3	1,68	22	26	31		Goe.5	Moderate
7,9	0,046	7,1	0,46	3,6	11	5	3240	Haa.1	Large
1,44	0,02	2,6	0,11	0,3	11	5		Haa.2	Moderate
18	0,022	7,6	0,45	3,9	11	5	3240	Haa.3	Large
4,4	0,046	5	0,3	2	11	5		Haa.4	Large
24,4	0,185	12,5	3,33	44	3772	75		Hart.1	Negligeable
27,8	0,183	13,2	3,57	50	36	31		Hart.2	Moderate
27,9	0,067	10,2	1,75	18	3772	75		Hart.3	Negligeable
12,9	0,036	6,2	0,73	4,5	369	67	1008	Kam.1	Minor
21	0,131	10	2,1	27	6024	73	252	Kam.2	Negligeable
21	0,131	10	2,1	27	61	31	1800	Kam.3	Moderate
29,5	0,17	13,8	3,43	49	61	13		Kam.4	Large
22,3	0,062	9,1	1,5	14	81	32	1080	Kam.5	Minor
7,2	0,016	4,1	0,3	1,2	11002	75	864	Kli.1	Negligeable
7,8	0,077	6,8	0,86	6	6,1	23	1728	Kli.2	Minor
12,9	0,09	8,5	1,5	11,4	6,1	23	1728	Kli.3	Moderate
8,6	0,077	7,2	0,9	6,5	11002	73	864	Kli.4	Minor
8,6	0,077	7,2	0,9	6,5	6,1	23	1728	Kli.5	Minor
0,8	0,078	3	0,2	0,6	5385	67	630	Mok.1	Negligeable
0,98	0,147	4	0,35	1,4	29	19	2025	Mok.2	Moderate
1,1	0,146	4,2	0,38	1,6	0,7	3	2430	Mok.3	Moderate
1,2	0,114	3,9	0,35	1,3	5385	67	630	Mok.4	Negligeable
3,6	0,085	5,7	0,53	3	5385	67	630	Mok.5	Negligeable
18	0,113	10,4	1,3	20	29	19	2025	Mok.6	Large
18	0,113	10,4	1,3	20	0,7	3	2430	Mok.7	Large
3,9	0,06	5,3	0,44	2,3	5385	67	630	Mok.8	Negligeable
27,6	0,665	20	5,6	180	29	19	2025	Mok.9	Extensive
27,6	0,665	20	5,6	180	0,7	3	2430	Mok.10	Extensive
1,1	0,148	3,8	0,41	1,6	1053	46	972	Osp.1	Negligeable
		4	0,47		108	25	1404	Osp.2	Moderate
1,11	0,174	4	0,47	1,9	1053	46	972	Osp.3	Minor
-	-	4,2	0,52		108	33	1404	Osp.4	Moderate
1,12	0,2	4,2	0,52	2,2	1053	41	972	Osp.5	Negligeable

Annexe B. Graphics data sources

B-1. Data source of **Figure 3-4**. *u_{mean} vs K, u_{mean} vs eGSI* and *u_{mean} vs $RMEI_B$*

Rock class (K) in terms of ease of excavation				Erosion class defined by Pells et al. 2016									
				Negligible		Minor		Moderate		Large		Extensive	
				u_{mean}	K	u_{mean}	K	u_{mean}	K	u_{mean}	K	u_{mean}	K
1, 2 et 3	Sedimentary		0 - 0,9					7,75	0,39	9,95	0,56	20	0,7
4	Rock	Easy	1 - 9,9			7	6,1	9,25	4,5	15	2,9		
5	Rock	Difficult	10 - 99,9			9,1	81	10,65	32,375	8,78	24,6	20	29
6	Rock	Very difficult	100 - 999	4,075	220,6	7,745	376	9,3	266,43	10,1	523		
7	Rock	Extrêmement difficile	1000 - 9999	9,7063	4563,8	10,03	3903	13,615	4165,4	15,43	3646	16,67	3721
8	Rock	Explosives	> 10 000	14,55	11210	7,2	11002						

Rock mass class (eGSI)			Erosion class defined by Pells et al. 2016									
			Negligible		Minor		Moderate		Large		Extensive	
			u_{mean}	eGSI	u_{mean}	eGSI	u_{mean}	eGSI	u_{mean}	eGSI	u_{mean}	eGSI
1	Very Bad	< 20					9	9	10	10	20	11
2	Bad	21 - 40	6	25	11	27	11	31	16	34	17	27
3	Medium	41 - 60	4	46	6	51	11	50	10	55		
4	Good	61 - 80	9	70	11	70	15	69	22	72		
5	Very Good	81 - 100										

Rock mass class ($RMEI_B$)		Erosion class defined by Pells et al. 2016									
		Negligible		Minor		Moderate		Large		Extensive	
		u_{mean}	$RMEI_B$	u_{mean}	$RMEI_B$	u_{mean}	$RMEI_B$	u_{mean}	$RMEI_B$	u_{mean}	$RMEI_B$
1	0 - 499	13,28	300	9,6	144						
2	500 - 999	5,45	743,4	9,267	655	17,83	936	18,5	715,5		
3	1000 - 1499	5,8	1242	5,611	1252	10,73	1229	9,6	1440		
4	1500 - 1999			10,28	1764	9,271	1799	18,6	1800	16,67	1755
5	2000 - 2499					3,533	2205	10,4	2228	20	2227,5
6	2500 - 2999			7,9	2925	8,6	2925	8,2667	2715		
7	> 3000							7,35	3240		

B-2. Data source of Figure 3-5. τ_b *vs K*, τ_b *vs eGSI* and τ_b *vs* $RMEI_B$

Rock class (K) in terms of ease of excavation				Erosion class defined by Pells et al. 2016									
				Negligible		Minor		Moderate		Large		Extensive	
				$\tau_{b\text{-mean}}$	K	$\tau_{b\text{-mean}}$	K	$\tau_{b\text{-mean}}$	K	$\tau_{b\text{-mean}}$	K	$\tau_{b\text{-mean}}$	K
1, 2 et 3	Sedimentary		0 - 0,9					1,445	0,39	2	0,56	5,6	0,7
4	Rock	Easy	1 - 9,9			0,88	6,1	1,1	4,5	2	2,9		
5	Rock	Difficult	10 - 99,9			1,5	81	3,0788	32,375	1,188	24,6	5,6	29
6	Rock	Very difficult	100 - 999	0,192	220,6	1,0909	376	1,734	266,43	2,75	523		
7	Rock	Extremely difficult	1000 - 9999	2,31125	4563	2,5608	3903	3,4615	4165,4	4,9183	3646,17	5,5	3721
8	Rock	Explosives	> 10 000	2,85	11210	0,9	11002						

Rock mass class (eGSI)			Erosion class defined by Pells et al. 2016									
			Negligible		Minor		Moderate		Large		Extensive	
			$\tau_{b\text{-mean}}$	eGSI	u_{mean}	eGSI	$\tau_{b\text{-mean}}$	eGSI	$\tau_{b\text{-mean}}$	eGSI	$\tau_{b\text{-mean}}$	eGSI
1	Very Bad	< 20					1,418	8,78	1,493	9,87	5,6	11
2	Bad	21 - 40	0,175	25	1,077	26,5	3,298	30,7	4,388	34	5,5	27,33
3	Medium	41 - 60	0,308	46	0,989	50,8	2,561	50,1	4,02	55		
4	Good	61 - 80	2,423	70,2	3,173	69,7	4,558	68,5	10	72		
5	Very Good	81 - 100										

Rock mass class ($RMEI_B$)		Erosion class defined by Pells et al. 2016									
		Negligible		Minor		Moderate		Large		Extensive	
		$\tau_{b\text{-mean}}$	$RMEI_B$	$\tau_{b\text{-mean}}$	$RMEI_B$	$\tau_{b\text{-mean}}$	$RMEI_B$	$\tau_{b\text{-mean}}$	$RMEI_B$	$\tau_{b\text{-mean}}$	$RMEI_B$
1	0 - 499	3,234	300	2,68	144						
2	500 - 999	0,817	743,4	2,037	655	4,1667	936	6	715,5		
3	1000 - 1499	0,46	1242	0,822	1252	3,105	1229	4,02	1440		
4	1500 - 1999			1,59	1764	1,7557	1799	4,933	1800	5,5	1755
5	2000 - 2499					0,29	2205	1,3	2228	5,6	2227,5
6	2500 - 2999			2,22	2925	2,45	2925	2,047	2715		
7	> 3000							0,455	3240		

B-3. Data source of Figure 3-6. $\prod_{UD}$ *vs K,* $\prod_{UD}$ *vs eGSI* and $\prod_{UD}$ *vs* $RMEI_B$

Rock class (K) in terms of ease of excavation				Erosion class defined by Pells et al. 2016									
				Negligible		Minor		Moderate		Large		Extensive	
				Π_{UD}	K	Π_{UD}	K	Π_{UD}	K	Π_{UD}	K	Π_{UD}	K
1, 2 et 3	Sedimentary		0 - 0,9					11,025	0,39	23	0,56	180	0,7
4	Rock	Easy	1 - 9,9			6,25	6,1	10,2	4,5	35	2,9		
5	Rock	Difficult	10 - 99,9			14	81	37,838	32,38	15,7	24,6	180	29
6	Rock	Very difficult	100 - 999	1,18	220,6	10,182	376	31,58	266,4	28	523		
7	Rock	Extremely difficult	1000 - 9999	32,413	4563	24,558	3903	62,477	4165	74,87	3646,2	257,73	3721
8	Rock	Explosives	> 10 000	83,1	11210	6,5	11002						

Rock mass class (eGSI)			Erosion class defined by Pells et al. 2016									
			Negligible		Minor		Moderate		Large		Extensive	
			Π_{UD}	eGSI	Π_{UD}	eGSI	Π_{UD}	eGSI	Π_{UD}	eGSI	Π_{UD}	eGSI
1	Very Bad	< 20					21,87	8,78	19,94	9,87	180	11
2	Bad	21 - 40	1,15	25	11,75	26,5	40,78	30,67	98,93	34	257,7	27,33
3	Medium	41 - 60	1,48	46	7,833	50,83	39,35	50,1	18	55		
4	Good	61 - 80	34,4	70,2	30,58	69,67	95	68,5	60	72		
5	Very Good	81 - 100										

Rock mass class ($RMEI_B$)		Erosion class defined by Pells et al. 2016									
		Negligible		Minor		Moderate		Large		Extensive	
		Π_{UD}	$RMEI_B$	Π_{UD}	$RMEI_B$	Π_{UD}	$RMEI_B$	Π_{UD}	$RMEI_B$	Π_{UD}	$RMEI_B$
1	0 - 499	54,76	300	18	144						
2	500 - 999	13,5	743,4	16,3	655	101	936	47,5	715,5		
3	1000 - 1499	2,8	1242	6,167	1252	48,14	1229	18	1440		
4	1500 - 1999			19,63	1764	19,93	1799	122,6	1800	257,7	1755
5	2000 - 2499					1,133	2205	20	2228	180	2227,5
6	2500 - 2999			17	2925	21,5	2925	19,17	2715		
7	> 3000							3,75	3240		

Annexe C. Avancement de la construction du modèle réduit

C-1. Plan de construction du modèle réduit

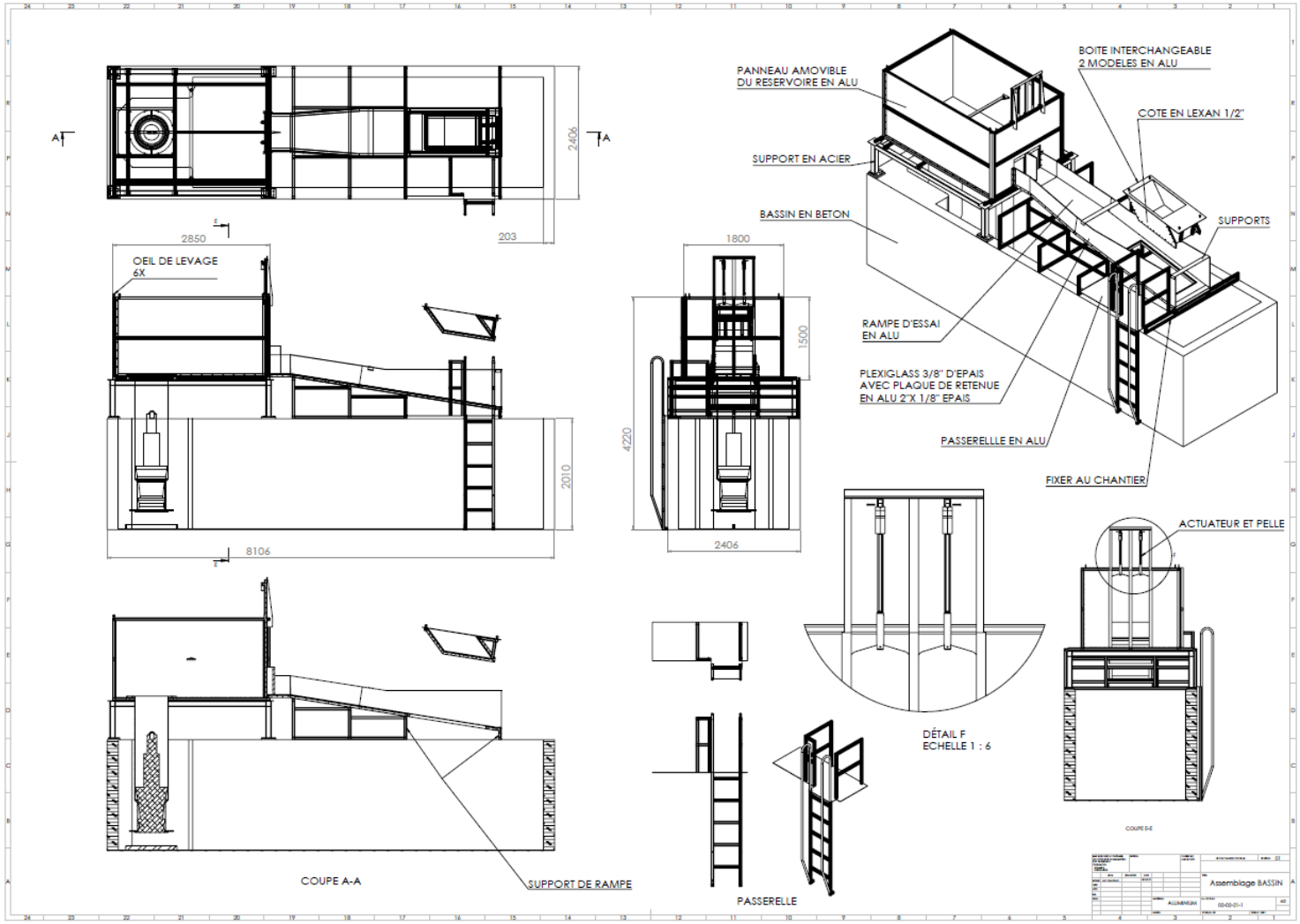

C-2. Dimensionnement du réservoir Amont (réservoir en Aluminium)

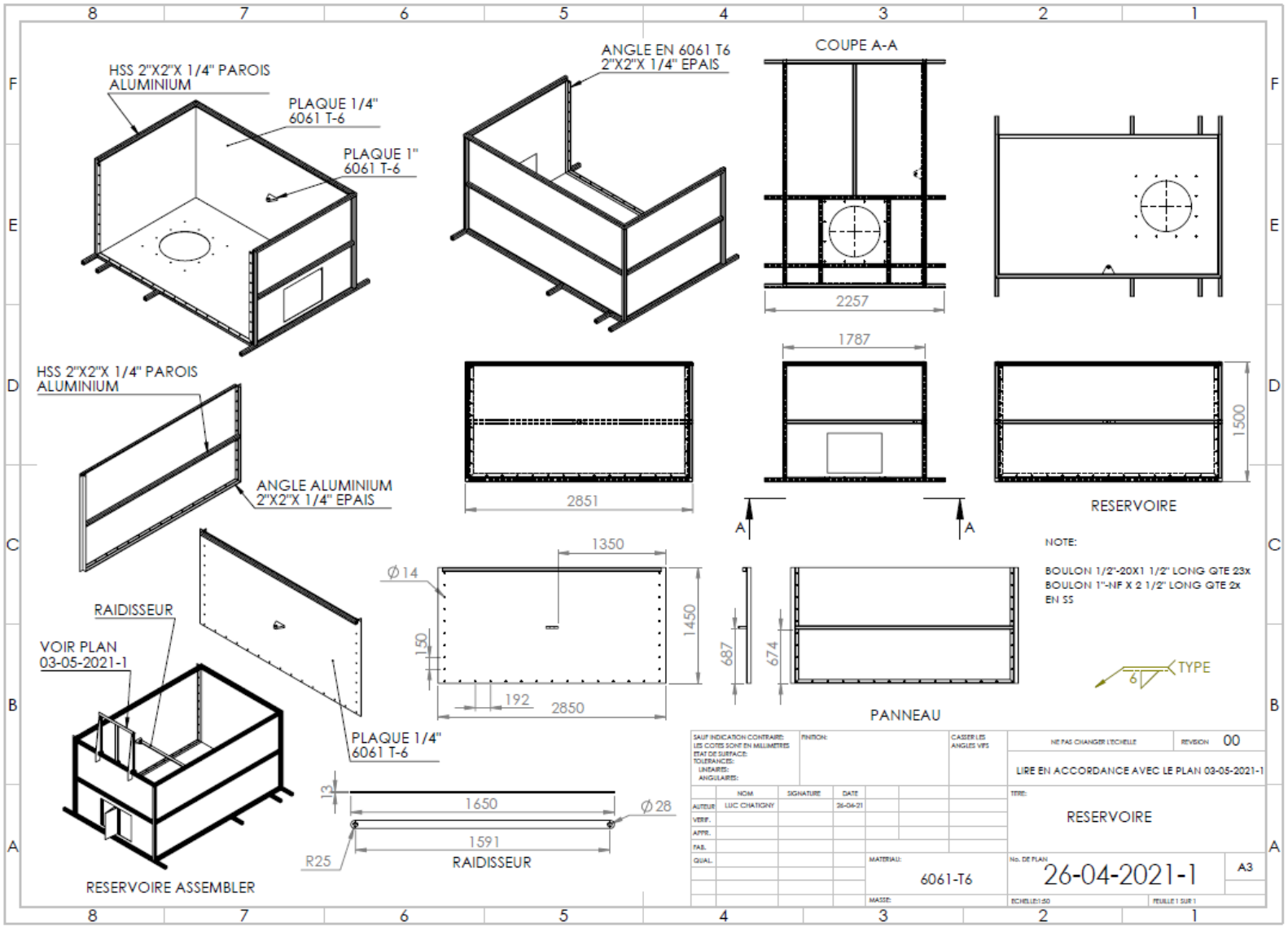

C-3. Dimensionnement de la boite réceptrice des blocs de bétons (Massif rocheux dans la section d'essai)

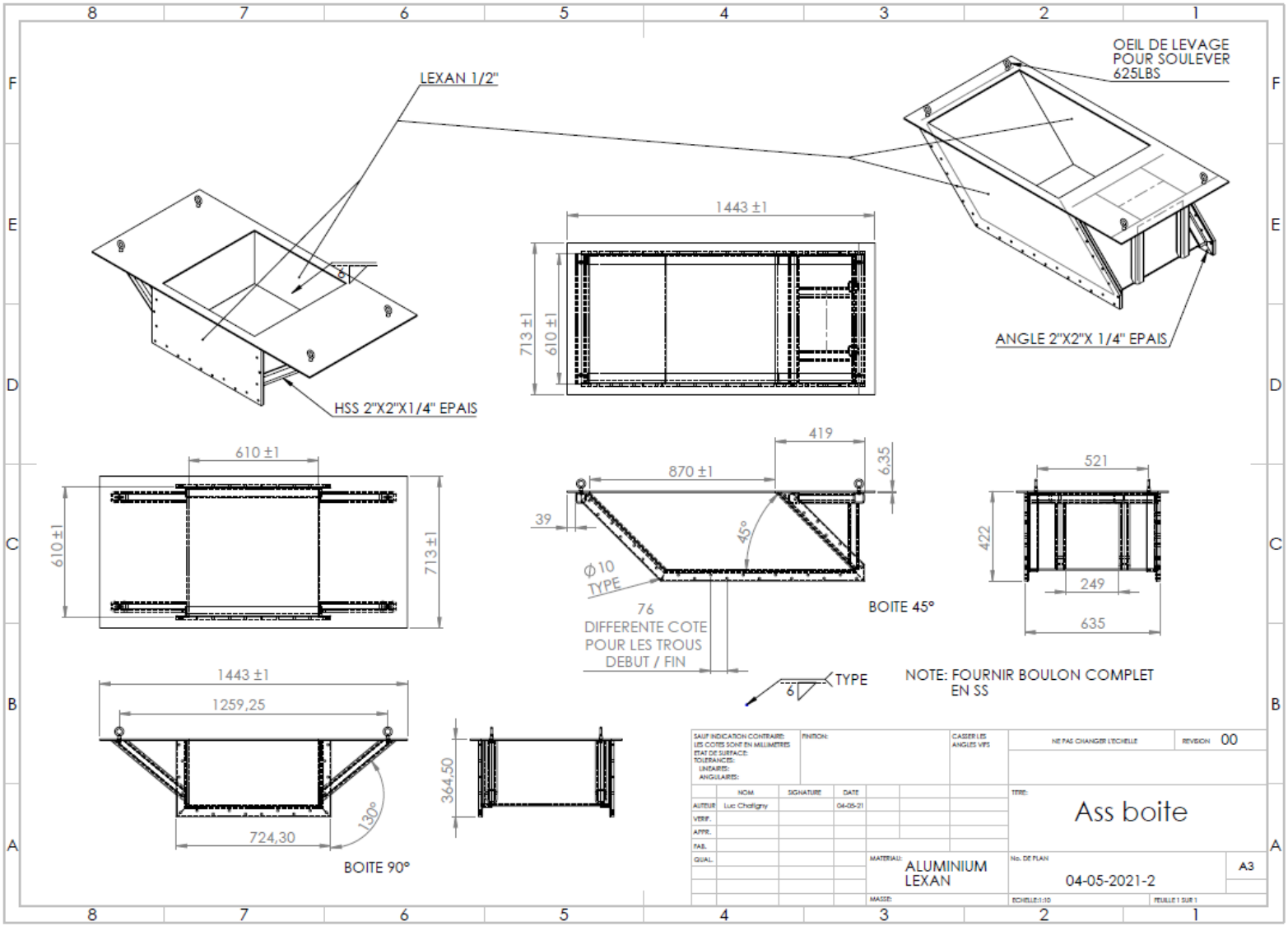

C-4. Dimensionnement de la portique (Système à double valve)

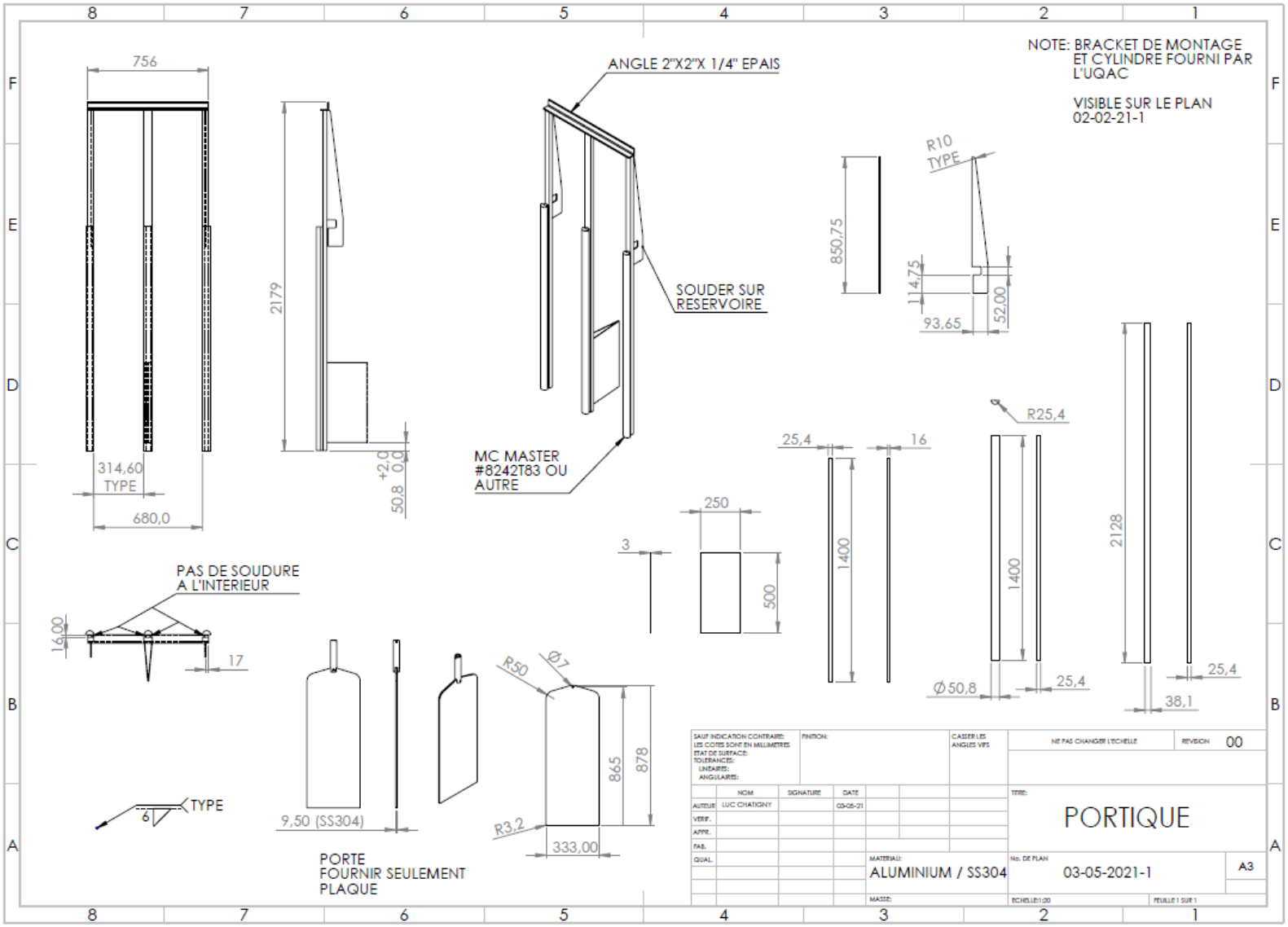

C-5. Dimensionnement du réservoir Avale (réservoir en béton)

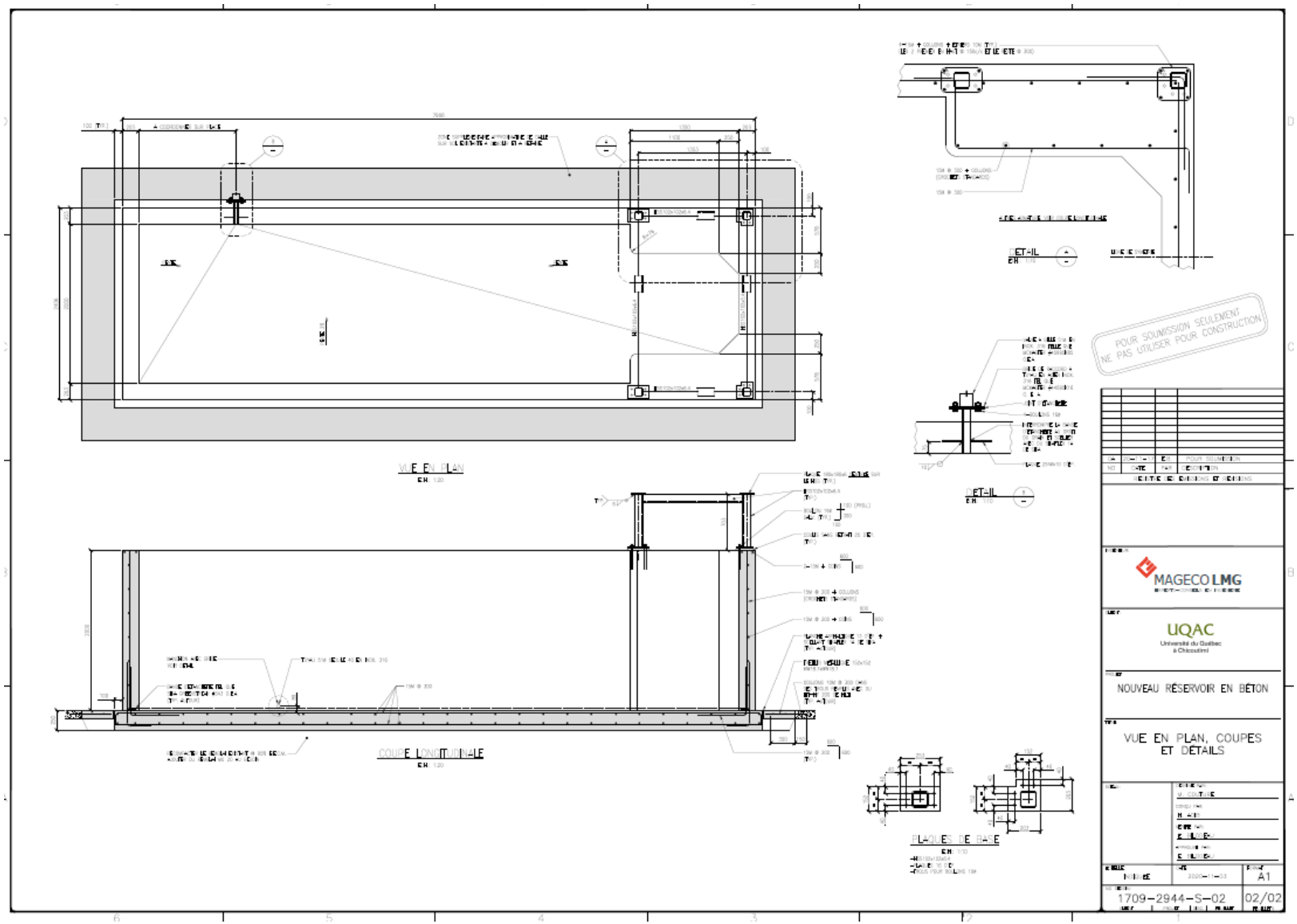
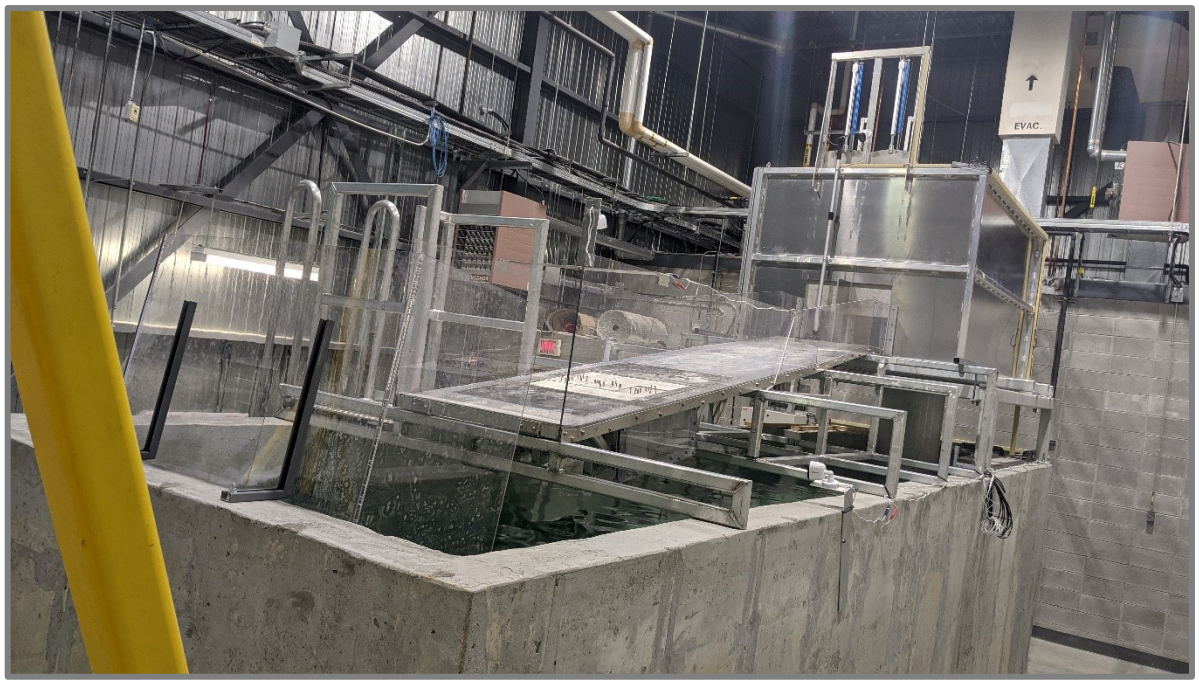
C-6. Modèle physique réduit construit